UNIVERSITÀ DELLA TUSCIA

FACOLTÀ DI SCIENZE MATEMATICHE FISICHE E NATURALI

DECOS: Dipartimento di Ecologia e Sviluppo Economico Sostenibile

Dottorato in Ecologia e Gestione delle Risorse Biologiche

XXIV Ciclo

"A new paradigm in coastal ecosystem assessment: linking ecology and geomorphology implementing the FHyL approach"

(SSD/BIO07**)**

Coordinatore: Dott. ssa Roberta Cimmaruta

Tutor: Dott. Andrea Taramelli

Dottoranda: Emiliana Valentini

Viterbo, 12/06/2013

To Antonello & Francesco

…"The reason death sticks so closely to life isn't biological. It is envy. Life is so beautiful that death has fallen in love with it, a jealous, possessive love that grabs at what it can….But life can go lightly over oblivion and gloom is but the passing shadow of a cloud"

(Revisited from Life of Pi, Yann Martel 2001)

My personal thanks to who profoundly influenced my sensibility in Life Sciences during these 4 years:

Thanks to my tutor Dr. Andrea Taramelli, expert in geophysics and geomorphology. He kindly introduced me the fascinating world of Earth Sciences and Remote Sensing. Through feedbacks from landscape to geomorphology he lighted my mind to innovative insights of research. Each day of these four years has been for me test and challenge in reasoning and learning...sincerely, thanks.

...*Space is a subject of research through space science (understanding the Universe) and a tool for research through science in space (research in life and earth sciences) and science from space…*

Thanks to Prof. Loreto Rossi and to his huge academic experience in teaching the Ecology. Every speech with him has been a lesson of inestimable value and suggested me how life interacts with its landscape and how ecosystems' structures, functions and services can be analyzed.

Thanks to Dr. Sergio Cappucci, his knowledge of coastal systems and sediment properties has been a precious source for the scientific discussions and to Eng. Claudia Giardino for the lessons in remote sensing of environment.

Thanks to Dr. Matteo Conti, colleague and friend during each day of the LiDLAZ project. I will never forget.

Thanks to Marco and Antonella, widely and immeasurably.

Always and wherever, thanks to my family.

PREFACE

In an era of changes, dynamic interaction of life and its landscape is determined by feedback at the interface between ecology and geomorphology. One of the main actual question in ecosystem analysis is how abundance, biomass and distribution of organism on the planet are dependent upon spatial and temporal variation in physical process (Reinhardt, 2010) and how abundance, biomass and distribution of organism are prevailing drivers in physical process (Haussmann, 2010; Corenblit et al., 2011). The hypothesis that land and water uses as well as other human activities, influence how the biosphere is changing in response to diverse set of climate pressures, led to the understanding that human activities are determining how physical process influence biodiversity and ecosystem services provision.

To contribute in understanding remote sensing technologies to monitor and maintain quality of life on this biosphere in view of predictable changes, this thesis, by moving from biological ecology to geomorphology within a variety of Earth System Science approaches (Viles et al., 2008; Roughgarden, et al., 2010), develop an holistic understanding of how complex spatial patterns can be investigated by means of innovative remote sensing application and how spatial vegetation pattern can influence and describe trends in coastal habitat distribution (Zhou et al., 2006).

An overall approach in terms of methodology and knowledge has been developed and named FHyL, Field measurements, Hyperspectral imagery and LiDAR altimetry. FHyL is a set of modular processes that moving through the path of fixed procedures produces descriptive and detailed biophysical maps of complex coastal ecosystems.

At the base of the innovative approach are both the new sub-pixel target detection algorithm that integrates linear mixing models with multisensory analysis and the use of existing techniques to obtain new ways of analyzing feedback from ecology and geomorphology in coastal ecosystem assessment.

This PhD thesis begin with an introduction that focuses the specific context of feedbacks between ecology and geomorphology and the increasing interests in remote sensing application for environmental studies and monitoring in coastal areas. An overview of the principles at the base of the implemented methodology is included and a brief introduction of the three cases studies is provided in order to underline specific complexities. Introduction ends with a summary of aims and purposes of the research.

The second chapter faces up with the methodology and shows in a schematic view the FHyL approach applied to different typologies of coastal areas.

Then, three chapters identify the three study cases developed through the FHyL approach:

- Coastal complex seabed;
- Coastal beach dune systems;
- Shallow muddy lake;

Each chapter is organized as a scientific paper with the introduction, methods, results and discussion, so that, for each of the three chapters, the state of the art and the references are provided, as well as the names of co-authors.

Conclusions take account of challenges and opportunity that recent advances in remote sensing offered to this research for accurate biophysical mapping.

The dissemination activities that supported the development of this thesis are listed at the end of the volume. They represented the end to end way used during thesis developments to test the scientific achievements.

This thesis has been mainly founded through ISPRA LIDLAZ research project by Lazio Region.

TABLE OF CONTENT

1. INTRODUCTION 1

RELEVANCE OF THE PRESENT WORK 2

PRINCIPAL DEFINITIONS 7

AIMS 10

CASE STUDY 1: Complex coastal seabed: Tarquinia (VT) 11

CASE STUDY 2: Coastal beach dune system: Sabaudia (LT) 12

CASE STUDY 3: The shallow muddy lake: Trasimeno (PG) 13

REFERENCES 14

2. FHYL: FIELD SPECTRAL LIBRARIES, AIRBORNE HYPERSPECTRAL IMAGES AND TOPOGRAPHIC AND BATHYMETRIC LIDAR DATA FOR COMPLEX COASTAL MAPPING 17

2.1METHODOLOGY 18

2.1.1 PREPROCESSING STEPS 18

2.1.2 MODULE 1 – LIDAR-MIVIS EMERGED 19

2.1.3 MODULE 2 – LIDAR-MIVIS SUBMERGED 20

2.1.4 MODULE 3 – MIVIS-LIDAR EMERGED 20

2.1.5 MODULE 4 – MIVIS-LIDAR SUBMERGED 21

2.2RESULTS 22

3. FHYL: FIELD SPECTRAL LIBRARIES, AIRBORNE HYPERSPECTRAL IMAGES AND LIDAR ALTIMETRY FOR COMPLEX COASTAL SEABED MAPPING 23

3.1INTRODUCTION 24

3.2STUDY AREA 27

3.3MULTYSENSORY DATASET COLLECTION 28

3.3.1 FIELD SPECTRAL PROPERTIES 29

3.3.2 AIRBORNE HYPERSPECTRAL IMAGERY 31

3.4METHODOLOGY 32

3.4.1 FIELD SPECTRAL LIBRARY 33

3.4.2 IMAGE PREPROCESSING 33

3.4.3 MULTISENSORY SPECTRAL MIXTURE ANALYSIS 34

3.5RESULTS 36

3.6DISCUSSION 51

3.7CONCLUSIONS 55

3.8REFERENCES 56

4. USE OF AIRBORNE LIDAR AND HYPERSPECTRAL DATA TO STUDY THE SANDY BEACH MORPHOLOGY ALONG THE LAZIO REGION COAST (ITALY) 60

4.1INTRODUCTION 61

4.2STUDY AREA 65

4.3DATA AND MATERIALS 66

4.3.1 LIDAR ACQUISITION 68
4.3.2 MIVIS DATA AND VALIDATION MEASUREMENTS 70

4.4METHODS AND METHODOLOGY 74

4.3.1 ANALYSIS OF LIDAR DATA 74
4.3.2 SHORELINES EXTRACTION 75
4.3.3 EXTRACTION OF THE FOOT AND THE INNER EDGE OF THE DUNES 75
4.3.4 MORPHOMETRIC ANALYSIS OF AEOLIAN DEPOSITS 77
4.3.5 EXTRACTION OF VEGETATED AREAS 78
4.3.6 PRINCIPAL COMPONENT ANALYSIS (PCA) 79
4.3.7 PRESENCE/ABSENCE OF VEGETATION 80
4.3.8 LANDFORM VEGETATION COVER STRUCTURE 80

4.5RESULTS AND DISCUSSION 83

4.6CONCLUSIONS 98

4.7REFERENCES 101

5. HABITAT MAPPING WITH COMBINED FIELD, HYPERSPECTRAL AND LIDAR DETECTION IN A SHALLOW MUDDY LAKE 106

5.1INTRODUCTION 107

5.2CASE STUDY 110

5.3MATERIALS AND METHDOS 112

5.3.1 BIO OPTICAL MODELING OF WATERS 113
5.3.2 DOUBLE STEP CLASSIFICATION 114

5.4RESULTS AND DISCUSSION 116

5.4.1 WATER QUALITY MAPS 116
5.4.2 STEP 1. LIDAR DSM ANALYSIS 117
5.4.3 AQUATIC VEGETATION MAPS 118

5.5CONCLUSIONS 125

5.6REFERENCES 126

6. CONCLUSIONS 130

7. KEY DISSEMINATION ACTIVITIES 133

1. INTRODUCTION

Coastal environments can be considered as mosaics of 'interacting ecosystems' (Risser, 1995). This view implies relationships between landscape and water in more (i.e. emerged nearshore) or less (i.e. submerged nearshore/shallow waters) evident feedbacks. Coastal areas are targeted by urbanization and industrial development causing rapidly undergoing adjustments and evolving at different time and space scales in response to varying conditions external to the system.

Utilization of the coasts increased dramatically during the 20th century, a trend that seems certain to continue through the 21st century. Coastal population growth led to widespread conversion of natural coastal landscapes to agriculture, aquaculture, as well as industrial and residential uses both in marine and freshwaters ecosystem (Valiela, 2006). It has been estimated that 23% of the world's population lives within 100 km distance of the marine coast and <100 m above sea level, and population density in coastal regions is about three times higher than the global average (Small and Nicholls, 2003).

Sandy beaches are widespread present along seacoasts and wetlands dominate most temperate and tropical latitude. They both represent important recreational assets and buffer zones of waters, animals and vegetation. In some areas they are very productive and commercially exploited.

For example, most beaches worldwide represent important touristic resources as well as a source of sediments for buildings and beach - nourishment (Regnauld et al., 2004). Europe's wetlands moreover, support a large diversity of plant and animal species and are also the source of a wide range of public coastal goods and services, including tourism and the supply of fresh waters and food (Costanza, 1997). Wetlands represent around 6% of the Earth's land area – some 570 million hectares, of which only 2% are lakes that supply freshwaters and an enormous range of plant and animal requirements. However, wetlands are among the most highly threatened ecosystems on the planet, with 50% of the world's wetlands having disappeared in the last century. Land reclamation through the filling of wetlands and expansion of coastlines threatened conservation efforts and biodiversity.

In response to the loss of land, coastal provision (nutrient cycling, waves and storms attenuation, sediments bid and biological communities sustain) can become reduced and large-scale ecosystem conversion for agriculture and aquaculture, urban and industrial development, is determining rapid changes in the natural evolution of ecosystems.

At the present it is essential understanding spatiotemporal variations in coastal dynamics in order to assess sources of complexity in ecosystems and in order to make appropriate information of biological and physical process across a wide range of scale.

In example, the problem of indeterminate boundaries has been explored by a number of writers in the description of vegetation communities (Roberts, 1989; Moraczewski, 1993a; Moraczewski, 1993b). If a plant community is defined by the presence of a certain proportion of a plant, then is it reasonable to identify a different community because there is 1% less than that proportion?

Landscape metrics are in widespread use, but previous research has highlighted problems over scale and error in the reliability of the metric values.

A major challenge in coastal management is then determining whether observed changes are natural or they resulted from alteration in external factors (such as climate change and exploitation), exceeding an internal threshold (such as vegetation disappearing or switching to a new location or soil sealing by buildings), or short-term disturbances within natural and atrophic pressures (such as chronic disturbances). Manager and decision makers, stakeholders and general public at the present need to quantitatively understand through the support of environmental and Earth Observation (EO) science, which is the right decision process to minimize risks for population and correctly use natural resources.

This thesis explores the variation of environmental gradients when it is difficult distinguish exactly where one changes into another; when the ecotone is not an abrupt transition it but has a spatial extent in its own right.

RELEVANCE OF THE PRESENT WORK

To rightly assess natural resources conservation and sustainable development strategies the decision process is generally supported by the 'Decision Support Systems (DSSs)' that include spatial data infrastructures and GIS based interface/database. Through tools that allow 'querying' these systems, they can give direct feedback from calculated indicators in terms of tabular and cartographic outputs. These instruments need to be frequently updated with environmental information and new algorithms are needed to ‘translate’ data processing into added biophysical value maps. Many of the recent advances hinge on the ideas that quantitative tools like space-borne data are useful in complex system understanding (Murray et al., 2009).

Remote sensing is a very powerful instrument to link ecological resilience to governance structures, economy and society. New remote sensing sensors are very powerful tools for coastal monitoring and investigation (Brock & Purkis, 2009), since they allow collection of spatially continuous information over vast areas in short time frames. In this view, space helps in responding to the grand challenges on Earth ageing population in Europe and growing population worldwide. It has the capability of supporting climate changes and natural resources monitoring, security, innovation and competitiveness development in landscape observation.

The article n. 189 (2007) of Lisbon treaty cites:

“1. *To promote scientific and technical progress, industrial competitiveness and the implementation of its policies, the Union shall draw up a European space policy. To this end, it may promote joint initiatives, support research and technological development and coordinate the efforts needed for the exploration and exploitation of space.*

2. *To contribute to attaining the objectives referred to in paragraph 1, the European Parliament and the Council, acting in accordance with the ordinary legislative procedure, shall establish the necessary measures, which may take the form of a European space program….*”

Copernicus, previously known as Global Monitoring for Environment and Security (GMES), is the European Programme for the establishment of a European capacity for Earth Observation. The Global Monitoring for Environment and Security mechanism deliver information on security and environment. Copernicus consists of a complex set of systems which collect data from multiple sources: earth observation satellites and in situ sensors such as ground stations, airborne and sea-borne sensors. The European Space Agency is developing five new satellite missions called Sentinels specifically for the operational needs of the Copernicus programme. The Sentinel missions are based on a constellation of two satellites to fulfill revisit and coverage requirements, providing robust datasets from radar and multi-spectral imaging instruments for land, waters and atmospheric monitoring. Moreover from 2014, European satellite navigation system Galileo, born to provide civil positioning system, will provide satellite navigation signals for government uses such as police, military and security services in addition to signals for navigation devices for cars and shipping.

Projects of that sort indeed include space science and exploration, together with the global response to major challenges on Earth such as climate change, the management of the environment and dwindling natural resources, as well as security on Earth.

The space industry helps to improve the performance of the wider industry partly through non-space sectors or space industry leading research organizations and universities.

Beyond all these advances Europe intends to remain a serious global player, in the current space know-how and in future global space initiatives and towards a flagship program, the Horizon 2020 actions in space, European Community will implement space sciences through main pillars based on enabling technologies. We are probably preparing more structured ways of space observations by developing a deeper synergy between ground-based, airborne and space techniques and field data collection.

The space sector has shown an exceptional dynamism, growing in real terms at around 9% a year since 1999, showing also, at national level, spin-offs at almost 5%. The Oxford Economics (2010), using data from 25 European economies and the United States and Canada suggest that such spill-over effects amount to research and technological investment by the aerospace industry generating a social return of around 70%. Also for these reasons major space initiatives are increasingly becoming global endeavors as the costs involved go beyond the resources available to any single nation.

Looking at the extra – European countries, US National Aeronautics and Space Administration (NASA) issues a press release (NASA, 2012) highlighting the development of air- borne sensors for monitoring the Earth system and the potential role of Earth system scientist in studying landscape evolution and bio – hydro - atmosphere interact. The USA National Ecological Observatory Network (NEON) is a bold effort to expand horizons in the science of large-scale ecology. Building on recent progress in many fields of applied ecology and remote sensing application in ecology, NEON's goal is to improve understanding and forecasting of ecological change at continental scales by testing airborne remote sensing technologies (Figure 1.1).

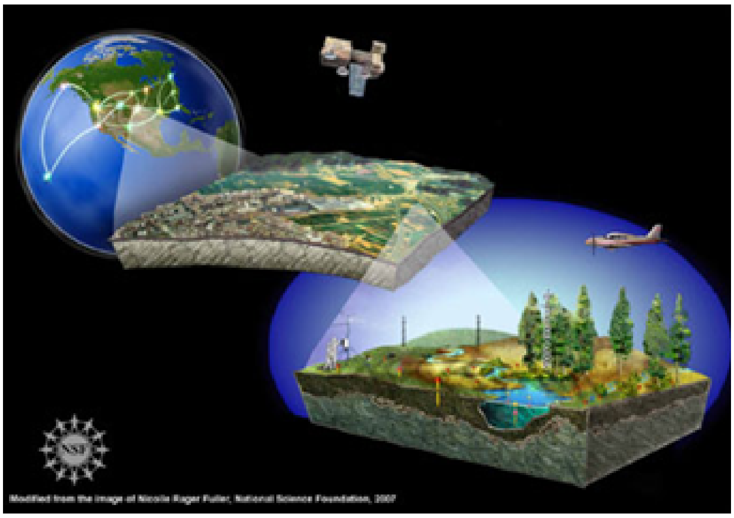

Figure 1.1 - The USA National Ecological Observatory Network (NEON)

If the political and socio economic attention in space technology is worldwide arising, the same is happening all through the environmental sciences because these techniques actually provides the scientific community with extensive dataset to infer earth surface process, landforms and ecosystem functioning.

Airborne remote sensing (Figure 1.2), although often more expensive and with limitation in high frequency acquisition, give much more insights then satellite. It allows a mission to be planned carefully, taking into account all possible constraints. Multi sensor airborne remote sensing provides data sets in environmental sector with maps of habitat heterogeneity (Artigas and Yang, 2005; Pignatti et al., 2009) studies of vegetation cover in wetlands (Barducci et al., 2009), maps of invasive plants distribution (Lawrence et al., 2006; Tsai et al., 2007), and species composition (Boschetti et al., 2007; Calvo et al., 2003; Giardino et al., 2009; Marani et al., 2006). Mumby and Edwards (2002) assessed maps of spatial vegetation composition in shallow waters and they provide unique constraints on different depositional processes, as well as on mechanisms by which vegetation properties controls ecosystem dynamics.

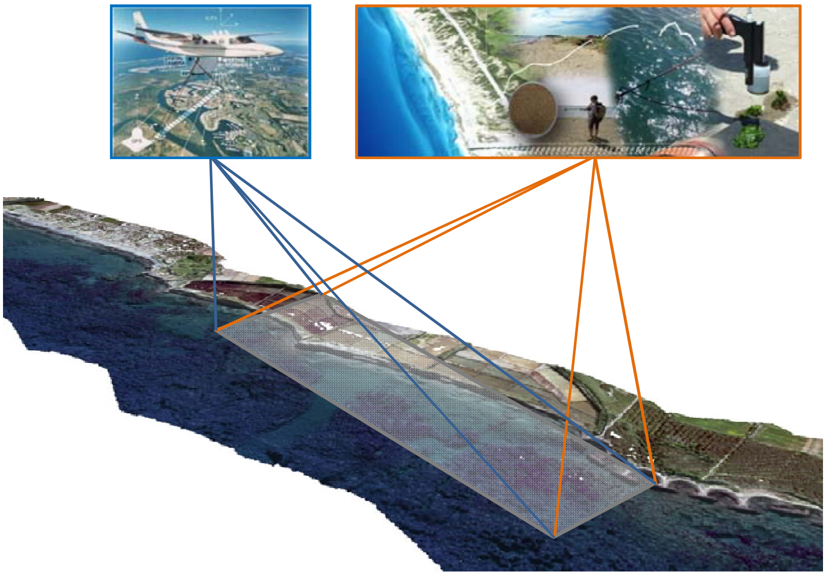

Figure 1.2 - Schematic representation of airborne and field measurements along the coastline. The coastal image is obtained by the 3d LiDAR bathymetry and MIVIS hyperspectral image.

Moreover, the technique is not hampered by the (in) accessibility of a site, which is often a problem in coastal areas. The knowledge of near-coast characteristics against coastal erosion are in fact, achieved covering large surfaces in a short time in order to study vegetation patterns and morphology along coastal zones (Deronde et al., 2006; Taramelli et al., 2011).

The principle of airborne 'hyperspectral' remote sensing is based on spectroscopy. From an aircraft a location reflects and absorbs sun light in different spectral bands in such a manner that for each pixel a quasi-continuous (depending on the number of bands) reflectance spectrum is obtained (Figure 1.3). The reflected radiance measured by the sensor is converted to reflectance values which are defined as the ratio of the intensity of the reflected light to the intensity of the incoming light in function of the wavelength. High spectral and spatial resolution images acquired with airborne hyperspectral sensors offer the opportunity to map environmental feature in great detail. Among these, presence/absence and structure of vegetation represent important indicators from optical remote sensing because of their interaction with sun light for photosynthesis.

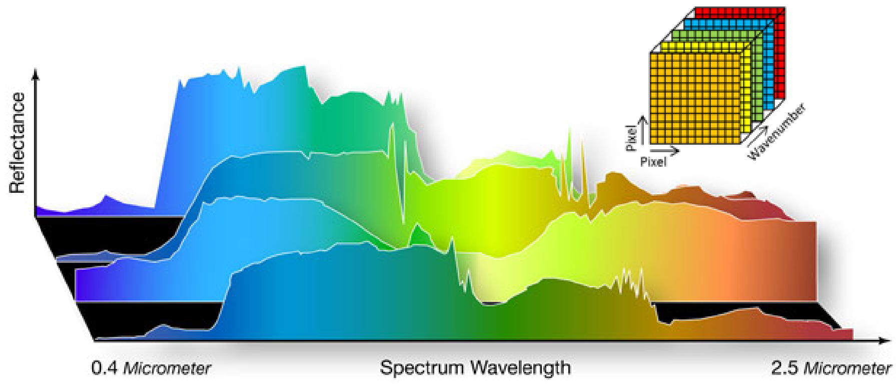

Figure 1.3 - Example of vegetation (the first and the last) and substrate (the central two) reflectance profiles. Hyperspectral pixel is schematized in a 3D view.

Hyperspectral remote sensing has been used to make large-scale inventories of vegetation cover, macrophytes and sea grasses distribution and corals (Pinnel., 2007). Retrieval methods may involve classification techniques (Reguzzoni et al., 2003), decision tree classifier (Bresciani et al., 2010) and semi-analytical bio-optical modeling (Giardino et al., 2007), the latter is able to simultaneously derive a number of water quality components (e.g., chlorophyll-a concentrations) beside bottom albedo and bottom depth (Brando et al., 2009; Lee et al., 2001). These parameters are important for identifying feeding areas, for evaluation of erosion/deposition processes function of the system exposure, for advancement/retreat monitoring of the coastline on the properties and for vegetation on both emerged and submerged areas (Valentini et al., 2012).

The green part of the solar spectrum is less absorbed causing plants to exhibit a green color. Because different plant species have different leaf pigments, internal cell structure and moisture content, they reflect light in a different way (Han & Rundquist, 2003; Lee & Carder, 2004).

The differences between the reflectance in the visible (VIS) and the reflectance in the near infrared (NIR) part of the spectrum is used to distinguish between vegetation types. Typical spectral response characteristic of green plants are strong increased reflectance of the NIR which appears around 0.69 μm. This is the so called red-edge (Zarco-Tejada, & Miller, 1999). The absorption of the near infrared part of the spectrum is due to the leaf cell internal structure and reflectance features are defined by position and slope of the red-edge. By measuring the amount of absorption due to pigments at lower wavelength and the amount of reflection at the green peaks against the red plateau reflectance values, clustering of species is possible.

Shallow seabed habitat mapping and geomorphology by airborne remote sensing has been applied successfully in optically clear shallow waters and by multisensory analysis (Dekker et al., 2005; Phinn et al., 2005, 2008) with a special focus in coral reef communities identification (Kutser & Jupp, 2006a). Less effort has been devoted to sedimentary seabed mapping and very few studies involve benthic seaweeds identification (Wittlinger & Zimmerman, 2000) from remote sensing. Forms, biomass, phenology, composition and vegetation cover percent are generally quantified with good accuracy in the emerged environment, while the quantification in underwater environment is complicated by the physical effect of the sea waters (Silva et al, 2008).

In this study a physic-based approach was applied to Multi-spectral IR and Visible Imaging Spectrometer (MIVIS) data. The main methodology is the Spectral Mixture Analysis (SMA). It is based on a physical representation of spectrally mixed pixels as areal fractions of spectral endmembers. SMA simulates the physical process of mixed radiance measurement in the IFOV with a linear mixture model. Inverting the linear mixture model yields quantitative estimates of the areal abundance (fractions) of specific targets (endmembers) within each pixel (Adams et al., 1986, 1993; Gillespie et al., 1990; Settle & Drake, 1993; Smith et al., 1990).

By representing each pixel as a combination of spectrally pure endmembers, the resulting fraction images provide continuous field representations of the spectrally heterogeneous gradations that characterize the Earth surface (Figure 1.4). In applications where discrete thematic classes are required, endmember fraction maps can be ‘‘hardened’’ to provide a more consistent definition of themes than is provided by statistical classification methods (Adams et al., 1995; Ustin, 2004).

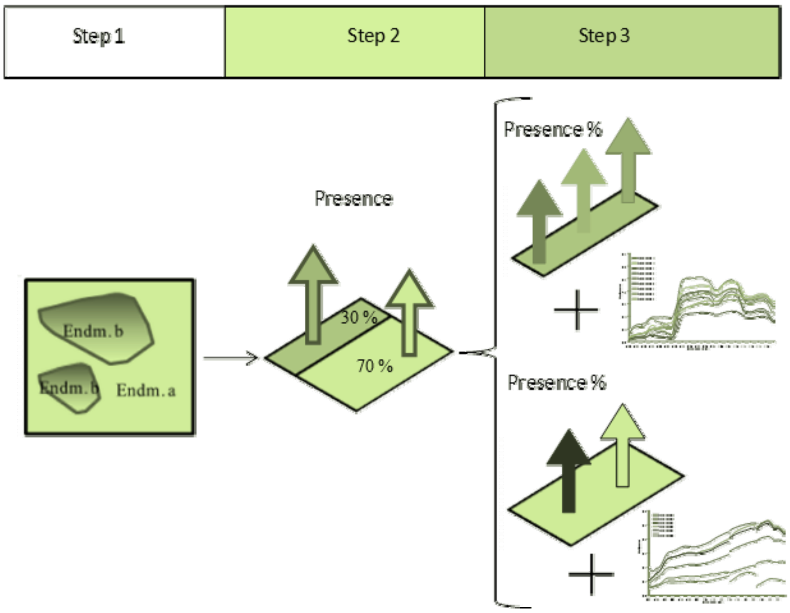

Figure 1.4 - Spectral mixture analysis is represented applied to each pixel. A step by step spectral analysis allows the dissection of spectral gradients into discrete classes. Endmember are collected from principal component analysis and then fraction maps are combined to obtain thresholds. Field spectral measurements can enhance the classification sub pixel analysis.

Moving from empirical analysis of field and image spectra on the base of decision tree, data can be translated into combined biophysical maps of land cover and benthic vegetation. Moreover by implementing geomorphic analysis, a useful contribute is obtained by combining hyperspectral data with active sensors able to provides accurate Digital Terrain Models (DTMs), or surface models (DSMs) of nearshore coastal areas (Pallottini et al., 2010). In recent years for the construction of DSM and DTM, on a wide scale range regardless of the site characteristics, laser altimetry technology is spreading through the use of LIDAR airborne sensors (Deronde et al., 2006). This approach provides 3D digital representations (point clouds) of extremely wide surfaces (from squared km to hundreds of squared km), with high density (cm-m) and high accuracy (cm-dm), solving large part of the above critical states for direct in situ measurement, mostly in areas where the access is difficult with traditional technologies (i.e. shallower bathymetries shrub lands and wetlands). However, the high costs of LIDAR flights instrument, can significantly affect the planning of acquisitions with high temporal frequency (Brock & Purkis, 2009) reducing the possibility to investigate on temporal evolution of coastal processes at seasonal scale. As a consequence, determination of feedback mechanisms between ecology and geomorphology can be compromised and their impact cannot be quantified.

AIMS

In this thesis by combining field radiometry with contemporary airborne hyperspectral imagery and LiDAR altimetry an innovative approach with the application of Spectral Mixture Analysis (SMA) is proposed in order to define shallow seabed properties, freshwaters macrophytes presence and dune habitat at the finest scale. The implemented FHyL (Field spectral libraries, airborne Hyperspectral imagery and LiDAR altimetry) processing chain leads to an innovative mapping results obtained by an integration of multisensory data. Presence and typology of vegetated and not vegetated coast (both emerged and shallow submerged) is represented as the abundance of each physical response within the hyperspectral reflectance by building multisensory and multidimensional hyperspectral - LiDAR mixture space. FHyL represents a way to classify and map vegetation presence and distribution, as well as ecology and geomorphology of shallow habitat and beaches dunes systems.

The present research is a novel input for spatial and temporal analysis in biophysical studies, modeling and monitoring.

CASE STUDY 1: Complex coastal seabed: Tarquinia (VT)

The considered coastal ecosystem is very complex from the ecological and geomorphological point of view. The inner part of the continental platform, where the submerged beach is characterized by continuous low slope in the nearshore seabed and by the presence of seagrass, hosts a series of bedrock outcrops and sandy channel network connected to the coastal basin. The presence, fragmentation and state of regression of seagrass meadows, reflect the health of the coast and endemic species such *Posidonia oceanica*, are considered main indicators of coastal status. Upper limit of seagrass appears at shallower bathymetries in the area of Tarquinia Lido (about 3-4 m).

By a redistribution of the material deposited on the beach after the Saline enlargement that area is considered at risk of erosive trend particularly intense at the salt work and in the immediately Northern area at the mouth of Marta river. Beach dune nourishment and defense structure lead to a progressive change of the shallower near shore seabed habitat and the available approach in coastal management reveal the importance of the sedimentary balance and losses of sediments between 4-5000 m^3/year/km of coastline in the physiographic unit. In this context seagrass represent a major driver of sedimentary process and the evolving composition of vegetated seabed can reveal retreating and fragmentation.

General public and local stakeholders are now conscious of the importance of these coastal marine ecosystems and a conservation process that involve universities and public institution has been implemented.

CASE STUDY 2: Coastal beach dune system: Sabaudia (LT)

For the purposes of proper management and planning and in accordance with the principles of Integrated Coastal Zone Management (ICZM) the coastal system studied and analyzed in its ecological and geomorphologic dynamics represent an important natural barrier from meteomarine pressure as well as a source of sediment and recreation. Therefore, it is necessary to identify parameters as expression of health/vulnerability status of to develop indicators of changes.

The dune system parallel to the coastline, related to sand bar is the result of increasing sea level action and increasing importance over time of the winds. Both the proportion and amplitude of these "convex system" increase from north to south and are mostly established by specialized coastal vegetation, typical of the Mediterranean. This dune cord lives on the base of the interaction between aeolian transport and vegetation root that stabilize the sands through specialized root systems triggering positive feedback mechanisms between the biological communities and sediments (i.e. deposition of particles on vegetated areas), giving dynamic stability and resilience to the system exposed to natural and manmade disturbances.

In the 50's the dynamics of the system, orthogonal to the shoreline, was blocked by the construction of the coastal road at its dune crest longitudinal axis. Then runoff phenomena triggered the development and enlargement of blowouts. In addition, the erosive wave action increased erosion at the base of the dune. In the late 80s, the central part of the area has been seriously damaged by a storm event, and as a result has not been opened to traffic. In that part of the dunes, a series of remedial and preservation of the beach-dune system has been tested in the last 20 years. More recently, an important structure, orthogonal to the shore line, linked to the Nuclear Power Station located in the northern part of the system has been removed. As a consequence, a significant volume of sedimentis now drifted southward by long shore currents, providing a sediment input to the system that, in near future, should nourish the emerged beach.

CASE STUDY 3: The shallow muddy lake: Trasimeno (PG)

Lake Trasimeno is located in central Italy and, despite its extension it is very shallow and smooth in slope. Its hydrological regime depends strictly on the local climate. In general, the high concentration of phytoplankton contributes to the turbidity due to the lake bed, making lake's waters unclear (average depth of the Secchi disc depth 1 m). Macrophytes characterize this ecosystem, indicating prerequisite conditions of soils and hydrology. Macrophytes are an essential part of the productive zone in the Trasimeno Lake and, by equilibrium with algal growth they contribute to the uptake of nutrients and pollutants, determining bottom quality, composition and stability and providing structural, food, shelter and breeding habitats for aquatic communities. Reeds and macrophytes respectively, are representative of Trasimeno coastal vegetation mostly abundant in the eastern part of the basin.

The low water levels, strictly influenced by seasonal rain, the nutrient loads from agriculture and livestock, civilian's discharges, tourism activities contribute to the process of eutrophication of the lake's waters. Decreasing of both biodiversity of the fish fauna, invasive species and vegetation distribution from land to lake bed, cause continuous changes in bathymetries. Important supports in lake management are bathymetric dataset to monitor evolution of accretion/erosion. These data are very difficult to obtain because of the environmental impediments. For these areas, vegetation maps coupled with bathymetries can provide biophysical indicators and represent an adjunct values to monitor summer blooms and reeds retreating towards the shore face.

REFERENCES

1. Adams J. B., M. O. Smith & P. E. Johnson, 1986. Spectral mixture modeling; A new analysis of rock and soil types at the Viking Lander 1 site, *Journal of Geophysical Research*, 91, 8098-8122.

2. Adams, J.B., M.O. Smith & A.R. Gillespie, 1993. Imaging Spectroscopy: Interpretation based on spectral mixture analysis, in Remote Geochemical Analysis: *Elemental and Mineralogical Composition*, edited by C.M. Pieters, and P. Englert, pp. 145-166, Cambridge University Press, New York.

3. Adams J. B., Sabol, D. E., Kapos, V., Almeida Filho, R., Roberts, D. A., Smith, M. O., & Gillespie, A. R. (1995). Classification of multispectral images based on fractions of endmembers: Application to land-cover change in the Brazilian Amazon. *Remote Sensing of Environment*, *52*(2), 137-154.

4. Artigas F & Yang J. 2005. Hyperspectral remote sensing of marsh species and plant vigour gradient in the New Jersey Meadowlands. *International Journal of Remote Sensing*. 26: 5209–5220.

5. Barducci, A., Guzzi, D., Marcoionni, P., & Pippi, I. (2009). Aerospace wetland monitoring by hyperspectral imaging sensors: A case study in the coastal zone of San Rossore Natural Park. *Journal of environmental management*, 90(7), 2278-2286.

6. Boschetti M, Boschetti L, Oliveri S, Casati L & Canova I. 2007. Tree species mapping with Airborne hyper-spectral MIVIS data: the Ticino Park study case. *International Journal of Remote Sensing* 28: 1251–1261.

7. Brando, V.E., Anstee, J.M., Wettle M., Dekker A.G., Phinn S.R., & Roelfsema, C. (2009). A physics based retrieval and quality assessment of bathymetry from suboptimal hyperspectral data, Rem. Sens. of Environ., 113, 775-770.

8. Bresciani M., Giardino C., Musanti M., Martinelli A., Taramelli A., & Valentini, E. (2010). Mappatura delle macrofite del lago Trasimeno tramite tecniche di telerilevamento. Special Issue Conference SITE, Bolzano 2009.

9. Brock, J. C., & Purkis, S. J. (2009). The emerging role of lidar remote sensing in coastal research and resource management. *Journal of Coastal Research*, 1-5.

10. Calvo S, Ciraolo G, La Loggia G. 2003. Monitoring *Posidonia oceanica* meadows in a Mediterranean coastal lagoon (Stagnone, Italy) by means of neural network and ISODATA classification methods. *International Journal of Remote Sensing* 24 : 2703–2716.

11. Corenblit D., Baas A. C., Bornette G., Darrozes J., Delmotte S., Francis R. A., ... & Steiger J. (2011). Feedbacks between geomorphology and biota controlling Earth surface processes and landforms: A review of foundation concepts and current understandings. *Earth-Science Reviews*, *106*(3), 307-331.

12. Costanza R., d'Arge R., De Groot R., Farber S., Grasso M., Hannon B., ... & Van den Belt M. (1997). The value of the world's ecosystem services and natural capital. *Nature*, *387*(6630), 253-260.

13. Davidson-Arnott RGD., MacQuarrie K, Aagaard T. 2005. The effect of wind gusts, moisture content and fetch length on sand transport on a beach. *Geomorphology* 68 : 115–129.

14. Dekker A.G., Brando V.E., & Anstee J.M. (2005). Retrospective seagrass change detection in a shallow coastal tidal Australian lake. *Remote Sensing of Environment*, 97, 415-433.

15. Deronde B., Houthuys R., Debruyn W., Fransaer D., Lancker V. V., & Henriet, J. P. (2006). Use of airborne hyperspectral data and laserscan data to study beach morphodynamics along the Belgian coast. *Journal of coastal research*, 1108-1117.

16. Giardino C., Bartoli M., Candiani G., Bresciani M., & Pellegrini L. (2007). Recent changes in macrophyte colonisation patterns: an imaging spectrometry-based evaluation of southern Lake Garda (northern Italy). *J. of App. Rem. Sens*., (SPIE), **1**, 011509.

17. Gillespie A., Smith J., Adarns M. & Willis S., 1990. Spectral mixture analysis of multispectral thermal infrared images, Proc. 2nd Thermal IR MUltispectral Scanner (TIMS) Workshop, JPL Publ. 90-33, pp. 57-74.

18. Han L., & Rundquist D. C. (2003). The spectral responses of Ceratophyllum demersum at varying depths in an experimental tank. *International Journal of Remote Sensing*, 24(4), 859-864.

19. Haussmann N. S. (2011). Biogeomorphology: understanding different research approaches. *Earth Surface Processes and Landforms,* 36 (1), 136-138.
20. Kutser T., & Jupp T. L. B. (2006a). On the possibility of mapping to the species level based on their optical signature. *Estuarine and Coastal Shelf Science*, 69, 607-614.
21. Kutser T., Vahtmae E., & Metsamaa, L. (2006b). Spectral library of macroalgae and benthic substrates in Estonian coastal waters. *Proceedings of the Estonian Academy of Sciences*, 55: 329-340.
22. Lawrence RL, Wood SD, Sheley RL. 2006. Mapping invasive plants using hyperspectral imagery and Breiman Cutler classifications (RandomForest). *Remote Sensing of Environment* 100: 356–362.
23. Lee Z., Carder K.L., Chen R.F. & Peacock, T.G. (2001). Properties of the water column and bottom derived from Airborne Visible Infrared Imaging Specrometer (AVIRIS) data. *J. Geophys. Res.,* **106**, 11,639-11,651.
24. Lee Z. & Carder K. L. (2004). Absorption spectrum of phytoplankton pigments derived from hyperspectral remote-sensing reflectance. *Remote Sensing of Environment*, 89, 361-368.
25. Marani M, Belluco E, Ferrari S, Silvestri S, D'Alpaos A, Lanzoni, S, Feola, A, Rinaldo, A. (20069. Analysis, synthesis and modelling of high-resolution observations of salt-marsh ecogeomorphological patterns in the Venice lagoon. *Estuarine, Coastal and Shelf Science* **69**: 414-426, doi:10.1016/j.ecss.2006.05.021.
26. Moraczewski I.R. (1993a). Fuzzy logic for phytosociology. Generalizations and prediction. Vegetation 106: (13–20.
27. Moraczewski I.R. (1993b). Fuzzy logic for phytosociology 1 Syntaxa as vague concepts. Vegetation 106: 1–1.
28. Mumby PJ, Edwards AJ. 2002. Mapping marine environments with IKONOS imagery-Enhanced spatial resolution can deliver greater thematic accuracy. *Remote Sensing of Environment* 82: 248–257.
29. MurrayA. B., LazarusE., Ashton A., Baas A., Coco G., Coulthard T., ... & Reinhardt, L. (2009). Geomorphology, complexity, and the emerging science of the Earth's surface. *Geomorphology*, *103*(3), 496-505.
30. Phinn S., Dekker A. G., Brando V. E. & Roelfsema, C. (2005). Mapping water quality and substrate cover in optically complex coastal and reef waters: an integrated approach. *Marine Pollution Bulletin*, 51(1-4), 459–469.
31. Phinn S., Roelfsema C., Dekker A., Brando V. &Anstee J. (2008). Mapping seagrass species, cover and biomass in shallow waters: An assessment of satellite multi-spectral and airborne hyper-spectral imaging systems in Moreton Bay (Australia). *Remote Sensing of Environment*, 112, 3413–3425.
32. Pinnel, N. (2007). A method for mapping submerged macrophytes in lakes using hyperspectral remote sensing. Ph.D. Thesis, Department für Ökologie und Ökosystemmanagement, Fachbereich für Limnologie, Technische Universität München, Germany (2007).
33. Reguzzoni M., Sansò F., Venuti G., & Brivio P.A. (2003). Bayesian classification by data augmentation. *Int. J. Rem. Sens*. **24**, 3961-3981.
34. Pignatti S., Cavalli R.M., Cuomo V., Fusilli L., Pascucci S., Poscolieri M., Santini F. 2009. Evaluating Hyperion capability for land cover mapping in a fragmented ecosystem: Pollino National Park, Italy. *Remote Sensing of Environment* 113: 622–634.
35. Regnauld H., Pirazzoli P. A., Morvan G., & Ruz M. (2004). Impacts of storms and evolution of the coastline in western France. *Marine geology*, *210*(1), 325-337.
36. Reinhardt L., Jerolmack D., Cardinale B. J., Vanacker V., & Wright J. (2010). Dynamic interactions of life and its landscape: feedbacks at the interface of geomorphology and ecology. *Earth Surface Processes and Landforms*, *35*(1), 78-101.
37. Risser P. G. (1995). The status of the science examining ecotones. *BioScience*, 318-325.
38. Roberts D.W. 1989. Fuzzy systems vegetation theory. Vegetatio 83:71–80.
39. Roughgarden J., Running S. W. & Matson P. A. (1991). What Does Remote Sensing Do For Ecology? *Ecology* 72:1918–1922. http://dx.doi.org/10.2307/1941546.
40. Settle J. J., & Drake N. A. (1993). Linear mixing and the estimation of ground cover

proportions. *International Journal of Remote Sensing*, *14*(6), 1159-1177.
41. Silva T. S., Costa M. P., Melack J. M., & Novo E. M. (2008). Remote sensing of aquatic vegetation: theory and applications. *Environmental Monitoring and Assessment*, 140, 131–145.
42. Small C, Steckler M, Seeber L, Akhter SH, Goodbred Jr S, Mia B, Imam B. (2009). Spectroscopy of sediments in the Ganges-Brahmaputra delta: Spectral effects of moisture, grain size and lithology. Remote Sensing of Environment 113: 342–361.
43. Small C. & Lu J., W., T., 2006. Estimation and vicarious validation of urban vegetation abundance by spectral mixture analysis. Remote sensing of environment 100: 441–456.
44. Small C. 2004. The Landsat ETM+ spectral mixing space. Remote Sensing of Environment 93: 1–17.
45. Small C. 2009. The Color of Cities. In Global mapping of human settlement: experiences, datasets, and prospects. CRC Press; 59–106.
46. Small C., & Nicholls R. J. (2003). A global analysis of human settlement in coastal zones. *Journal of Coastal Research*, 584-599.
47. Smith M. O., Ustin S. L., Adams J. B., & Gillespie A. R. (1990). Vegetation in deserts: I. A regional measure of abundance from multispectral images. *Remote sensing of Environment*, 31(1), 1-2.
48. Taramelli A. (2011). Detecting Landforms Using Quantitative Radar Roughness Characterization and Spectral Mixing Analysis. *Geocomputation, Sustainability and Environmental Planning*, 348, 225-249.
49. Tsai F, Lin EK, Yoshino K. (2007). Spectrally segmented principal component analysis of hyperspectral imagery for mapping invasive plant species. *International Journal of Remote Sensing* 28: 1023–1039.
50. Ustin S. L., Roberts D. A., Gamon J. A., Asner G. P., & Green R. O. (2004). Using imaging spectroscopy to study ecosystem processes and properties. *BioScience*, *54*(6), 523-534.
51. Valentini E., Taramelli A., Bresciani M., Giardino C., Filipponi F., Targusi M., Manzo C., & Disperati L. (2012). Spectral libraries for emerged and submerged sandy beach using hyperspectral data. ESA – Ecological Society of America, 97th Annual Meeting Book of Abstracts and Poster session 2012, http://cdn.f1000.com/posters/docs/251665544.
52. Valiela I. (2006). *Global coastal change*. Blackwell Pub.
53. Viles H. A., et al. (2008). "Biogeomorphological disturbance regimes: progress in linking ecological and geomorphological systems." *Earth Surface Processes and Landforms* 33(9): 1419-1435.
54. Wittlinger, S. K., & Zimmerman, R. C. (2000). Hyperspectral remote sensing of subtidal macroalgal assemblages in optically shallow waters. *Proc. Ocean Optics* XV. SDROM.
55. Zarco-Tejada P. J., & Miller J. R. (1999). Land cover mapping at BOREAS using red edge spectral parameters from CASI imagery. *Journal of Geophysical Research*, *104*(D22), 27921-27933.
56. Zhou D. M., Gong H. L., Hu J. M., & Wu F. L. (2006). Application of satellite remote sensing technology to wetland research. *Remote sensing technology and application*, *21*(6), 577-583.

2. FHyL: Field Spectral Libraries, Airborne Hyperspectral Images and Topographic and Bathymetric LiDAR Data for Complex Coastal Mapping

Andrea Taramelli[1], Emiliana Valentini[1], Carlo Innocenti[1], Sergio Cappucci[2],

[1] ISPRA – Institute for Environmental Protection and Research – Rome

[2] ENEA - Italian Agency for New Technology, Energy and Environment - Rome

Remote sensing of coastal ecosystems provides fundamental information for the effective assessment of valuable natural habitat. A synoptic view of the shallow submerged and emerged coastal landscape can offer the quantitative ability to obtain spatially explicit data over large and complex areas, where the heterogeneity of habitat is mixed by vegetation and sediment interactions at the interface between seabed and beach dune system. In the present paper, by combining field radiometry with contemporary airborne hyperspectral imagery and topographic and bathymetric LiDAR data an innovative approach with the application of Spectral Mixture Analysis (SMA) and Multiple Linear Regression models is proposed in order to define shallow coastal seabed, beach and dune habitat at the finest scale. The implemented FHyL (Field spectral libraries, airborne Hyperspectral imagery and LiDAR altimetry) processing chain leads to an innovative mapping results obtained by an integration of multisensory data. Presence and typology of vegetated and not vegetated beach is represented as the abundance of each physical response within the hyperspectral reflectance by building multisensory and multidimensional hyperspectral - LiDAR mixture space. An accurate estimation of the mineralogical and grain size proprieties of the beach sediment was finally achieved, using field and airborne spectral libraries combined with sediment sampling in a multiple linear regression statistical model.

Therefore, FHyL represents the multisensory data fusion process to classify and map vegetation presence and distribution, as well as sediment properties and geomorphology of complex coastal seabed, and beaches dunes systems. The present research is a novel input for multilayered and multi temporal analysis in biophysical studies and modeling of coast evolution.

2.1 METHODOLOGY

Two airborne surveys with MIVIS hyperspectral and LiDAR Hawkeye II sensors, during the spring 2009 and 2010 provided the hyperspectral, topographic and bathymetric dataset. Several field surveys were carried out during the airborne acquisitions providing spectral data for enhancement and validation of remote records. A modular approach has been used to develop the FHyL processing chain (Figure 1). FHyL consists of four main modules and two preprocessing steps: each module differs for the analyzed environment (emerged and submerged) and for the approach in the sensors integration (Hyperspectral, LiDAR and Field); in the two preprocessing steps, one for each sensor, the data is prepared for main analysis.

2.1.1 PREPROCESSING STEPS

The geometrically calibrated hyperspectral dataset was corrected for atmospheric influence using ATCOR4, based on the radiometric transfer model MODTRAN4 (and implemented by Schläpfer Applications) and is designed for the atmospheric correction of remotely sensed data acquired from aerial platform that suffer from distortions. All the analyses started with the definition of the Region of Interests (ROIs). Baseline MIVIS imagery required the gradual generation of masks to reduce the extent of image itself and to define the best subsets for the final habitat processing (seabed and dunes). Picking MIVIS thermal bands it was possible to define a threshold temperature value, to mask emerged and submerged areas on an empirical basis supported by field validation measurements. MIVIS and LiDAR were coupled by interpolating the filtered LiDAR point cloud on a raster with the same extent of the MIVIS one (with 3x3 m cells) and layer stacked as a new band. Field Spectral Libraries were resampled on MIVIS bands spectral resolution so that the data were comparable. For collected sediment samples, the results of mineralogical and grain size analysis, the resampled field spectral measures and MIVIS spectral measures were linked by means of spatial coordinate.

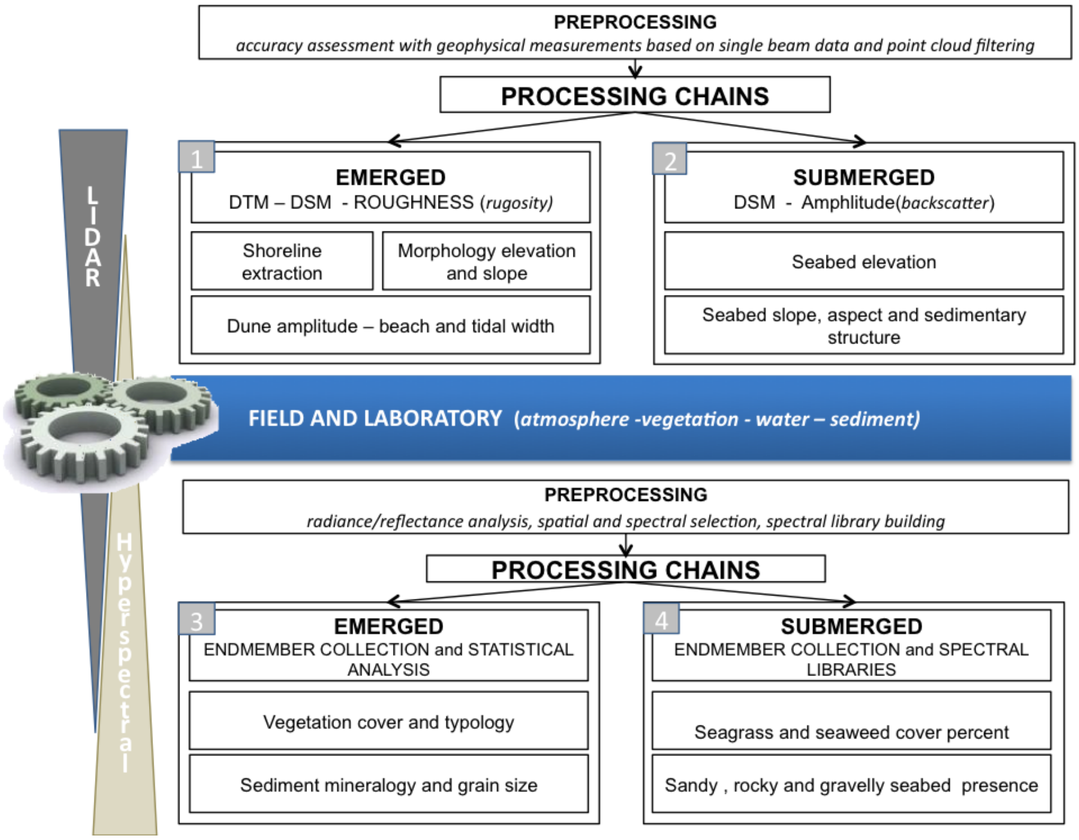

Figure 2.1 -– FHyL processing modules

2.1.2 MODULE 1 – LIDAR-MIVIS EMERGED

The analysis of the LiDAR elevation data allowed a complete morphological characterization of the emerged beach and dune environments and leads to obtain results such as accurate shoreline position, DSM, dune amplitude and elevation, slope, dune foot and the inner edge. In this case the evaluation of vegetation indexes was used to get a synoptic view of biomass distribution of vegetation on coastal dunes that supported accurate foot and inner edges extraction and the discussion of the preliminary definition of beach-dunes polygons.

2.1.3 MODULE 2 – LIDAR-MIVIS SUBMERGED

By calculating the standard deviation of the LiDAR point cloud on a 4 x 4 m grid, we observed and classified seafloor topography and rugosity Consolidated and unconsolidated seabed was then classified on the base of an accurate interpretation. By the application of morphometric slope and curvature parameters the sand bars and complex sedimentary structure were analyzed. Size, orientation and asymmetry of several bedforms observed in shallow water were described and correlated to longshore current, waves and wind regime to better understand their formation and evolutionary trend. Then, selecting the hyperspectral subset for submerged environment the analysis of sandy bars and the definition of different sectors along the coastal stretch was enhanced by introducing combined indexes of spectral bands or band ratios and parameters such as sandy bar order, extent and their relation to emerged landscape.

2.1.4 MODULE 3 – MIVIS-LIDAR EMERGED

Beach and dune polygons, obtained on the base of module 1 were used to define two sets of ROI, one for the dune cords and one for the near shore emerged beach. For dune cords multisensory mixing space has been generated on the base of PC rotation scatterplots (0,43 - 1,55 µm). The PCA multidimensional space identified for each dune polygon quotes of the scatter plots on the base of the first two or more dimensions as pure pixels. Two, three and four pure pixels were selected for vegetation, sands and eventually atrophic structures (EM) and used as training sets for running the maximum likelihood classification for vegetation presence and absence. Then by considering dune geomorphologies and the spectral profiles enhanced the habitat classification (trees, shrub and grasses).

On the beach subset, multitemporal and distributed sediment samplings were collected during the first MIVIS acquisition. The sampling data were pre-processed as described above, and an algorithm to find and test all the possible multiple linear regression models between sedimentological characteristics and spectral properties was implemented. As result for the mean phi, and for each of the principal mineralogical phases present on the beach (quartz, calcite, albite, sanidine and pyroxene) two multiple linear regression model were developed one using the band values extracted from the

MIVIS (using just the range 0,46 - 2,5 μm), and one using the band values obtained by the field spectral measurements and resample on the MIVIS's ones. The first method doesn't need field spectral data, but is applicable only if sampling is contemporary with MIVIS acquisition, the second one permit to use not contemporary sampling for the model calibration.

2.1.5 MODULE 4 – MIVIS-LIDAR SUBMERGED

A high-resolution airborne sensor spectral data in combination with innovative assimilation from field radiometric observation and from LiDAR bathymetry develops a multidimensional and multisensory mixture space. The processing chain starts by integrating morphologies into the hyperspectral mixing space (0,43 – 0,72 μm) and then the EM collection from image is used to achieve an image based linear mixture model of fraction that describes the composition of each mixed pixel. With a spectral resampling of Field Spectral Library on MIVIS hyperspectral bands, single and multiple spectral signal enhanced the image based EM collection in order to obtain different mixing of fraction maps. The endmembers were evaluated against the consistency in the topology of the multisensory mixture space and the spectral separation between cover typologies and water absorption was observed and analyzed. Field surveys and video shot validated the final decision tree classification where fraction maps are considered predictor variables whereas the classes to be mapped (habitat) are referred to the target variables properties by expert based rules.

2.2 RESULTS

The objective of the FHyL analysis is to provide a baseline to assess cover properties for mapping near shore regions by vegetation and sediment description.

Biophysical maps are obtained with 4x4 m resolution. Vegetation composition and distribution is grouped in different classes, 2 for seabed (0 -6 m of depth) and 3 for dunes (1-30 m of height). For the emerged area, an accurate grain size and mineralogical sediment features estimation permitted to appreciate variation occurring at both large scale (along the entire stretch of coast) and micro scale (few meters). Two different regression models were tested for sedimentological feature estimation: the first uses MIVIS data and is applicable to contemporary sampling; the second uses auxiliary field spec measures and don't need contemporary sampling. The spectral library introduced in the linear mixture model for SMA both lowered the reflectance and enhanced the variety of vegetated and not vegetated seabed leading to a magnification of results. Meanwhile, in the emerged AOIs the spectral library introduced in the linear mixture model allowed to clearly distinguish spectral properties of vegetation communities and part of the moisture contribution within the beach areas. The present research suggest that morphology is the driving factor for: (1) vegetated habitat classification; (2) hyperspectral image content enhancement; (3) the implemented final maps contributes to the knowledge of relationships between seabed and (4) seawaters mixed absorption as well as between sediment and vegetation interaction.

The strategy of combining high and very high resolution spectral measurements in a multisensory and multi resolution analysis includes different way of data fusion to assimilate spectral and spatial variability in complex coastal mapping.

3. FHyL: Field spectral libraries, airborne Hyperspectral images and LiDAR altimetry for complex coastal seabed mapping

Emiliana Valentini[1] & Andrea Taramelli[1], Carlo Innocenti[1]

ISPRA – Institute for Environmental Protection and Research – Rome

ABSTRACT

Remote sensing of coastal ecosystems provides fundamental information for the effective assessment of valuable natural habitat. A synoptic view of the shallow coastal seascape can offer the quantitative ability to obtain spatially explicit data over complex areas, where the heterogeneity of habitat is mixed by vegetation and sediment interactions at the interface between seabed and seawaters. In this paper by combining field radiometry with contemporary airborne hyperspectral imagery and LiDAR altimetry acquisition, an innovative approach with the application of Spectral Mixture Analysis (SMA) is proposed in order to define shallow coastal seabed habitat at the finest scale. The implemented FHyL (Field spectral libraries, airborne Hyperspectral imagery and LiDAR altimetry) processing chain leads to an innovative mapping results obtained by an integration of multisensory data. By building a multisensory hyperspectral - Lidar mixture space, the presence of covered and uncovered seabed is represented as the abundance of each physical response within the hyperspectral reflectance. The introduction of field spectral libraries into the linear mixture model improved the classification representing the ecological spectral variability into discrete seabed habitat classes. Through the FHyL implementation using visible and near infrared wavelength finally highlighted how biophysical properties recorded by spectral signatures are distributed in presence and absence of seawaters. FHyL represents the multisensory and multispectral linear mixture model to classify seabed benthic habitat by vegetation presence, composition and abundance and by geomorphic features. The present research is a novel input for multilayered and multi temporal analysis in biophysical coastal studies and modeling.

Key worlds: FHyL, seagrass, seaweeds, hyperspectral, spectral libraries, SMA, LiDAR.

3.1 INTRODUCTION

Seascape areas are valuable environments where various habitats are each other linked by complex spatial interaction. In this interaction benthic vegetation contributes to the morphology of seabed with primary producers such as seagrasses and seaweeds that play a central role in many process of coastal ecosystems (Augier, 1986; Pergent-Martini et al., 2005; Fornes et al., 2006), stabilizing unconsolidated sediments by deposition (Cappucci et al., 2004, Friend et al., 2003), attenuating currents and wave energy and offering a productive environment to rich community of secondary producers (Basterretxea et al., 2004). The presence, fragmentation or state of regression of seagrass meadows in Mediterranean seas reflect the health status of the coast and endemic species such as the *P. oceanica,* are considered one of the main indicator of coastal status. In this context the characterization of habitat and studies of ecological properties and patterns (Fraschetti et al, 2005; Underwood et al., 2005) are focused on a wide range of spatial scale (Keitt & Urban, 2005) in a wide range of ecological application.

Remote sensing from satellites and aircraft has, over the past 30 years, revolutionized studies of the Earth's surface ecology and geomorphology (Cohen & Goward, 2004; Hurtt et al., 2003; Sellers et al., 1995) offering the possibility of modeling biological and morphological complexities at fine scale and at the shallowest bathymetries (Richardson L. & LeDrew E., 2006). Mapping shallow seabed habitat and geomorphologies by airborne remote sensing has been applied successfully in optically clear shallow waters and by multisensory analysis (Dekker et al., 2005; Phinn et al., 2005, 2008) with a special focus in coral reef communities identification (Kutser & Jupp, 2006a). Less effort has been devoted to sedimentary seabed mapping and very few studies involve benthic seaweeds identification (Wittlinger & Zimmerman, 2000) from remote sensing. Forms, biomass, phenology, composition and vegetation cover percent are generally quantified with good accuracy in the emerged environment, while the quantification in underwater environment is complicated by the physical effect of the sea waters (Silva et al, 2008).

In shallow waters, seabed mapping is influenced by the scattering and absorption of radiation by optically active targets such as organic and inorganic particles (Han & Rundquist, 2003; Lee & Carder, 2004). Given sufficient spectral resolution, traditionally supervised and unsupervised classifications underestimate or overestimate cover classes content because the mixture of each pixels is not detected at the scale where many spatial patterns occur. These small (cm to m) spatial scales tends to contain heterogeneous mixed habitat properties and innovative assimilation of different spectral resolutions from ground and remote observations can provide a quantitative method to define these complexities.

The concept of the mixed signatures has been recognized long ago, and the development of an end-to-end understanding and model led to quantitative applications of Spectral Mixture Analysis - SMA (Smith et al., 1990) to measure land cover percent of vegetation in several studies of semiarid regions (Taramelli et al., 2012; Taramelli, 2011). Linear mixture models are based on the observation that radiances reflected from surfaces and constituted by different endmembers (EM = spectrally distinct components) mix linearly in proportion to ground cover percent within the instantaneous field of view (IFOV). A mixing space is generally represented with low dimensional orthogonal projections of the principal components (PCs) and the eigenvalues distribution provides a quantitative estimate of the variance on the base of spectral bands information (Green & Boardman, 2000; Price, 1997; Sabol et al., 1992). The multidimensional feature space therefore provides a spectral mixing space that can be used to collect the individual spectra as a combination of spectral endmembers (Johnson et al., 1985). Nonetheless linear mixture models from medium to coarse satellite imagery (Small, 2004; Small et al., 2009) can be not enough detailed when applied to complex environments that show considerable variability as the coastal one. Instead hyperspectral data (i.e. MIVIS) now available from several airborne sensors (George, 1997; Lewis, 2001) allow better discrimination between pigments and the identification not only of seagrass community presence but also of broad macroalgal groups (Murphy et al., 2008; Valentini et al., 2012). The increased use of hyperspectral sensors in mapping and in differentiating between vegetation cover class and species of macrophytes in shallow water has been demonstrated in the lagoon of Venice (Alberotanza et al., 2006); in a lagoon coast of the island of Sicily (Calvo et al., 2003) and in several internal lakes for macrophytes identification (Giardino et al., 2007). Within the available remote data sources, hyperspectral imagery is best suited to this task because it provides a calibrated baseline and both the spatial and radiometrical resolution necessary to distinguish among important seabed and seawater characteristics. Physical descriptors of surface morphology and sedimentology can improve the definition of these key seabed properties. In this task, passive hyperspectral assimilated to active sensors such as radar and LiDAR, enhance the limit where is still possible to retrieve spectral information. The usefulness of data fusion of hyperspectral with optical and bathymetric (Lyzenga, 1978) to module the effect of the seawater and the seabed reflectance is well recognized since years (Lyzenga, 1985; Bierwirth et al., 1993). Others major examples are the integration of hyperspectral and fluorescence with LiDAR topography that made possible to differentiate between benthic green and blue-green seaweed biomass (Bazzani & Cecchi, 1995) with unique spectral properties. The overall approach is that first, the high spectral resolution is useful to identify different relationships between reflectance properties in the visible and near-infrared (Hakvoort et al., 2002) and second, the high spatial resolution (i.e. 3x3 m) of airborne sensors offer optimal capabilities for shallow seabed habitat mapping (Groom et al., 2006; Keitt & Urban, 2005; Ustin et al., 2004; Wulder et al., 2004). Recent enhancements in seabed mapping are based on field radiometry that offers the simultaneous, narrow and contiguous bands needed to study these complex environments (Barillè et al., 2011; Hochberg & Atkinson, 2008; Murphy et al., 2005, Asner et al., 2012). Two studies focusing on coral reef mapping demonstrated that spectral signatures of seawater and seabed differ until about 7 - 8 m of depth (Call et al., 2003; Karpouzli & Malthus, 2004) and below this threshold they cannot be distinguished. In-situ measurements of target at 6 – 8m of depth in optically clear waters demonstrate that reflectance of vegetated seabed due to the added effect of vegetation and sea water absorption, results generally lower if compared with sandy and rocky seabed (Paringit& Nadaoks, 2003). Moreover, many pigments have spectrally distinct absorption features that can be coupled with the interesting possibility of mapping the sandy and clayey reflective sediments (Rainey et al., 2003).

This study develops a processing chain FHyL that generate high accuracy in mapping complex coastal seabed in terms of habitat classification and morphological properties. The complex coastal areas investigated in the present study, include a shallow coastal seabed (0 -18 m of depth) dominated by optically clear seawaters. Multisensory technology to obtain multidimensional data fusion has been achieved by introducing

LiDAR altimetry into the hyperspectral mixing space where seabed and sea waters properties are distributed. When implementing the linear spectral mixture model, the collection of spectrally distinct components (EM) is then magnified with the integration of the Spectral Library.

The methodology has been implemented by using: 1) a multidimensional – multisensory biophysical mixing space to select the most suitable endmembers to account for both physical and environmental properties provided by hyperspectral and LiDAR dimensions; 2) a field spectral library to assimilate the high environmental variability into the spectral mixture model; 3) a decision tree classification to represent the spectral variability provided by the multidimensional analysis into discrete seabed habitat classes.

3.2 STUDY AREA

The study area is included into a physiographic unit in the Central Tyrrhenian sea (Mediterranean - Italy) that lies from the Orbetello promontory to the Civitavecchia harbor along 60 km of mixed sandy and organogenic coastal seabed (Figure 3.1).

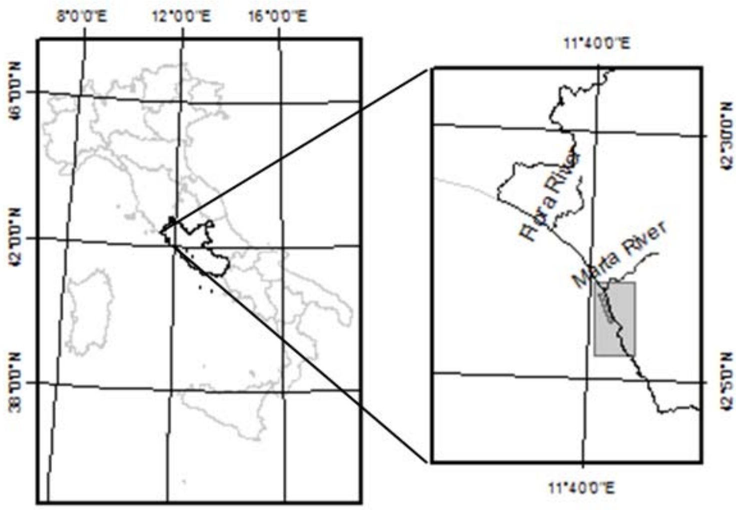

Figure 3.1 - Study area localized in the Central Tyrrhenian coast (Mediterranean - Italy).

In this coastal stretch the sedimentary continental platform is characterized by continuous low slope (1,2 -1,7 %) with meadows of *Posidonia oceanica* often interrupted by the sandy channel network connected to the coastline. Scattered seabed of other seagrass species and benthic seaweed corresponds to seabed complex morphology and sediment supply (AA. VV, 1996). Two subareas can be identified where patches of *Posidonia oceanica* are generally interspersed with organogenic deposits. The northern subarea, with the upper limit over 10m of depth is broken near the mouth of the river Fiora. This river influence the distribution of organogenic deposits up to 20 m and impacts the profile of the entire sandy stretch over the Marta river mouth where the second subarea of seagrass appears at shallower bathymetries (AA. VV, 1996). Here, consolidated outcrops that in front of the Tarquinia saltwork are mostly covered by P. oceanica break up sandy bars parallel to the coastline between 5 m and 10 m depth. The seagrass upper limit in this area is around - 4 m and its cover percent varies from 20% and 100% (AA. VV, 1996). Benthic seaweeds are present in response of hard structure and gravelly patches of bedrock in shallow waters. The second subarea has depth range between 0 –18 m along 4,5 km of shallow sedimentary seabed. Several rocky and organogenic outcrops, a sandy paleo-riverbed with high level of seagrass and seaweeds presence characterize it (AA. VV, 1996).

3.3 MULTYSENSORY DATASET COLLECTION

Two airborne surveys with MIVIS hyperspectral and Hawkeye LiDAR sensors, during the spring 2009 and 2010 provided the hyperspectral and bathymetric dataset. Four field surveys per year during the airborne acquisition provided data for validation and analysis assimilation and integration (Figure 2). The use of Field Spectroradiometer allowed building a Field Spectral Library with the spectral features of consolidated and unconsolidated seabed, benthic seagrasses and seaweeds targets. Moreover, high definition video shot through the study area (Figure 3.2) and available cartographic archives completed the overall dataset for image ground truth and interpretation. Positioning of all measures was obtained with a Trimble GPS navigation system with an error around 5m.

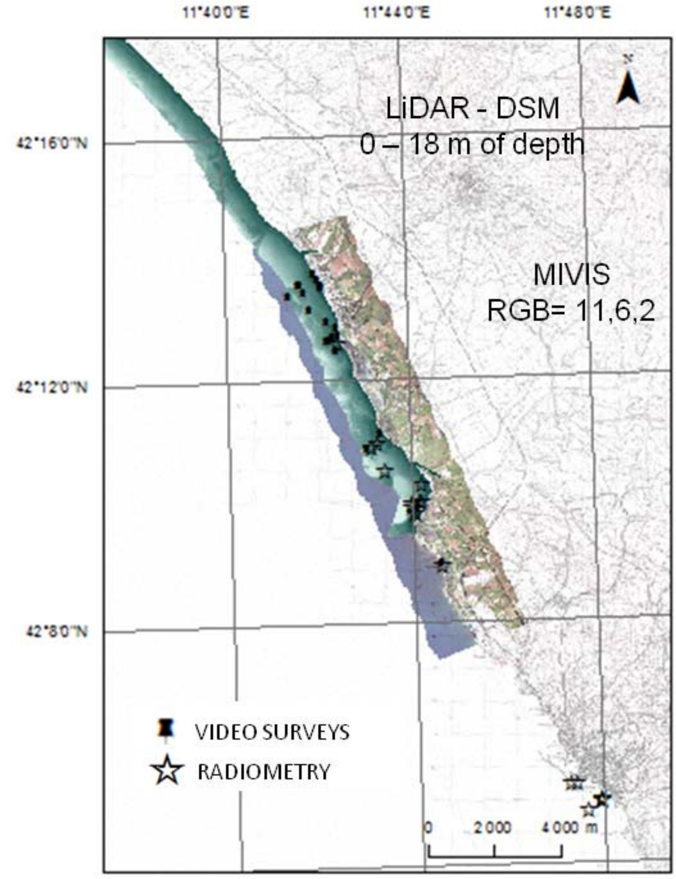

Figure 3.2 - Multisensory dataset. IGM official cartography with hyperspectral MIVIS image in true colors (R,G,B = 11, 6, 2) and LiDAR Digital Surface Model (DSM). Field surveys station are represented with black stars for both video and radiometric stations and with pins for only video shot stations.

3.3.1 FIELD SPECTRAL PROPERTIES

The ASD Field Spectroradiometer FR Pro, operating in the spectral range between 0.35 μm and 2.50 μm (Table 3.1) was used to measure spectral reflectance of the surfaces after the normalization with reference Spectralon panel used to simulate the Lambert' surface properties. In our field campaign we propose to focus the analysis of reflectance variations mainly on vegetation patterns and bedform presence.

Table 3.1 - Field Spectroradiometer FR pro details.

Fieldspec FR Pro SPECIFICATION	SPECTRAL INTERVAL (μm)	SPECTRAL RESOLUTION (μm)	SAMPLING INTERVAL (μm)
SPECTRAL RANGE	0.35 – 1.00 1.00 – 2.50	0.3 0.1	0.14 0.20
DIGITAL RESOLUTION	14 bit		
FIELD OF VIEW	5° – 25°		
SPECTRAL ACCURACY	± 0.01μm		

Surveys of the optical properties of the shallow seabed were carried out through the study area (Figure 3.2) within the 15 m depth limit on a variety of vegetation density and seabed typologies. Measures of the spectral reflectance led to a collection of 1000 reflectance spectra of 20 radiometric target. Basic analytical measures such as seagrass leaf length, epiphytes percent cover, leaves density and seaweed identification were made directly in situ or at laboratory and samples sediment for grain size and organic content were also collected. Field Spectroradiometer was used first to define *P. oceanica* spectral reflectance and to better understand the influence of epiphytes in its overall signature. The in situ measurements of *P. oceanica*, were carried out on sandy and mixed (rocky and sandy) seabed, on densely and homogeneously distributed *P. oceanica* with and without epiphytes. The two main groups of marine algae (Red and Green) were measured both insitu and exsitu and laboratory identification was made at species level.

International protocols for Apparent and Inherent Optical Properties (AOP) were applied to connect reflectance from seawaters of Total Suspended Matter (TSM), Chlorophyll (Chl) and Yellow Substances (YS) on imagery and reflectance from seabed into the spectral arrangements of hyperspectral imagery. Indicators of seawater quality were estimated using bio optical models with backscatter coefficient bb (λ) of the water, the Secchi depth and the concentration of chlorophyll were also measured insitu for the simulation and validation.

3.3.2 *AIRBORNE HYPERSPECTRAL IMAGERY*

The Multispectral Infrared Visible Imaging Spectrometer MIVIS (Table 3.2) is a passive whiskbroom scanner where the sunlight collimated by the scan head is distributed by means of dichroic filters into 4 modules that simultaneously record the radiation from 0.43 µm and 12.70 µm, coming from the Earth surface (Daedalus, 1993). On 08/05/2009 and 06/06/2010 two flight acquisitions along 40 km^2 of coast with the MIVIS hyperspectral sensor registered the at sensor radiance (Figure 3.2b) in 2 hyperspectral images called *Run* with 102 spectral bands and 3x3m pixel resolution.

Table 3.2 - Hyperspectral MIVIS sensor details

MIVIS TECHNICAL DETAILS	NUMBER OFBANDS	SPECTRAL INTERVAL (µm)	SPECTRAL RESOLUTION (µm)
I module	1-20	0.43 – 0.83 VIS	0.2
II module	21-28	1.15 – 1.55 NIR	0.5
III module	29-92	1.98 – 2.48 MIR	0.09
IV module	93-102	8.18 – 12.70 TIR	3.4– 5.4
IFOV/FoV	2 mrad / 71.06°		
SCAN/SEC	25 m/sec		
DIGITAL ACCURACY	12bit x pixel, ±1 bit		
SPATIAL RESOLUTION	3 x 3 m with 1500m of flight height		

All images were georeferenced directly by the company who made the airborne acquisition (BLOM). Measurement of the optical thickness of the atmosphere (AOT) with an EKO photometer recorded absorbance and attenuation values for atmospherically influenced wavelengths between 0.50 µm and 0.70 µm. By interpolating the 0.56 µm values the exponential model of decay during the day 6/06/2010 from 8.00 am to 3.00 pm (local time) provides the estimate of the model aerosol necessary for atmospheric correction operations in airborne hyperspectral images. Thanks to ground measurements during the second airborne acquisition we also validated temperature recorded by the IV module MIVIS thermal bands.

3.3 *LIDAR DATA*

Contemporary with hyperspectral acquisition, LiDAR Hawkeye sensor (Table 3.3) provided the point cloud collection for morphological and physical analysis. LiDAR equipment based on an active sensor that sends out laser beam at near infrared and green wavelength, scans across Earth surface and then measures the time it take for the laser beam to bounce back and the way it gets deflected by the surface under survey (Schnurr, 2009).

Table 3.3 - Bathymetric LiDAR sensor details

LiDAR HawkEyeII DETAILS	NUMBER OF BANDS	LASER PULSE WAVELENGHTH(μm)
BATHIMETRIC	NIR	1.06
	GREEN	0.53
FLIGHT HEIGTH	500 m	
FREQUENCY	Bathy 4000 Hz	
DENSITY	1-4 pt/m²	
SWATH	300 – 330 m	
ACCURACY	Bathy Horizontal (x, y) ±2.5 m / Vertical (z) ±0.25 m	
DEPTH RANGE	3 times Secchi depth	
SPATIAL RESOLUTION	4 x 4 m with 500m of flight height	

Specific survey for geophysical measurements with Echo sounder provided the accuracy of the Digital Surface Model (DSM) obtained by LiDAR.

3.4 METHODOLOGY

A hierarchical approach of spectral data has been used to develop the FHyL processing chain. We use the high resolution airborne sensor spectral data in combination with innovative assimilation from field radiometric observation and from LiDAR altimetry to develop a multidimensional and multisensory mixture space. In order to apply the FHyL, first the Region of Interest was obtained by a spatial resampling of LiDAR DSM 4x4 on the base of the hyperspectral 3x3m spatial resolution. By selecting the spectral subset between 0.46μm and 0,70 μm we also produced a spectral resampling of Field Spectral Library at MIVIS spectral resolution. Field Spectral Libraries and LiDAR DSM were used to magnify the dimensions of the hyperspectral mixing space and the variables of the linear spectral mixture model.

3.4.1 *FIELD SPECTRAL LIBRARY*

At first three field radiometric measurements were applied: a) in situ, b) ex situ and c) in contact in order to collect pure and mixed spectral signatures. The three measures mainly differ in the distance of the probe from the target analyzed. a) and b) are based on natural reflectance of investigated surfaces and the final signature is affected by water or atmosphere while c) can be considered pure, as the reflectance is derived from a source of artificial light and is virtually measured placing the sensor in contact with the target. Main targets separated each sample and four reflectance spectra were measured for each target. Measures of spectral signatures were expressed as reflectance on a scale between 0 and 1. Field Spectral Library was finally built and processed according to the international standard of the main spectral libraries published online by the United States Geological Survey (USGS - http://speclab.cr.usgs.gov), the Jet Propulsion Laboratory (JPL-http://asterweb.jpl.nasa.gov/speclib) and the John Hopkins University (JHU - ftprocky.eps.jhu.edu). By clustering spectral profiles of seagrass, seaweeds, sandy, rocky and gravelly seabed a built-in spectral library with 20 signatures of different targets was associated with descriptive forms containing station data, characteristics of each target, type of measure and the description of the target spectral behavior. Field Spectral Library was resampled at the radiometric resolution of the MIVIS sensor using the "Spectral Library resampling" tool in ENVI ® in order to have the optical relationships with specific properties and the target characteristics smoothed and comparable with the radiometric resolution of MIVIS images.

3.4.2 *IMAGE PREPROCESSING*

The geometrically calibrated hyperspectral dataset was corrected for atmospheric influence using ATCOR4, based on the radiometric transfer model MODTRAN4 (Richter, 2009 - DLR, German Aerospace Center, Remote Sensing Data Center, Wessling) and implemented by Schläpfer Applications. ATCOR4 ® is designed for the atmospheric correction of remotely sensed data acquired from aerial platform. Airborne sensors are much more unstable and sensitive to wind motion, the scanned data can therefore suffer from distortions related to pitch, yaw and roll of the aircraft and instrumental variables such as FOV from very narrow to large systems and push broom scanner have to be considered. To cope with these possible sources of error and distortion of remote sensing data, the code ATCOR4 ® uses, among other data input, a metafile containing information on the sensor about the geometry of flight azimuth, zenith of acquisition and flight altitude.

All the analyses started with the definition of the Region of Interest. MIVIS imagery required the gradual generation of masks to reduce the extent of image itself and to define the best subset for the final seabed processing. Picking one out of the 10 thermal band of the MIVIS sensor (n. 93, 8.20µm - 8.60 µm) it was possible to define a threshold temperature value, identified in 19.5°C, to mask emerged land. The value has been defined on an empirical basis; drawing transects perpendicular to the shoreline and determining the most appropriate value for discrimination of the emerged and submerged area. During 2009 MIVIS acquisition we validated thermal bands value with field temperature measurements.

LiDAR 4x4m DSM was interpolated at the 3x3m MIVIS hyperspectral resolution and stacked on the subset as an adjunct band. By calculating the standard deviation of the LiDAR point cloud on a 4 x 4 m grid, we observed and classified seafloor rugosity in terms of parameters (elevation, slope, aspect) that helps in classify the seabed in consolidated and unconsolidated. Through the analysis of morphological parameters and by standard deviation classification we calculate the correlation with hyperspectral MIVIS bands in order to define the spatial mask for a reduction of the spectral subset. The final spatial subset was defined between -3 and -18 m (two class of different rugosity) that leads to a reduction from 20 to 13 hyperspectral bands, with a wavelength between 0,46 µm and 0,70 µm.

3.4.3 MULTISENSORY SPECTRAL MIXTURE ANALYSIS

Hyperspectral MIVIS pure and mixed pixels have undergone to SMA in order to discriminate vegetated and not vegetated seabed fractional abundance. A multisensory mixing space has been generated on the base of PC rotation scatterplots. The pixel spectra from the apexes indicate pure endmembers and pixels located along the straight edges represent binary mixtures of those endmembers. The endmembers were evaluated against the consistency in the topology of the mixing space and the spectral separation between seabed typologies and the seawaters absorption effect was observed and analyzed. To quantify seawater absorption on different fractions we first observed the spatial distribution of bathymetric values along the mixing space trajectories and then by sampling spectral signature along the PC1 vs PC2 multisensory space we evaluate the relationship between depth and reflectance properties. The processing chain starts by integrating bathymetries and morphologies into the hyperspectral mixing space (Figure 3.4) and then the EM collection from image is used to achieve an image based mixture model of fraction that describes the composition of each mixed pixel in the final fractions maps. Then based on the Field Spectral Libraries resampled on MIVIS bands, we imported single and multiple spectral signals into the image EM collection in order to obtain a different mixture of fraction maps. No constrain was applied for the linear spectral mixture model of equations and physically impossible values outside the range of 0.0–1.0 were however considered. Root mean square (RMS) error was used to evaluate the accuracy of the mathematical results and to provide a quantitative measure of how fractions fit with the estimate of the observed environment.

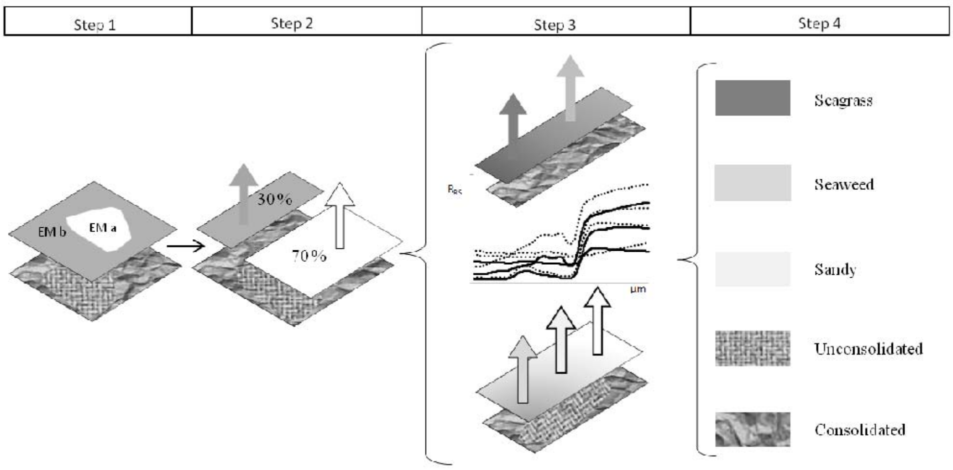

Figure 3.3 - Hyperspectral, LiDAR and Field spectral library (FHyL) processing procedure. Starting from Hyperspectral – LiDAR (Step1), multisensory Spectral Mixture Analysis provides cover percent (Step 2) fraction maps. Coupling the linear mixture model with single and multiple spectra from Field spectral library (Step 3) the number of detectable targets is increased at level of seabed habitat classification and seafloor properties (Step 4).

For each final fraction map the distribution of values has been analyzed and then by using a decision tree the final classification was obtained. Decision trees provide a more rational approach than traditional statistical supervised classification. A decision tree allows the user to specify the exact logical basis of class assignment in the form of conditional language of arbitrary complexity. In other words, decision trees let the user provide a physical basis for which pixels end up in a class. In any thematic classification, each pixel is assigned membership in one, and only one, class. In areas where the cover is discrete and homogenous, this is a reasonable approach but most of the seabed is not discrete and homogenous but rather gradational and heterogeneous. This requires that artificial distinctions be introduced where none exist in reality. In our case fraction maps are considered predictor variables whereas the class to be mapped (habitat) are referred to the target variables properties. The classification tree assign each pixel to a habitat class and where possible a cover percent class on the base of each variable values distribution. Selected fractions are graphically combined in a multilayered map of the seabed that defines seafloor physical properties as consolidated and unconsolidated seabed and seagrass and seaweeds distribution and abundance.

3.5 RESULTS

The final 20 signature of the Field Spectral Library (Table 3.4) showed absolute reflectance intensities that varies, in a 0-1 scale, between 0 and 0.6 for the signatures measured with contact and ex-situ, between 0 and 0.06 for the signatures sampled in-situ (Figure 3.4). Each selected signature was compared with available international reference with good agreement in profile and intensity of spectral profiles (Kutser et al. 2006b, Baldridge et al., 2009).

Table 3.4 - Field spectral library. Summary of shallow seabed targets with station detail an type of measurements (in grey are listed signature plotted in Figure 4). The main absorption (in black) and reflection (in white) peaks observed with Fieldspec FR Pro are pointed along the spectrum and with lines, spectral absorption (in black) and reflection (in white) range of interest are reported.

Code	Target Name	Depth	Date	GMT Time	Secchi depth
SLSUBLAZS01	*P. oceanica* (in contact)	4.00	20110401	10.00	4.00
SLSUBLAZS02	*P.oceanica* with epiphytes (in contact)	4.00	20110401	11.00	4.00
SLSUBLAZS03	Decomposing *P. oceanica* (in contact)	4.00	20110401	9.10	4.00
SLSUBLAZS04	Dry *Posidonia oceanica* (in-situ)	0.00	20100513	10.30	0.00
SLSUBLAZS05	*P. oceanica* (in-situ)	4.00	20110331	13:20	4.00
SLSUBLAZS06	*P. oceanica* with epiphytes (in-situ)	3.50	20110401	10:30	3.50
SLSUBLAZS07	*P. oceanica* on roky seabed (in-situ)	2.50	20110401	10:45	2.50
SLSUBLAZS08	*P. oceanica* on mixed seabed (in-situ)	1.00	20110401	12.15	1.00
SLSUBLAZS09	Red seaweed (ex-situ)	0.50	20100513	10.30	0.50
SLSUBLAZS10	Red seaweed (ex-situ)	0.50	20100513	11:40	0.50
SLSUBLAZS11	Green seaweed (ex-situ)	0.50	20100513	12:50	0.50
SLSUBLAZS12	Dead seaweed (ex-situ)	0.50	20100513	11:00	0.50
SLSUBLAZS13	Red seaweed (in-situ)	0.50	20100513	11:20	0.50
SLSUBLAZS14	Red seaweed (in-situ)	0.50	20100513	15:30	0.50
SLSUBLAZS15	Green seaweed (in-situ)	0.50	20100513	16:30	0.50
SLSUBLAZS16	Seaweeds on roky seabed (in-situ)	2.50	20110401	11:30	2.00
SLSUBLAZS17	Seaweds on sandy seabed (in-situ)	7.00	20110401	11:45	5.50
SLSUBLAZS18	Roky seabed (in-situ)	13.00	20110401	13:20	8.00
SLSUBLAZS19	Gravelly seabed (in-situ)	5.00	20110331	12.55	5.00
SLSUBLAZS20	Sandy seabed (in-situ)	3.00	20100528	10.00	3.00

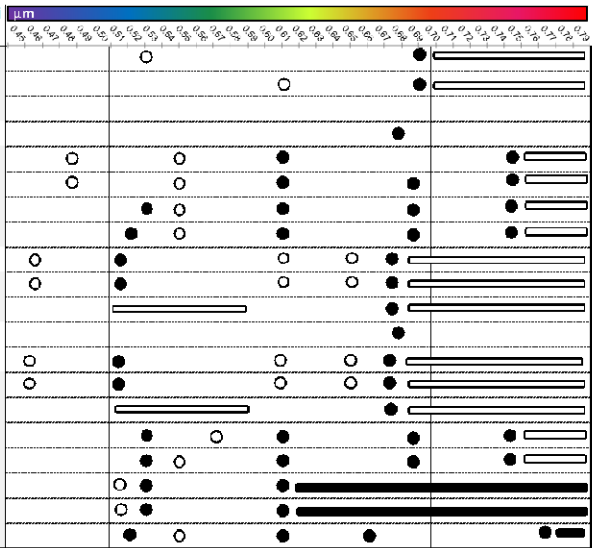

In situ *P. oceanica* showed spectral behavior with average absolute reflectance values generally lower than 0.6. In contact and ex situ measures reveal peaks of absorption between at 0.65 µm and the higher reflection between 0.70 µm and 0.90 µm (Figure 4a). Due to the leaf seasonal cycle especially during the colder months, these plants goes through a phase where leafs are completely or in part covered from organisms that give a speckled appearance white-pink, in contrast with the dark green of the leaves. In the spectral profile of selected leaf with high cover percent of epiphytes, more reflection than the not colonized foliage is observed both at green wavelengths (0,60 - 0.65 µm) and at the red edge (0.70 µm), where minimum in reflectance (8-15%) are registered (Figure 3.4a). The reflectance profiles of in situ patches of less dense *P. oceanica*, especially around the 0.55µm and 0.60 µm are influenced by the optical contribution of sands or rocks (Figure 3.4c) and epiphytes effects resulted lowered.

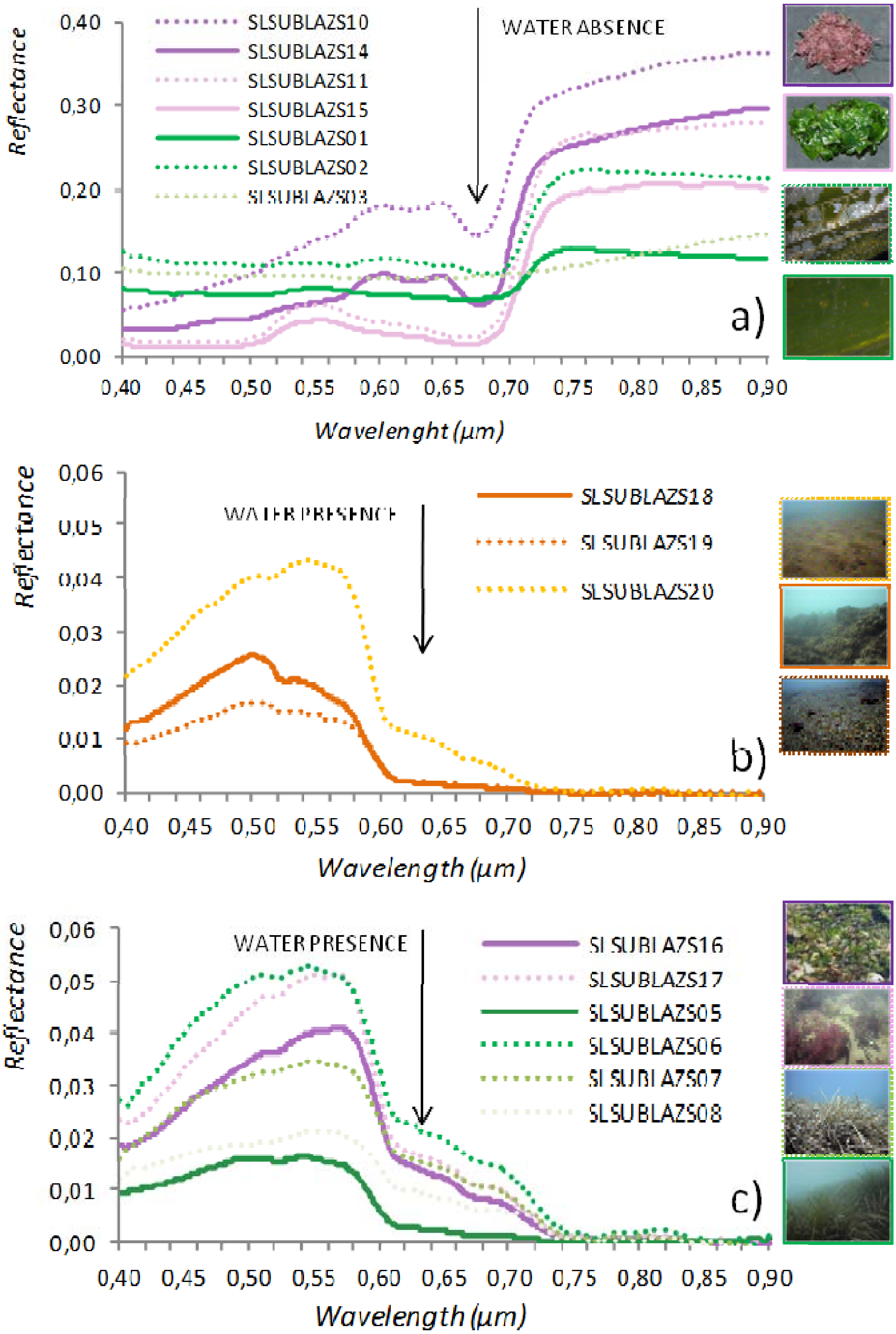

Figure 3.4 - Spectral profiles from the Field spectral library listed in Table 5. 4a) In contact signature of *P. oceanica* with and without epiphytes and ex situ spectral signatures of seagrass and seaweeds; 4b) in situ seafloor signatures; 4c) in situ mixed seabed typologies

Specific absorption peaks of algal pigments at 0.50 µm and 0.65 µm are observed (Figure 3.4a). Red seaweed (*Rodophytes*), represent the higher reflectance vegetation values measured over 0.68 µm and they have a wide range of absorption peaks between 0.50 µm and 0. 65 µm due to the presence of phycobiliproteins. Green seaweed (C*hlorophytes*) exhibits absorption peaks all through the spectrum 0.45 µm and 0.60 µm due to the presence of chlorophyll b and carotenoids that contribute at 0.50 µm (Figure 3.4a). In situ spectral behavior of red and green seaweeds, as observed for seagrass, are influenced by the presence of rocky and sandy seabed and between 0,55 µm and 0,65 µm reflectance features become less distinct (Figure 3.4c) than these measured exsitu.
Comparison between seabed typologies (Figure 3.4b) showed that they differ mostly at lower wavelengths. The sandy reflectance represents the higher value (maximum 0,05) between 0.54 µm and 0.57 µm. The gradient of the curve is reduced gradually absorbing red reflectance as for the gravelly and rocky patches. Both gravelly and rocky patches showed very similar profiles with maximum in reflectance between 0.48 µm and 0.54 µm and lower increases in absorption if compared with the sandy (maximum 0,03). Then the profile goes through the extinction of reflectance between 0.57 µm and 0.63 µm. Gravel seabed lower reflectance values at 0,028 are related to the shadowing and scattering effects. When the three seabed typologies are measured insitu with the presence of vegetation (Figure 3.4c), the more reflective sandy seabed, generally preserve both higher intensities and spectral profile instead of gravelly and rocky seabed that between 0,60 µm and 0,65 µm become deeply influenced by absorption of vegetation. Based on the above, the insitu seabed spectral profiles resulted directly dependent by the rugosity that influences the scattering phenomena and thus the radiometric response.
The overall spectral characteristics of the in situ response can be summarized as a mixtures of low reflectance in the blue, between 0.40 µm and 0.50 µm that increase moving through the green between 0.55 µm and 0.57 µm and decrease again between 0.66 µm and 0.70 µm with the absorption peak between 0.67 µm and 0.68 µm.
Field measurements allowed calibration and validation (Table 3.5) of hyperspectral MIVIS imagery acquisition (r = 0,92 *p-value* < *0,05*). Measurement of the optical thickness of the atmosphere (AOT) showed heterogeneous profiles especially between 0.5 µm and 0.7 µm, indicating a mean value of 0.125 (AOT) that corresponds to an

average visibility of 48 meters for the model that provided high atmospheric correction accuracy (r = 0,90 *p-value < 0,05*). Good correspondence was observed also for the thermal wavelength against insitu thermal profiles (r = 0,76 *p-value < 0,05).* Echo sounder profiles are compared with that of LiDAR DSM until 8 m of depth where their profile are overlapped (r = 0,70 p-value < 0,05). The purpose of this is twofold: first, LiDAR bathymetric allow to identify the depth associated with the spectral endmembers, secondly, field validation allows to identify significant intermediary of spectral characteristics of particular significance changing with depth.

Table 3.5 – Ground truth in airborne hyperspectral MIVIS imagery and LiDAR altimetry.

MIVIS VISIBLE	MIVIS THERMAL	MIVIS ATM CORRECTION	LiDAR (until 8 m depth)
R=0.92	R=0.76	R=0.90	R=0. 70

The multidimensional image PC rotation (Table 3.6) provides as expected, high score on the PC1 (93.08%) that represent the main source of spectral information about seabed. The PC1 results to be less affected by seawater effects. PC2 (4,99%) is the one that collect seawater absorption effects and plotted against LiDAR bathymetry interesting evidence are highlighted below - 6 m. The remaining PC3-PC5(1,35%) mixed in a single additive image contributes to the qualitative interpretation of seabed variance.

Table 3.6 - PCA results

	MIN/100	MAX/100	DEV ST/100	% OF VARIANCE	CUMULATIVE VARIANCE	PC - IMAGE
PC1	-4.11	17.71	0.28	93.08%	93.08%	
PC2	-2.63	1.49	0.07	4,99%	98.07%	
PC3	-1.62	0.88	0.05	0,89%	98.96%	
PC4	-0.62	1.01	0.03	0,25%	99.21%	
PC5	-0.64	0.57	0.02	0,21%	99.42%	

The PC1 vs PC2 2d scatterplot (Figure 3.5) shows a tetrahedral mixing space bounded by three distinct spectral endmembers and that the reflectance properties are distributed with specific directions along the axes. The bathymetric hyperspectral mixing space built on the base of hyperspectral and Lidar data highlighted the optical threshold close to the bathymetries – 3 m and – 6 m along the PC2 axes and seabed composition along PC1 with different trajectories of vegetation and sand abundance. Over – 6 m this effect disappears and the ability of seabed detection is reduced by mixed sea water and seabed darkness absorption effects. A detailed analysis of the outline and properties of the mixing space led to clarify the dependence between seawaters and PC2. By sampling spectral profiles along 2 transects (left and right edge) of the PC1 vs PC2 mixing space we verified the distribution of the water depth along the vegetated and not vegetated seabed. By selecting shallow sea waters effect through a spectral sampling every single meter of depth, from -1 to -10 m for not vegetated seabed and from -3 to -10 m of the vegetated seabed, we measured changes of the spectral response at each wavelength along the bathymetric gradient (Figure 3.5b, 3.5c).

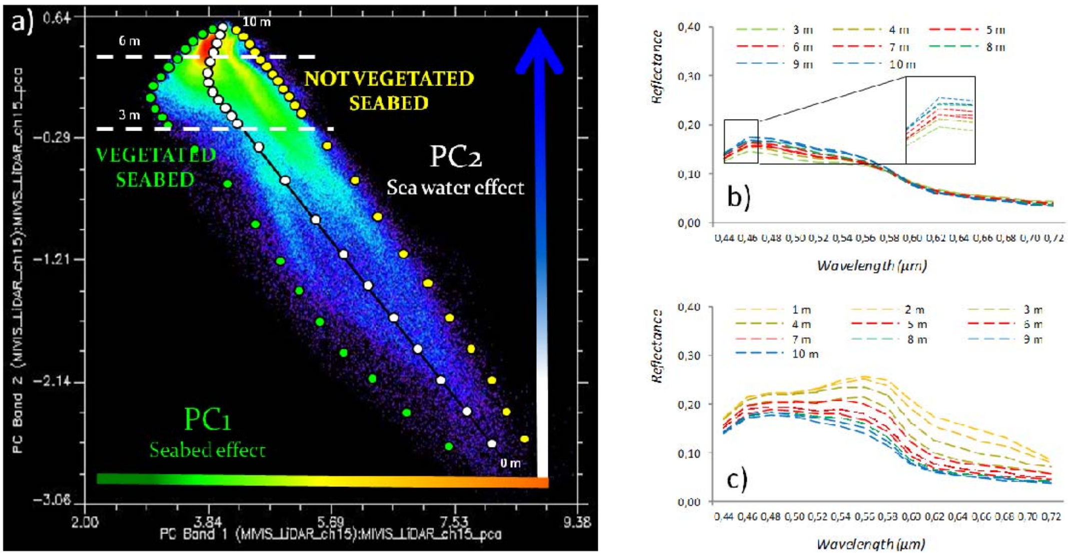

Figure 3.5 - a) Multidimensional – Multisensory mixing space on the base of the PC1vsPC2 scatterplot. The main observed features are highlighted; b) Vegetated seabed and c) not vegetated seabed signatures are sampled from the lower apex towards the upper in order to observe seawater depth along specific trajectories.

Spectral sampling of the mixing space showed the progressive decrease of the values of radiance moving over 0.58 µm due to the increasing water presence. The left edge of the mixing space can be associated to the vegetated seabed where reflectance varies with increasing depth in all bands, up to - 8 m. An inversion of the trend, moving toward increased levels of reflectance in the first part of the spectrum (0.44 µm and 0.59 µm) changes in decreased levels of reflectance in the lower part of the spectrum. To be noted is that the mixing space register vegetated seabed only over - 3 m depth. It is possible that this change in spectral trend is due to the change of the seabed features hedges and then to the interaction with residual algal and leaves at the surf zone. We also noted that the radiance gradually decreases with increasing depth, until - 6 m. After this depth, both vegetated and not vegetated seabed looks more like sea water absorption than seabed.

Between the depth of 3 m and 8 m of the mixing space we selected a collection of three endmembers (EM) to describe the heterogeneity of seabed. The 3 endmember for spectral unmixing were: a) not vegetated seabed b) vegetated seabed and c) depth (Figure 3.6a). The unconstrained linear spectral mixture model obtained with the three endmember collection showed good approximation of the darker part of the image, represented by vegetation and rocky or organogenic seabed. The average RMS error was generally low until 6m of depth suggesting the validity of the three endmember selected. By collecting endmember at the edge of the mixing space, the linear equation system was deprived of intermediate reflectance not available in the 2^{nd}, 3^{rd} and 4^{th} dimension of the mixing space edges. Linear transformations of the dataset, such as reflectance retrieval, didn't not change the linear addition of endmember as long as the same linear transformations were performed on the endmember. This makes reflectance retrieval areas of the pixel suitable for seabed reflectance recognition.

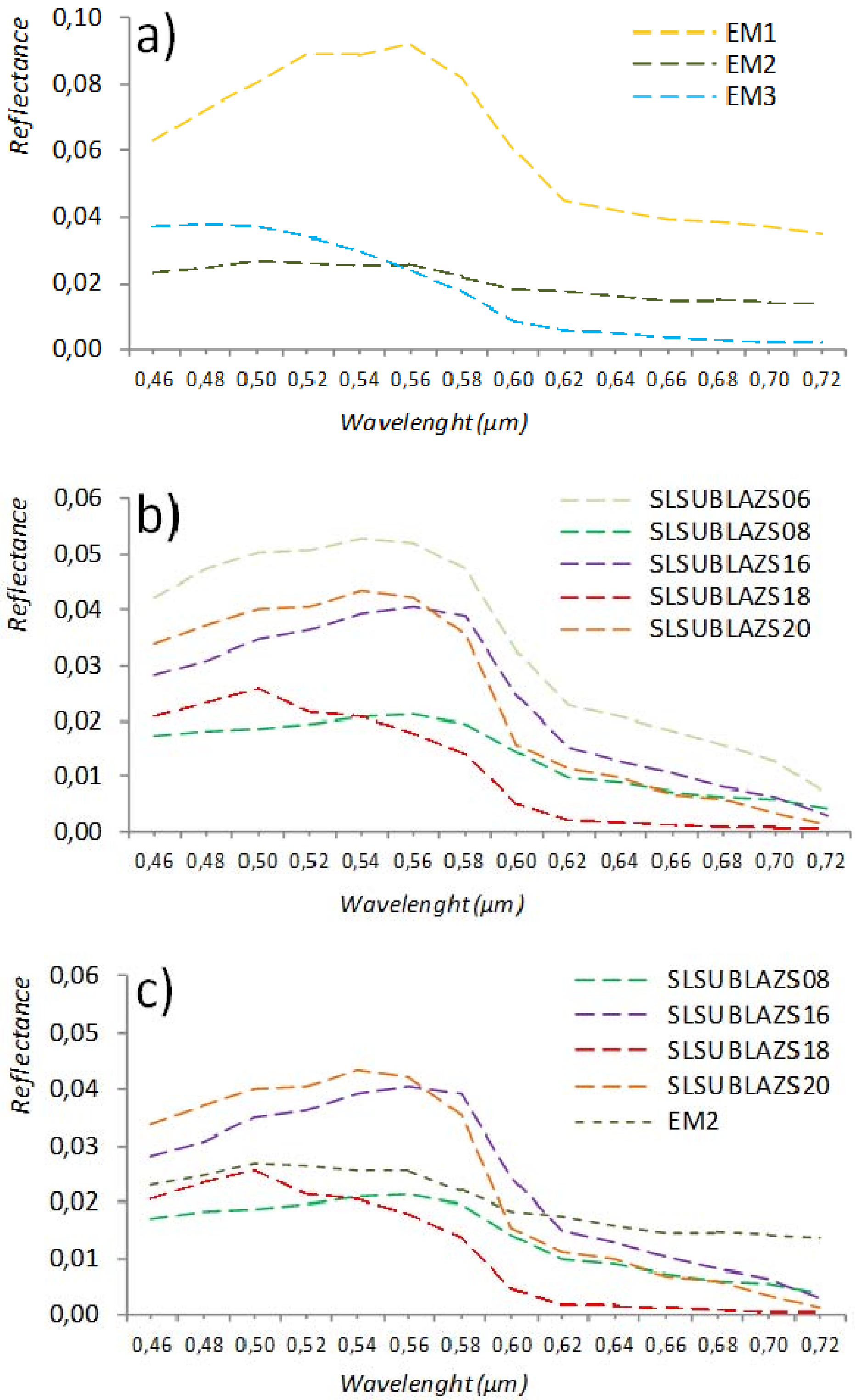

Figure 3.6 - Figure 6 – Spectral collection a) Image based (EM) b) Field Spectral Library based c) Combined Image and Field spectral library based.

From the Field Spectral Library, considering the high level of absorption within the shallow seabed, five profiles were summarized in a single collection for the image based mixture models analysis. Working on a linear spectral mixture model based on field spectral collection it was possible to discuss diagnostic peak (Figure 3.6b) along reflectance profiles. Clustering of the PCs, reveals spectral similarity along the edge of the mixing space and we expect some insight might be gained from the relative contributions of field spectra to the PCs. The third mixed spectral collection was obtained by introducing a variety of image and Spectral Library based reference spectra (Figure 3.6c). The fraction map of seaweeds on rocky ground made possible the identification between -3m and -6m of depth of the presences of extensive algal cover involving gravel and mixed sandy and rocky seabed. In addition, the sandy seabed introduced from Field spectral library led to a better resolution of the sandy patches. In order to define the best solutions for the system variables and to provide an adequate number of information we notice that the projections of 4 endmembers extracted from the spectral libraries account for the 99% of the spectral variance. The clustering of different spectral set of signature was repeated and the best fitting result was based on a collection of four EM signatures extracted from the spectral library and one EM signatures from the mixing space. The vegetated seabed EM pick the missing intermediate reflectance observed on the seabed due to the gradient generated from seagrass with the rocky seabed and sea waters absorption. Fraction map of sandy and rocky seabed, as well as seaweed cover represent significant spectral contributions in the range of low reflectance signal. The RMS error of the third mixture model resulted the lowest in terms of mean and maximum values compared to the image based mixture model (Table 3.7). The continuous structure and the EMs within the mixing space fallow specific trajectories that enhance the ability to resolve complex mixtures and to determine the multidimensional natural- space.

Table 3.7 - The three spectral mixture model results. To be noted the lower RMS error in image and Field spectral library case.

	Full Scene 2,824,125 points	EM name	min	max	mean	dev.st
Image	EM1	not vegetated seabed	-2,41	5,39	-0,06	0,22
	EM2	vegetated seabed	-0,39	1,21	0,05	0,14
	EM3	depth	-0,77	1,27	0,09	0,22
		RMS error	0,00	31,07	1,38	3,45
Field Spectral Libr	SLSUBLAZS08	*P. oceanica* on mixed seabed (in-situ)	-6,30	5,57	0,05	0,56
	SLSUBLAZS16	Seaweeds on roky seabed (in-situ)	-4,98	2,28	-0,04	0,21
	SLSUBLAZS18	Roky seabed (in-situ)	-2,22	2,28	0,09	0,29
	SLSUBLAZS20	Sandy seabed (in-situ)	-0,87	1,45	0,02	0,12
	SLSUBLAZS06	*P. oceanica* with epiphytes (in-situ)	-1,93	6,43	0,06	0,29
		RMS error	0,00	25,92	1,22	3,09
Image and Field Spectral Library	SLSUBLAZS08	*P. oceanica* on mixed seabed (in-situ)	-4,52	4,83	0,10	0,48
	SLSUBLAZS16	Seaweeds on roky seabed (in-situ)	-1,97	3,04	0,00	0,25
	SLSUBLAZS18	Roky seabed (in-situ)	-1,01	2,18	0,11	0,30
	SLSUBLAZS20	Sandy seabed (in-situ)	-1,09	1,38	0,02	0,10
	EM2	vegetated seabed	-0,99	3,44	0,02	0,14
		RMS error	0,00	16,39	1,07	2,22

Endmember fraction and RMSerror distribution illustrate the trade off associated with the five endmembers. To obtain a clear understanding of the radiometric profiles associated to the seabed through the mixture models the 5 fraction (Figure 3.7) were analyzed in terms of distribution of more reliable values to extract cover classes. The *P. oceanica* on mixed sandy and rocky seabed (Figure 3.7a) showed a cover percent distribution extremely consistent between – 3m and – 6m. Seaweeds obtained by importing signature from Field spectral library appeared complementary to the fraction *P. oceanica* on mixed seabed confirming the existence of specific radiometric properties associated with vegetation (Figure 3.7b). The introduction of the vegetated seabed EM, extracted from the image proved to be basic for the lowering the maximum RMS error. By adding such information, vegetation fraction maps fit more closely to the reality but the similarity of the seafloor morphologies (Figure 3.7c) reduce the inversion as indicated by the negative fractions values of both seafloors and mixed seabed. The bedrock was in this model the less accurate fraction in terms of geometry detected (Figure 3.7d), also if associated with LiDAR standard deviation.

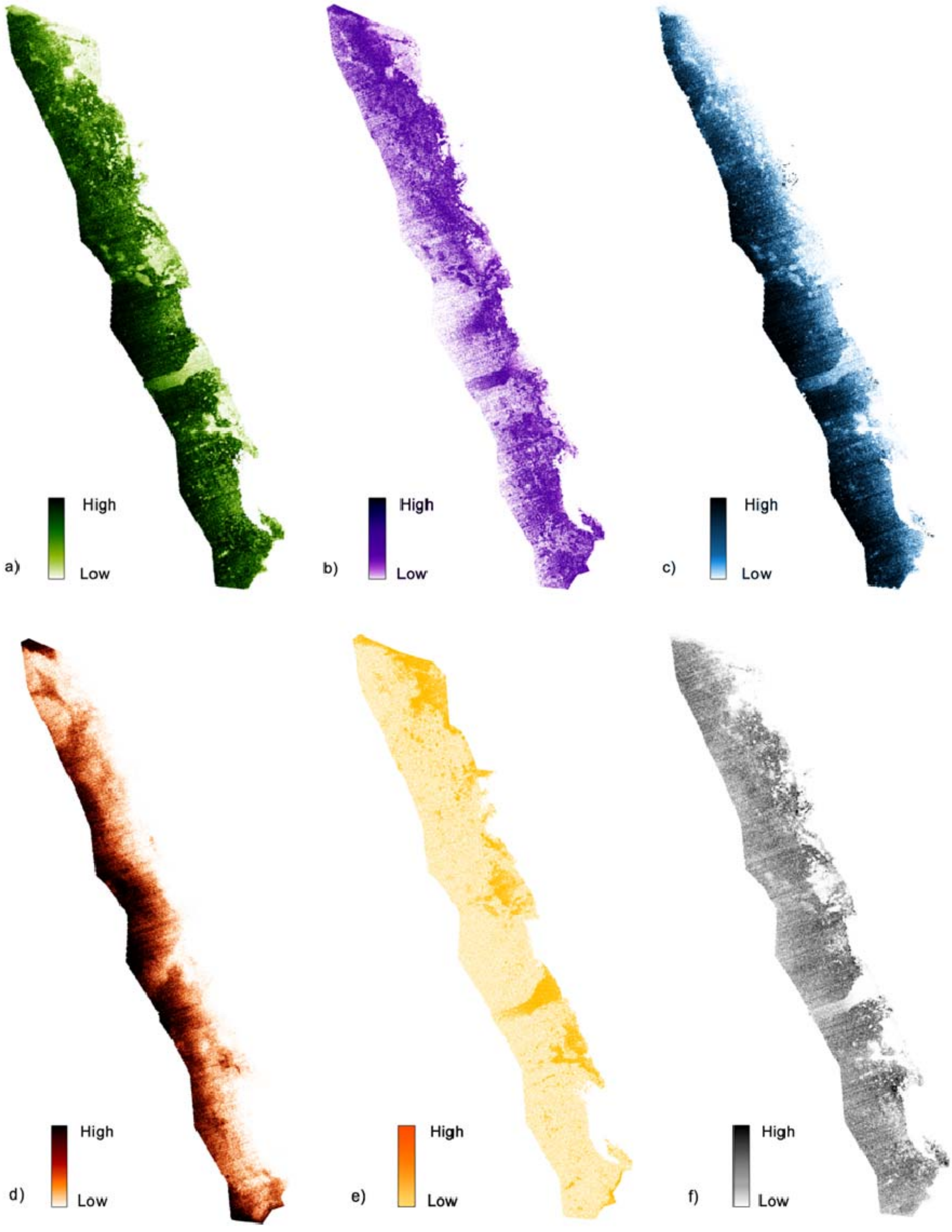

Figure 3.7 - Fraction maps obtained by combined Image and Field spectral library spectral mixture model: a) *P. oceanica* on mixed sandy and rocky seabed; b) seaweeds on rocky seabed; c) EM vegetated seabed; d) rocky seabed; e) sandy seabed; f) RMS error.

The fraction associated with sand (Figure 3.7e) can be considered the most accurate since it is linked to a spectral behavior highly reflective able to reduce the effect of absorption function due to sea waters effect. RMS error (Figure 3.7f) showed lower values where sandy seabed was mapped and good reliability below 6 - 8 m of depth that allowed bettering defining limits of vegetation patches. When coupled with LiDAR standard deviation, sandy seabed limits has been enhanced in terms of ability of unconsolidated seabed retrieval. Finally, the linear Pearson product – moment of seagrass and seaweeds fraction maps against bathymetry didn't reveal high correlation. Anyway the residual fraction of sea waters effect was removed with a normalization based on the linear model coefficient of 0,07 for both *P. oceanica* on mixed seabed and seaweeds. Coupling with seagrasses and seaweeds abundances, the two main habitat are identified and then four cover percent classes represent cover gradients.

High definition video shot through the study area completed the ground truth of the final fraction maps. A detailed crosscheck analysis between GPS track of each movie with the fraction values revealed that the mixed mixture model adequately predicted the boundary and the cover percent. Spectral signature of *P. oceanica* and seaweeds more or less dense on sandy bottoms from 3 m of depth to the limit of 10 m were detected. In areas where *P. oceanica* patches are dense and comprised between - 3 m and - 6 m, accuracy of mapping allowed classification of cover percent. Where the effect of the sandy or rocky seabed on the spectral behavior is almost null and the entire field of view of the sensor is occupied by the set of physical contributions from leaves and algal tissues a major group of marine algae showed specific absorption peaks at blue and green wavelength.

The FHyL processing chain produce a final composite layout of selected fraction maps classifing 2 main benthic habitat: the vegetated seabeds with cover percent and the main seafloor properties that describes the consolidated and unconsolidated areas. By combining the RMS error with vegetated seabed EM a preliminary identefication of accuracy thresholds are identified. We choose a multylayerd composition on the base of a simple decision tree where fractions are combined on the base of their abundance (Figure 3.8).

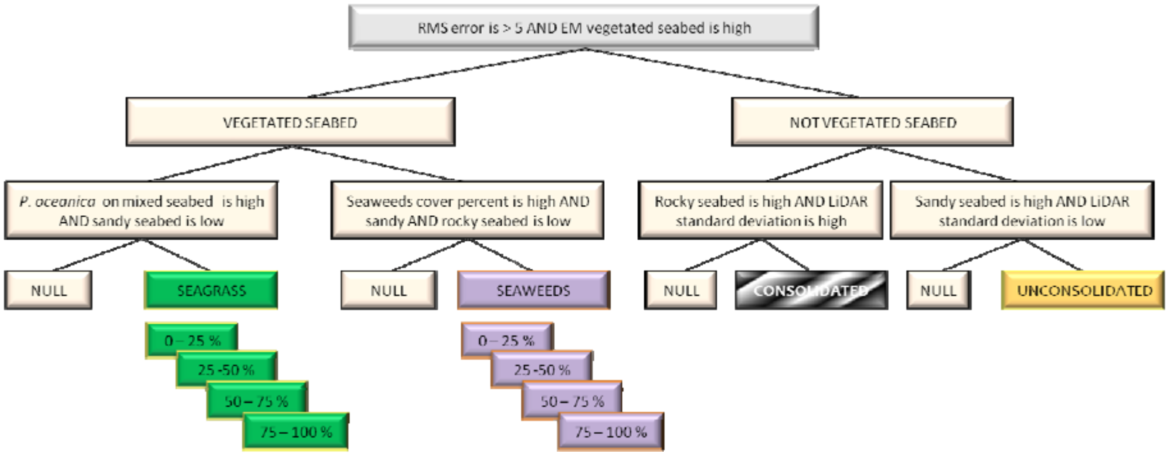

Figure 3.8 - Decision tree for seabed habitat and seafloor properties mapping. Colored box represent layers in the final map (Figure 3.9).

The resulted map of stretch of coast, describe the heterogeneity of cover typologies and habitat within the seabed (Figure 3.9).

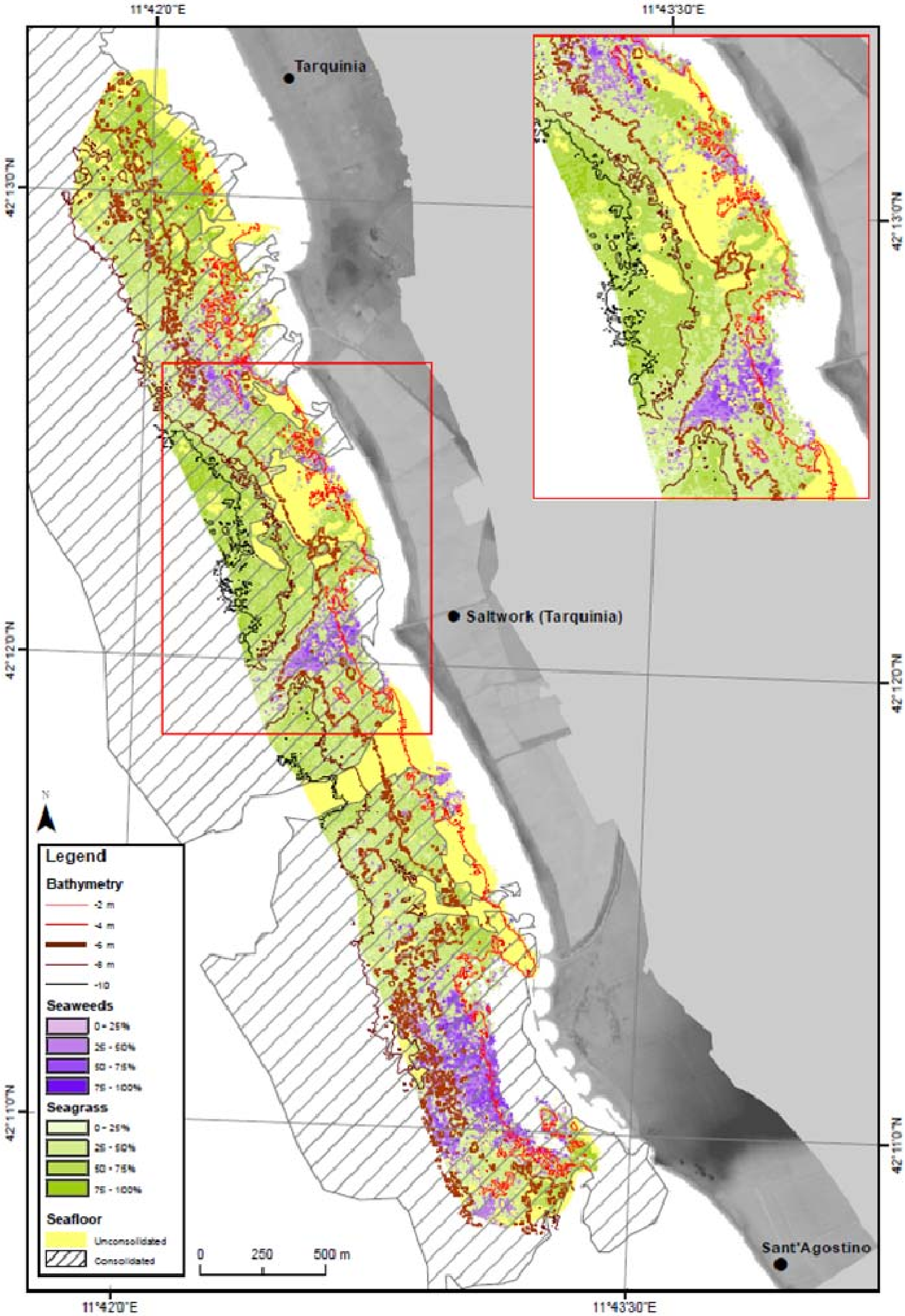

Figure 3.9 - Final map with legend of seabed habitat and seafloor properties. Grey is land and highlight is used to indicate the accuracy threshold at – 6 m of depth.

The distribution of *P. oceanica* is organized in two large populations belonging to the upper limits of the deepest meadows. Both are characterized by a strong fragmentation of the upper limit interspersed with rocky outcrops and sandy cavity. The patches in the north, bounded by the river Marta freshwaters, consists of an area with cover between 25% and 50% at the shallowest bathymetries that is not properly the meadow upper limit but probably just contiguous pioneer patches. That is in coherence with the evolving state of the area, where pioneer seagrass other than *P. oceanic*a has been mapped in recent years. Moving in front of the Saline saltwork, the level of heterogeneity increases and the upper limit become populated by vegetated patches between -3m and -6m, bounded by the sandy network of channel that crosscut major patches. In this section, we observe the presence of extensive seaweed cover on the rocky outcrops. The same seaweeds are detected by moving to the center of the salt work. Probably coastal microcirculation and coastal management interventions limited the presence of seagrass and encouraged the development of seaweeds benthic colonization. Going beyond the paleo sandy riverbed, the patch located at the south side grows up in shallow water around 3m of depth. Sedimentary dynamics also stimulates flowering and seaweeds and enable recolonisation. In the same area sandy seabed offer to *P. oceanica* the possibility of reaching 50% of cover with homogeneous spatial distribution. Hard defense structure define the end of this shallow emergency of the upper limit of *P. ocenica* meadows and pebbles of different sizes favorites the presence of seaweed communities that results homogeneously distributed with high degree of presence. Patch of organogenic outcrops are probably present in the southern areas, where consolidated seafloor resulted in correspondence of sandy seafloor.

3.6 DISCUSSION

The objective of the FHyL analysis is to provide a baseline to assess seabed cover discrimination for mapping underwater regions and to generate inputs to the regional managers. The first task, implemented here, is to determine the extent to which airborne hyperspectral data assimilated with field radiometry and LiDAR altimetry can distinguish important shallow seabed cover typologies and the seafloor properties within a complex submerged ecosystem. The study started from using the SMA on the hyperspectral images and therefore the influence of seawaters and geomorphic properties derived from LiDAR, enabled the introduction of a spatial and a spectral limitation relative to the very shallow environment. Bathymetric LiDAR has been a major contribution to understand the effects of absorption and reflection recorded by the hyperspectral sensor. Using the LiDAR point cloud standard deviation and DSM , the limits of radiometric data were identified as well as the validity of the hyperspectral acquisition and its boundary conditions (wind, cloud cover, fog, waves) that reveal the potential of the sensor itself in penetration capacity of optically clear seawaters below 6 m of depth. The average values of reflectance in the visible and near infrared of the seabed varies as a function of two main variables: geomorphic features and vegetation presence respectively and when measured in the presence of natural light, both determines a marked lowering of the average reflectance intensity.

Observing fractions, irregular forms increases through the southern direction where the presence of *P. oceanica* on mixed seabed is interspersed with seaweeds on the consolidated part of the seafloor. Once these forms has been determined and validated by video shot, it was possible to develop a procedure for mapping the spatial distribution on the seabed at a finest scale. Looking at the mixing space, all the pixels below 3 m of depth didn't allowed spectral variability dissection and they were not included into the final mixture models because of the effects of very shallow seawaters, sun glint and scatter of the littoral zone. Moving towards increases in depth the ability of dissecting contribution of mixed seabed increases, nevertheless the overall reflectance profiles decline. Particular extension of the mixing space over the 3 m of depth highlights where vegetation presence grow up and a clear dissection of vegetated and not vegetated seabed up to 6 m of depth is possible. Over this range 3 / 6 m the mixing space become thin and dense with a progressive end to a single apex. Here, seawaters absorption extinguishes vegetated and non-vegetated seabed contribution and the darkness dominates the mixture of pixels. Similar results have been obtained during the implementation of bio optical simulations of hyperspectral images for bathymetries ranging from 1 to 10 m. In this case sandy seabed showed over 6-7 m of depth, reflectance values reduced to about 5% against the same simulated signal with depth of 1 m and about 4% is observed in the presence of vegetation (ISPRA, 2012).

On this evidence the mixing space suggested that the optical characteristics of the seabed could be investigated mainly on the PC1 axis where we were able to distinguish the two main seabed, vegetated and not vegetated. The PC2 axis, instead, goes progressively describing the variation that causes the increase of the sea water effect on the spectral signatures. This strong influence enhanced the potential of the multisensory analysis for the development of the FHyL method that aims at extracting biophysical information using the assimilation of field spectral libraries and LiDAR bathymetry. Opposite, FHyL demonstrates the lower limits of the hyperspectral mixing space in distinguishing seabed typologies without field radiometry and LiDAR standard deviation amplitude.

Assimilating field spectral library within the mixture model, lead to a more detailed seabed habitat classification with the identification of the major patches of seagrass or green and red seaweeds through the absorption features of chlorophyll and other pigments. The assimilation of spectral library to understand the mixture effects of different signals on the inversion model provided ratios between visible and infrared moving from contact probe to insitu measurements and highlights the threshold values moving from presence and the absence of seawater (Figure 10) in different part of the spectrum. This is a key aspect of the FHyL analysis applied to the submerged area and breaking down into the albedo according to the range of the visible, we observed that the first variable associated to the contact probe in seagrass identification is the epiphytes presence instead of the reflectance properties of insitu measurements, where seawaters absorption influences the total reflectance with high reflective sands and low reflective rocks that may increase or reduce the total view of each pixel.

Looking at the ratios between infrared and visible wavelength we observe negative values where absorption of seabed is increased by higher density of vegetation or seafloor irregularities. Mapping radiances by pure spectral profiles converts a physical measure of reflected radiance to physically meaningful estimates of a basic biophysical property of each target.

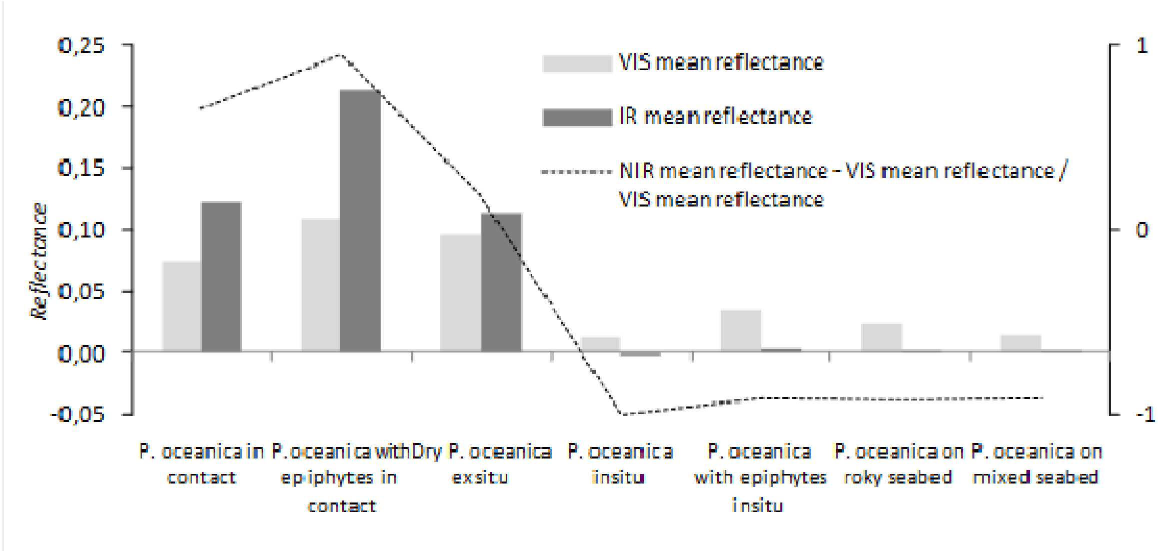

Figure 3.10 - NIR-VIS index summary. The histogram represents the average reflectance value in the VIS (light grey) and NIR (dark grey) of each target indicated under bars. On the left side reflectance axe and on the right side the value of the NIR-VIS index represented with the dotted line.

It is evident the presence of a strong absorption for non-sandy seabed all through the image associated with the vegetation absorption. To obtain a detailed identification of consolidated and unconsolidated seabed it has been necessary the integration of both fraction maps values and LiDAR standard deviation in accordance with the data fusion analysis.

The final map, based on expert ecological effort about the selection of important seabed properties to be represented evidences seaweed distribution probably connected with the circulation system changes, looking at hard barriers and saltwork presence. The sandy beach of S' Agostino has historically been the sandy southern edge of the seagrass meadow even at lower bathymetries, now this limit is represented by benthic seaweeds that colonize pebbles in front of the hard defense barriers. In this area, close to the hard structures, patches of consolidated seabed overlay the unconsolidated one. Although it can be interpreted as an error, observing the finest published seagrass cartography (Diviacco et al., 2001) realized with Side Scan Sonar (SSS) and by consulting experts, we understand that, as an adjunct information, the final map is able to define the organogenic seafloor, usually called *matte* (assemblage of intermingled dead rhizomes with sediment).

3.7 CONCLUSIONS

This study develops a processing chain where the spectral mixture analysis of pixels resulted a valid method for the identification of a variety of different shallow seabed typologies. *P. oceanica* presence and the degrees of cover as well as the arrangements of the scattered patches of seaweeds are obtained by applying the FHyL processing chain that uses a multisensory data fusion to output detailed biophysical map. By integrating LiDAR bathymetry and point cloud standard deviation the range between 3 and 6 m of depth has been identified as the threshold range for accurate shallow seabed habitat mapping as well as for seafloor geomorphic characterization. The use of field radiometry and sampling to quantify abundance of cover classes not only offered a significant advantage over conventional approaches but it introduces the possibility for new insight in coastal habitat classification by traditional methods. If the spectral dissection of seawaters and seabed composition observed with LiDAR, field spectral library and the image based EMs collection leads to map seabed habitat at synoptic scale, in the range of wavelengths between green and blue, the added effect of the seawaters and vegetation absorption become combined and spectral signature of *P. oceanica* can be isolated in specific ranges of depth. Along the -3m line shallow seawater absorption generally combined with the suspended particulate matter and atmospheric moisture reduce imagery quality. The spectral library introduced in the linear mixture model both lowered the reflectance and enhanced the variety of vegetated and not vegetated seabed leading to a magnification of results. The strategy of combining high and very high resolution in a multisensory and multi resolution analysis includes different way of data fusion to assimilate spectral and spatial variability in complex coastal seabed mapping. Seafloor morphology become the driving factor for vegetated habitat classification and the implemented final map contributes to the knowledge of relationships between seabed and seawaters mixed absorption as well as between sediment and benthic vegetation interaction. FHyL is designed to gather and synthesize data for accurate multisensory analysis in complex coastal seabed habitat mapping and monitoring at regional and local scales.

Acknowledgements

The Lazio Region funds this research within the CAMP Project and a special thanks is addressed to Eng. Paolo Lupino for his interest through it all. Personal and great thanks goes to Luisa Nicoletti and Monica Targusi for contributions in biological interpretation of spectral data, to Federico Filipponi for data procecissing, to Raffaele Proietti for GIS expert solutions and to Alfredo Pazzini for field surveys.

3.8 REFERENCES

1. AA. VV. (1996). Morfologia e sedimentologia della spiaggia e della piattaforma continentale interna. In *Il mare del Lazio*, University of Rome 'Sapienza' and Latium Region press, 62-105.
2. Alberotanza, L., Cavalli, R. M., Pignatti, S., &Zandonella, A. (2006). Classification of submersed aquatic vegetation of the Venice lagoon using MIVIS airborne data. *Annals of Geophysics*, 49, 271-276.
3. Asner, G. P, Knapp, D. E., Boardman, J., Green R. O. (2012) Carnegie Airborne Observatory-2: Increasing science data dimensionality via high-fidelity multi-sensor fusion. *Remote Sensing of environment,* 124, 454-465.
4. Augier, H. (1986). L'herbier a *Posidonia oceanica*, son importance pour le littoral Mediterraneen, sa valeur comme indicateur biologique de l'etat de sante de la mer, son ultilisation dans la surveillance du milieu, les bilans ecologique et les etudes d'impact. *Vie. Mar*, 7, 85-113.
5. Baldridge, A. M., Hook, S. J., Grove, C. I., &Rivera, G. (2009). The ASTER spectral library version 2.0. *Remote Sensing of Environment*, 113, 711-715.
6. Barillé, L., Mouget, J. L., Méléder, V., Rosa, P., & Jesus, B. (2011). Spectral response of benthic diatoms with different sediment backgrounds. *Remote Sensing of Environment*, 115(4), 1034-1042.
7. Basterretxea, G., Orfila, A., Jordi, A., Casas, B., Lynett, P., Liu, P.-F., Duarte, C.M., &Tintore, J.(2004). Seasonal dynamics of a micro tidal pocket beach with *Posidonia oceanica* seabeds (Mallorca Spain). *Journal of Coastal Research*, 20(4), 1155–1164.
8. Bazzani, M. &Cecchi, G. (1995). Algae and mucillagine monitoring by fluorescence LiDAR experiments in field. *EARSeL, Advances in Remote Sensing*, 3, 90-101.
9. Bierwirth, P. N., Lee, T. J.,& Burne, R. V.(1993). Shallow sea-floor reflectance and water depth derived by unmixing multispectal imagery. *Photogrammetric Engineering and Remote sensing*, 59(3), 331-338.
10. Call, K. A., Hardy, J. T., &Wallin, D. O.(2003). Coral reef habitat discrimination using multivariate spectral analysis and satellite remote sensing. *International Journal of Remote sensing*, 24, 2627–2639.
11. Calvo, S., Ciraolo, G., & La Loggia, G. (2003). Monitoring *Posidonia oceanica* meadows in a Mediterranean coastal lagoon (Stagnone, Italy) by means of neural network and ISODATA classification methods. *International Journal of Remote Sensing*, 24(13), 2703-2716.
12. Cappucci, S., Amos, C.L., Hosoe, T., & Umgiesser, G., (2004). SLIM: a numerical model to evaluate the factors controlling the evolution of intertidal mudflats in Venice Lagoon, Italy. *Journal of Marine System*, 51/4: 257-280.
13. Cohen, W. B., & Goward, S. N. (2004). Landsat's role in ecological applications of remote sensing. *BioScience*, 54(6), 535-545.
14. Daedalus (1993). Daedalus Manual's Maintenance Manual AA5000 Multispectral Infrared and Visible Imaging Spectrometer (MIVIS), 2.
15. Dekker, A.G., Brando, V.E., & Anstee, J.M. (2005). Retrospective seagrass change detection in a shallow coastal tidal

Australian lake. *Remote Sensing of Environment*, 97, 415-433.
16. Diviacco G., Spada E.,& Virno Lamberti C. (2001). Le fanerogame marine del Lazio, ICRAM, 113 (Annex III).
17. Fornes, A., Basterretxea, G., Orfila, A., Jordi, A., Alvarez, A., & Tintore, J. (2006). Mapping *Posidonia oceanica* from IKONOS. *ISPRS journal of photogrammetry and remote sensing*, 60(5), 315-322.
18. Fraschetti, S., Terlizzi, A., & Benedetti-Cecchi, L. (2005). Patterns of distribution of marine assemblages from rocky shores: evidence of relevant scales of variation. *Marine Ecology Progress Series*, 206, 13-20.
19. Friend, P.L., Ciavola, P., Cappucci, S., & Santos, R., (2003). Bio-dependent bed parameters as a proxy tool for sediment stability in mixed habitat intertidal areas. *Journal of Coastal Research*, 23: 1899-1917.
20. George, D. G. (1997). Cover Bathymetric mapping using a Compact Airborne Spectrographic Imager (CASI). *International Journal of Remote Sensing*, 18(10), 2067-2071.
21. Giardino, C., Bartoli, M., Candiani, G., Bresciani, M., & Pellegrini, L. (2007). Recent changes in macrophyte colonisation patterns: an imaging spectrometry-based evaluation of southern Lake Garda (northern Italy). *Journal of Applied Remote Sensing*, 1, 011509.
22. Giardino, C., Candiani, G., Bresciani, M., Lee, Z., Gagliano S., & Pepe, M. (2012). BOMBER: a tool for estimating water quality and bottom properties from remote sensing images. *Computers & Geosciences*, (in press). Vol. doi:10.1016/j.cageo.
23. Green, R. O., & Boardman, J. (2000). Exploration of the relationship between information content and signal/noise ratio and spatial resolution in AVIRIS spectral data. In Green R. O. (Ed.), *Proceedings of the Ninth JPL Airborne Earth Science Workshop*, Pasadena, CA (pp. 195– 206).
24. Groom, G., Mücher, C. A., Ihse, M., & Wrbka, T. (2006). Remote sensing in landscape ecology: experiences and perspectives in a European context. *Landscape Ecology*, 21(3), 391-408.
25. Hakvoort, H., de Haan, J., Jordans, R., Vos, R., Peters, S., & Rijkeboer, M. (2002). Towards airborne remote sensing of water quality in The Netherlands—validation and error analysis. ISPRS *journal of photogrammetry and remote sensing*, 57(3), 171-183.
26. Han, L., & Rundquist, D. C. (2003). The spectral responses of Ceratophyllum demersum at varying depths in an experimental tank. *International Journal of Remote Sensing*, 24(4), 859-864.
27. Hochberg, E. J., & Atkinson, M. J. (2008). Coral reef benthic productivity based on optical absorptance and light-use efficiency. *Coral Reefs*, 27(1), 49-59.
28. Hooker, S. B., & Esaias, W. E. (1993). An overview of the SeaWiFS project. *Eos, Transactions American Geophysical Union*, 74(21), 241-246.
29. Hurtt, G., Xiao, X., Keller, M., Palace, M., Asner, G. P., Braswell, R., & Wickel, A. J. (2003). IKONOS imagery for the large scale biosphere–atmosphere experiment in Amazonia (LBA). *Remote Sensing of Environment*, 88(1), 111-127.
30. ISPRA, 2012. Rilievo di dettaglio della batimetria costiera laziale con tecnologie LiDAR e valutazione delle caratteristiche fisiche e biologiche in aree marine della costa laziale di specifico interesse ambientale, FASE 4. (Scientific Report-http://www.cmgizc.info/).
31. Johnson, P. E., Smith, M. O., & Adams, J. B. (1985). Quantitative analysis of planetary reflectance spectra with principal components analysis. *Journal of Geophysical Research*, 90, C81– C805.
32. Karpouzli, E., Malthus, T., & Place, C. (2004). Hyperspectral discrimination of coral reef benthic communities in the western Caribbean. *Coral Reefs*, 23(1), 141-151.
33. Keitt, T. H., & Urban, D. L. (2005). Scale-Specific Interface Using Wavelets. *Ecology*, 86, 2497–2504.
34. Kutser, T., & Jupp, T. L. B. (2006a). On the possibility of mapping to the species level based on their optical signature. *Estuarine and Coastal Shelf Science*, 69, 607-614.
35. Kutser, T., Vahtmae, E., & Metsamaa, L. (2006b). Spectral library of macroalgae and benthic substrates in Estonian coastal waters. *Proceedings of the Estonian Academy of Sciences*, 55, 329-340.
36. Lee, Z., & Carder, K. L. (2004). Absorption spectrum of phytoplankton pigments derived from hyperspectral remote-sensing reflectance. *Remote Sensing of Environment*, 89, 361-368.
37. Lewis, M. M. (2001). Discriminating vegetation with hyperspectral imagery - what is possible? In *Geoscience and Remote*

Sensing Symposium, 2001. IGARSS'01. IEEE 2001 International (Vol. 6, pp. 2899-2901). IEEE.

38. Lyzenga, D. R. (1978). Passive remote sensing techniques for mapping water depth and bottom features, *Applied Optics*, 17(3), 379-383.
39. Lyzenga, D.R. (1985). Shallow-water bathymetry using combined LiDAR and passive multispectral scanner data. *International Journal of Remote Sensing*, 6(1), 115-125.
40. Murphy, R. J., Tolhurst, T. J., Chapman, M. G., & Underwood, A. J. (2005). Remote-sensing of benthic chlorophyll: should ground-truth data be expressed in units of area or mass?*Journal of Experimental Marine Biology and Ecology*, 316, 69-77.
41. Murphy, R. J., Underwood, A. J., Tolhurst, T. J., &Chapman, M. G. (2008). Field-based remote sensing for experimental intertidal ecology: Case study using hyperspatial and hyperspectral data for New South Wales (Australia). *Remote Sensing of Environment*, 112, 3353-3365.
42. Paringit, E. C., & Nadaoks, K. (2003). Sediment yield modelling for small agricultural catchments: land-cover parameterization based on remote sensing data analysis. *Hydrological processes*, 17, 1845-1866.
43. Pergent-Martini, C., Leoni, V., Pasqualini, V., Ardizzone, G. D., Balestri, E., Bedini, R., Belluscio, A., Belsher, T., Borg, J., Boudouresque, C. F., Boumaza, S., Bouquegneau, J. M., Buia M. C., et al. (2005). Descriptors of *Posidonia oceanica*. *Ecological Indicators,* 5, 213-230.
44. Phinn, S., Dekker, A. G., Brando, V. E., & Roelfsema, C. (2005). Mapping water quality and substrate cover in optically complex coastal and reef waters: an integrated approach. *Marine Pollution Bulletin*, 51(1-4), 459–469.
45. Phinn, S., Roelfsema, C., Dekker, A., Brando, V., &Anstee, J. (2008). Mapping seagrass species, cover and biomass in shallow waters: An assessment of satellite multi-spectral and airborne hyper-spectral imaging systems in Moreton Bay (Australia). *Remote Sensing of Environment*, 112, 3413–3425.
46. Price, J. C. (1997). Spectral band selection for visible-near infrared remote sensing: Spectral-spatial resolution tradeoffs. *IEEE Transactions on Geoscience and Remote Sensing*, 35(5), 1277–1285.
47. Rainey, M. P., Tyler, A. N., Gilvear, D. J., Bryant, R. G., &McDonald, P. (2003). Mapping intertidal estuarine grain size distribution through airborne remote sensing. *Remote Sensing of Environment*, 86, 480-490.
48. Richardson, L., &Ledrew, E. (2006). Remote sensing of aquatic coastal ecosystem processes: Science & management applications, Remote sensing & digital image processing, 9.
49. Richter, R. (2009). Atmospheric/Topographic Correction for Satellite Imagery. *DLR report DLR-IB 565-01/09*, Wessling, Germany.
50. Sabol, D. E., Adams, J. B., & Smith, M. O. (1992). Quantitative sub-pixel spectral detection of targets in multispectral images. *Journal of Geophysical Research*, 97, 2659–2672.
51. Schnurr, D., Pettersson, M., & Grierson, H. (2004). Investigation, assessment and correction of systematic errors in large LiDAR dataset, Proceeding of the RSPSoc/BGS Meeting, 11-12 November, England.
52. Sellers, P. J., Meeson, B. W., Hall, F. G., Asrar, G., Murphy, R. E., Schiffer, R. A., & Try, P. D. (1995). Remote sensing of the land surface for studies of global change: Models—algorithms—experiments. *Remote Sensing of Environment*, 51(1), 3-26.
53. Silva, T. S., Costa, M. P., Melack, J. M., &Novo E. M. (2008). Remote sensing of aquatic vegetation: theory and applications. *Environmental Monitoring and Assessment*, 140, 131–145.
54. Small, C. (2004). The Landsat ETM+ spectral mixing space. *Remote Sensing of Environment*, 93, 1–17.
55. Small, C., Steckler, M., Seeber, L., Akhter, S.H., Goodbred, Jr. S., Mia, B.,&Imam, B. (2009). Spectroscopy of sediments in the Ganges-Brahmaputra delta: Spectral effects of moisture, grain size and lithology. *Remote Sensing of Environment*, 113, 342–361.
56. Smith, M. O., Ustin, S. L., Adams, J. B., & Gillespie, A. R. (1990). Vegetation in deserts: I. A regional measure of abundance from multispectral images. *Remote sensing of Environment*, 31(1), 1-2.
57. Taramelli, A. (2011). Detecting Landforms Using Quantitative Radar Roughness Characterization and Spectral Mixing Analysis. *Geocomputation, Sustainability and Environmental Planning*, 348, 225-249.

58. Taramelli, A., Pasqui, M., Barbour, J., Kirschbaum, D., Bottai, L., Busillo, C., Calastrini, F., Guarnieri, F.& Small, C. (2012). Spatial and temporal dust source variability in Northern China identified using advanced remote sensing analysis. *Earth Surface Processes and Landforms*. DOI: 10.1002/esp.3321
59. Underwood, A.J., Chapman, M.G., & Connell, S. D. (2000). Observation in ecology: you can't make progress on processes without understanding the patterns. *Journal of Expert Marine Biology and Ecology*, 250, 97-115
60. Ustin, S. L., Roberts, D. A., Gamon, J. A., Asner, G. P., & Green,R. O. (2004). Using Imaging Spectroscopy to Study Ecosystem Processes and Properties.*BioScience*, 54(6), 523-534.
61. Valentini, E., Taramelli, A., Bresciani, M., Giardino, C., Filipponi, F., Targusi, M., Manzo, C., & Disperati, L. (2012). Spectral libraries for emerged and submerged sandy beach using hyperspectral data. ESA – Ecological Society of America, 97th Annual Meeting Book of Abstracts and Poster session 2012, http://cdn.f1000.com/posters/docs/251665544.
62. Wittlinger, S. K., & Zimmerman, R. C. (2000). Hyperspectral remote sensing of subtidal macroalgal assemblages in optically shallow waters. *Proc. Ocean Optics* XV. SDROM.
63. Wulder, M. A., Hall, R. J., Coops, N. C., & Franklin, S. E. (2004). High spatial resolution remotely sensed data for ecosystem characterization. *BioScience,* 54, 511–521.

4. Use of Airborne Lidar and Hyperspectral data to study the sandy beach morphology along the Lazio region coast (Italy)

A. Taramelli [1], E. Valentini [1], C. Innocenti [1], S. Cappucci [2], M. Conti [1], E. Pallottini [1]

(*) ISPRA - Institute for Environmental Protection and Research, Rome, Italy
(**) ENEA – National Agency for new technologies, energy and sustainable development

ABSTRACT

Coastal landscape, and its evolution over time, provides the outline on which life must function and dictate the ecosystems and human activities that can exist or develop in a specific region. Basically emerged and submerged morphology, from terrestrial to aquatic environments, represents the structural feedback for sediment capping of coastal areas and influences coastal erosion and beach dunes system stabilization. This research addresses the feedbacks mechanism between morphology and linked ecosystem using multisource dataset (Hyperspectral - MIVIS and topographic/bathymetric LiDAR - Hakw-eye II). A physically based approach was applied to Hyperspectral and LiDAR airborne data, simultaneously acquired on 12 May 2009 in order to integrate geomorphological and ecological observations into detailed biophysical maps of the physiographic unit named Sabaudia (Lazio Region - Central Italy). The basic strategy was to highlight the different components of the coastal system through:

1) maps of coastal morphology, where the topography and bathymetry DSM were used to produce a) the contour line of the +0.3 m on the mean sea level, to obtain a tide independent shore line; 2) combined use of standard deviation maps and endmembers fraction maps, obtained by means of the Spectral Mixture Analysis (SMA) of hyperspectral data, to discriminate different types of bottom and surface cover. To extrapolate progressive evolution of the physiographic unit we have twisted a specific effort to quantify vegetation fractions pattern in emerged morphology highlighting the central role of the feedbacks between biological and physical processes that links the sand dune system stabilization to the shallow water seabed temporal evolution. The work did so far provide a good foundation for an intensive spatial analysis for the coastal sand-dunes system.

Keywords: Beach morphology, LiDAR-DSM, vegetation patterns, hyperspectral, spectral mixing analysis

4.1 INTRODUCTION

Sandy coasts are dynamic systems naturally subject to morphological and ecological changes due to factors external to the system. Coastal environments may also be subjected to occasional disturbances of varying spatial and temporal intensity (stochastic extreme event), after which they tend to recover to dynamical equilibrium (resilience of the system toward a steady state). Erosion is caused by a large number of factors such as changes of winds regimes and coastal current, increase of wave energy and coastal anthropization. The impact of human activities that involves the loss of coastal wetlands and deforestation; the construction of dams along the rivers and their discharge control, the construction of jetties at sea and other engineering works, is altering the natural equilibrium of coastal areas and consequently affect the distribution of renovated surface and ground water, sediments and nutrients in coastal habitats and beaches (Cappucci et al., 2011). The compromise of the delicate equilibrium governing the coastal habitats creates a major impact on all living habitats associated with this complex ecosystem. Understanding of conservation status, evolution method and coast dynamics is essential not only for the protection of habitats, but also for proper management of all components of the coast (Saye et al., 2005). Submerged beach, backshore and dune area are three separate interdependent elements in this full context. For that, we plausibly expect that changes affecting one of these three components have direct or indirect influence on the state of the other two (Psuty, 1988; Saye et al., 2005). For the purposes of proper management and planning, and in accordance with the principles of Integrated Coastal Zone Management (ICZM) the coastal system must be studied and analyzed in its three components, in terms of both physical and ecological approach (Irish and White, 1998; Rodriguez et al., 2009). Therefore, it is necessary to identify morphological and ecological parameters as expression of health/vulnerability status of coastal systems and, then to develop indicators of the changes made (Silvestri et al., 2003; Taramelli et al., 2010; Volpe et al., 2010).

The techniques that actually the Geomatics provides the scientific community are particularly suitable for collecting morphological and ecological information in order to identify and quantify the relative indicators. Among these, morphometric parameters related to ecological parameters (such as vegetation presence/absence and structure) are generally important and are of particular relevance in the dunes system coastal context

(Mason et al., 2010). They, in fact, represent the interface between the marine and terrestrial environments and the place where many biogeochemical processes take place (Taramelli et al., 2010; 2011). A great effort has been spent to discover patterns and relationships within dunes system areas, in order to reach a successful management and monitoring of these transitional environments (White and Wang, 2003; Pallottini and Cappucci, 2009; Pallottini et al., 2010; Simeoni et al., 2007). The quantitative morphological analysis applied to parts of the coastline, through investigating feedback mechanisms among them and properly integrated with ecological and environmental studies, is very useful to identify and assess any critical system, such as those related to erosion and/or extreme profile change (Bauer and Davidson-Arnott, 2003, Davidson-Arnott, 2005, Davidson-Arnott et al., 2005; Cappucci et al, 2004; Pallottini et al., 2010; Simeoni et al., 2000). An innovative approach recently used is the combination of two innovative remote sensing techniques that can be used to study the sediment dynamics and the vegetation patterns (both emerged and submerged), and hence the morphodynamics, along sandy shorelines (Deronde et al., 2003; Taramelli et al., 2011). Remote sensing in general is a very powerful tool for beach monitoring and investigation, since it allows collection of spatially continuous information over a vast area in a short time frame (Taramelli et al., 2009). Cracknell (1999) and subsequently Malthus and Mumby (2003) provided the starting overview of the capacities of remote sensing for estuarine and coastal zone studies. While the focus in these review articles is mainly on low-resolution remote sensing, Mumby and Edwards (2002) investigated the additional value of very high- resolution hyperspectral data. The latter is highly important in coastal areas as this environment is subject to fast changes in time (Adam et al., 1998; Silvestri et al., 2003; Brock and Purkis, 2009). Moreover, the technique is not hampered by the (in)accessibility of a site, which is often a problem in coastal areas. However, their fixed orbit limits the common spaceborne platforms, making use of sun-synchronous satellites (Wensink et al., 1997; Calkoen et al., 2001). This implies that acquisitions cannot be planned in time; hence, tides and weather often prohibit successful acquisitions. Airborne remote sensing on the other hand, although often more expensive and with limitation in high frequency acquisition, is much more flexible. It allows a mission to be planned carefully, taking into account all possible constraints. In addition, for implementing morphometric analysis, the necessary starting point is the availability of an accurate Digital Terrain Model (DTM), or at least a surface model (DSM) of onshore and nearshore coastal areas (backshore, dune and shallow water), datasets that may be obtained through several measurement techniques, in some cases affected by drawbacks (Pallottini et al., 2010). One of the most used methods for acquiring topographic data is the use of total station (expected accuracy 1-5 cm), and GPS RTK (Real Time Kinematics; 1-10 cm) (Morton et al., 1993; Pallottini et al. 2010). However, the use of these instruments involves a significant undertaking from the standpoint of logistics and acquisition of field data. From the logistics, for instance, the topographic survey of much vegetated coastal dunes or, in general, of not accessible areas, it can be very difficult or impossible. Thus, the density of data collected in situ by direct measurement techniques is often spatially heterogeneous, such as singular profiles of emerged beach and dune, or limited areas not so representative of study site (Andrews et al., 2002). In recent years, to overcome these problems and for the construction of DSM and DTM, on a wide scale range regardless of the site characteristics, laser altimetry technology is spreading through the use of LIDAR bathymetric airborne (Deronde et al., 2006; Taramelli et al., 2009). These two approaches measurements provide 3D digital representations (3D clouds) of extremely wide surfaces (from squared km to hundreds of squared km), with high density (cm-m) and high accuracy (cm-dm), solving large part of the above critical states for direct in situ measurement. However, currently the high costs of LIDAR flights with ranging greater than 300 m, can significantly affect the planning of acquisitions with high temporal frequency (Brock and Purkis, 2009).

Numerous examples of coastal monitoring studies may be cited, that integrate field data with remote sensing data (Adams et al., 2010; Arens, 1994; Atearn et al., 2010; Brook and Purkins, 2009; Davidson-Arnott et al. 2005; Goodman et al., 2008; Liu et al., 2011; Malthus and Mulby, 2003) in order to overcome the limitations of methodological approaches. Besides morphometric analysis, other study based on the use of Geomatics techniques can provide important support for the understand health/vulnerability status of coastal systems. Multispectral and hyperspectral remote sensing provides data sets allowing, for example in environmental sector, mapping of habitat heterogeneity (Artigas and Yang, 2005; Pignatti et al., 2009) study of vegetation cover in wetlands (Bellucci et al., 2006; Barducci et al., 2009), the mapping of invasive plants distribution

(Lawrence et al., 2006; Tsai et al., 2007), and mapping of plant species (Boschetti et al., 2007; Calvo et al., 2003; Giardino et al., 2009; Marani et al., 2006). Hyperspectral data analysis was also used to obtain quantitative information on mineral composition, grain size composition and water content of soils and sediments (Innocenti et al., 2011; Taramelli et al., 2012 in review). These parameters are important for identifying feeding areas, for evaluation of erosion/deposition processes function of the system exposure, for advancement/retreat monitoring of the coastline on the properties and for vegetation on the backshore of the beach.

MIVIS (Multi-spectral IR and Visible Imaging Spectrometer) and LiDAR (Light Detection and Ranging) airborne data simultaneously acquired are integrated with accurate field campaign and a collection of different biophysical parameter has been achieved. Different types of MIVIS-derived map of were merged to bathymetry and topography DSMs derived from LiDAR for generating the preliminary classification of the biophysical habitat.

4.2 STUDY AREA

The research area between Torre Astura and the San Felice Circeo Promontory (Figure 4.1) is sandy and is characterized by a dune system parallel to the coastline, which once ran without interruption throughout the physiographic units (Campo and La Monica, 2006), while today it covers about 80% (25 miles). The origin of these coastal dunes appears to be related to the formation of a sand bar as a result of increasing sea level rise within the age's Versiliana (Blanc et al., 1953; Giovagnotti et al., 1980), and by the increasing importance over time of the wind power action.

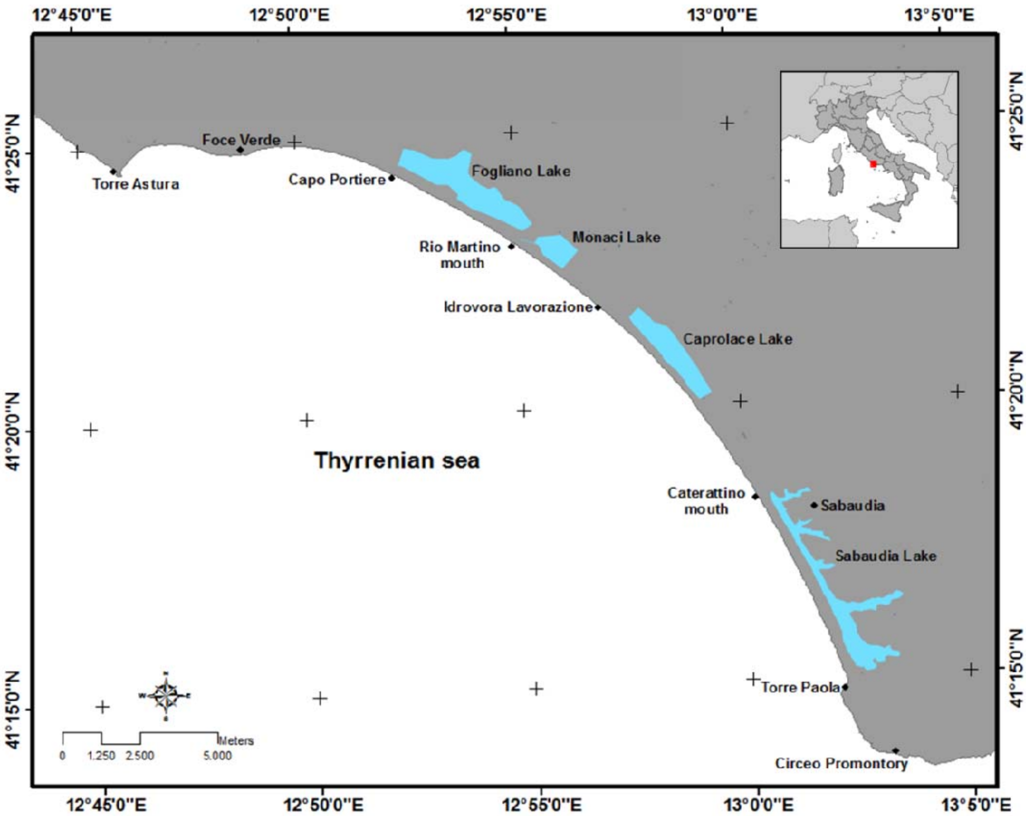

Figure 4.1 - Study area

Both the proportion and amplitude of these "convex system" increase from north to south to the 28 m maximum elevation above sea level and 250 m wide near Torre Paola (Campo and La Monica, 2006).

The dunes are mostly established by specialized Mediterranean coastal vegetation, (Giovagnotti et al., 1980; Pallottini and Cappucci, 2009; Pallottini et al., 2010). Due to the different exposure to wind and insolation, it is possible to distinguish two different sectors along the dunes: the side facing towards the coastal lakes, characterized by the presence of a well-structured tree and shrub vegetation, and the one facing the sea, characterized by a vegetation mostly xerophytic bush and halophyte, that can stabilize the sands and reduce aeolian transport through specialized root systems, thereby triggering positive feedback mechanisms between the biological and sedimentological components, which give dynamic stability and resilience to the system exposed to natural and manmade disturbances (Pallottini and Cappucci, 2009).

In the 50's the dynamics of the system, orthogonal to the shoreline, was blocked by the construction of the coastal road at its dune crest longitudinal axis. In addition, to prevent the free morphological evolution (i.e. the free feed and withdrawal that would limit the damage produced by the erosive wave action), increased erosion due to runoff phenomena contributed to making the entire coastal area more accessible during summer (Pallottini and Cappucci, 2009).

In the late 80s, the stretch of road between the mouth of the Rio Martino and the Idrovora Lavorazione (central part of the area) has been seriously damaged by a storm event, and as a result has not been opened to traffic and was the subject of remedial and preservation of the beach-dune system.

4.3 DATA AND MATERIALS

The methodology adopted in this paper is based on two types of airborne remote sensing data: hyperspectral imagery and LiDAR altimetry (Figure 4.2). Hyperspectral remote sensing, or imaging spectroscopy, is the acquisition of images in hundreds of (contiguous) spectral bands that for each pixel through complete reflectance spectrum (Goetz, 1992). Reflectance is defined as the ratio of the radiance of the reflected light over the radiance of the incoming light at a certain wavelength. Each pixel element contains a unique reflectance spectrum that can be used for the identification of the Earth's surface materials. When light interacts with the Earth's surface, certain wavelengths are preferentially absorbed, whereas other wavelengths are transmitted or reflected. The kind of material determines the degree to which light of different wavelengths is absorbed. The part of the sunlight not absorbed (or transmitted) is reflected and determines the colour of the material. In this way, each material has its own spectral signature by which it can be identified.

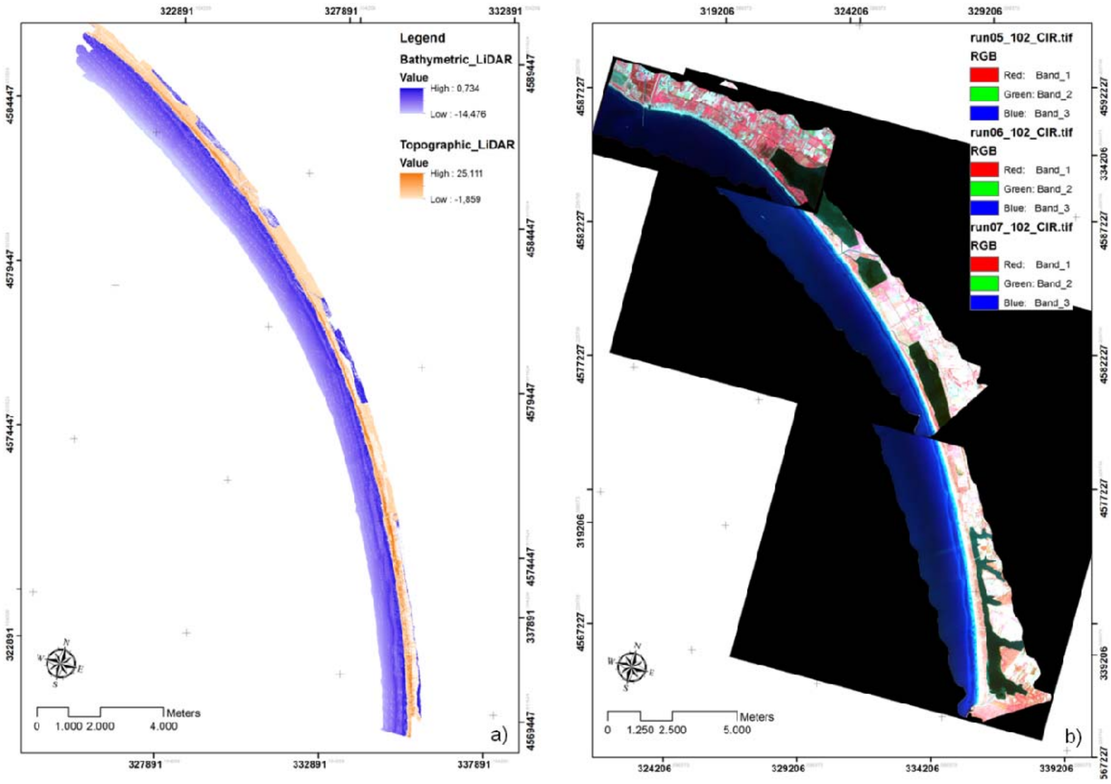

Figure 4.2 - a) Bathymetric and Topographic LiDAR and b) hyperspectral MIVIS datasets

LIDAR (light detection and ranging) is a scanner that deflects a laser beam across the flight line and detects its reflection, so that a swath of ground along the flight line is sampled point wise. The distance to the Earth's surface is determined by measuring the pulse return time. The position and altitude of the sensor is calculated by a GPS/IMU system (Global Positioning System/Inertial Measurement Unit). In combination with the scan angle, the 3D position of each laser beam spot on the surface can be determined. On flat not vegetated surfaces, a vertical accuracy of 5–10cm can be achieved. The development of LIDAR represents a technological breakthrough in topographic monitoring. A number of studies have demonstrated the ability of LIDAR data to accurately represent topography over large sections of coastline (Revell et al., 2002; Sallenger et al., 2003; White and Wang, 2003), and sequential LIDAR surveys have shown that shoreline changes can be monitored over time (Stockdon et al., 2002; Tebbens et al., 2002). Brock et al. (2002) provide a good overview of the basic principles of airborne laser altimetry.

4.3.1 LIDAR ACQUISITION

To achieve the objectives of this study we used the data acquired from May 2009 BLOM-CGR through simultaneous use of LiDAR sensors (topographic and bathymetric) and hyperspectral MIVIS (ISPRA, 2009a, 2010). The LiDAR sensor acquisition, for the purposes of this study, was executed by the sensor Hawk Eye II (Steinvall et al., 1994; Koppari et al., 1994; Schnurr, 2010), with a total of 42 strips for the Sabaudia Area (ISPRA, 2009b). The main difference between topographic and bathymetric Hawk Eye II LiDAR lies in the type of laser and related wavelengths of radiation used. The topographic LiDAR uses infrared wavelengths, unable to penetrate into the waters. The bathymetric LiDAR uses two distinct radiations and is characterized by different wavelengths: a band in the infrared (wavelength of 1064 nm) for the measurement of the free surface and one in the green band (wavelength of 532 nm) for the measurement of seabed (Schnurr, 2009; Taramelli et al., 2009). The cover strips ranges from a maximum altitude of about 346 m, and a minimum of about -26 m, for the Sabaudia Area. The depths identified by bathymetric LiDAR were determined for each pulse from the time differences between the feedback signal received from the water surface and the return signal received from the seabed. In fact, the two different channels that work as a receiver are used separately: one for the estimation of the return of a surface and the other to estimate the return from the bottom (Guenther et al., 1994). For this reason, we eliminate the effects of surface waves (Thomas and Guenther, 1990) and a series of errors of measurement on the surface (Guenther, 1986) that act on the bottom (Guenther and Thomas, 1984). Although a number of technical difficulties related to turbidity have been solved in different ways for different acquisition systems in literature, many of the limitations of bathymetric LiDAR involving the physics of light propagation in water were common also to our acquisition. The strips acquired during the overpass were arranged in parallel and overlap the sides for about 20-30%. The final point clouds LiDAR, due to non-homogeneity of the points' density (Guenther, 2007; Irish and White, 1998; Quadros et al., 2008; Schnurr, 2009), were therefore more focused on the edges of the strips (ISPRA, 2009; Innocenti et al., 2012).

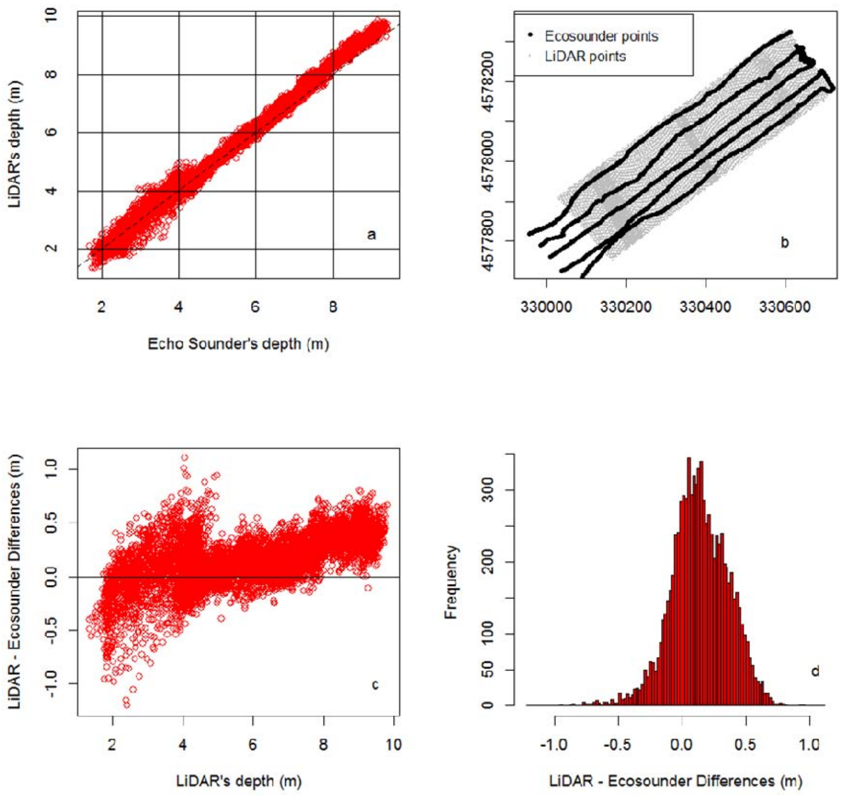

Figure 4.3 - a) Performance of the submerged LiDAR data with singlebeam acquisition. a) and b) show differences in the acquisition with singlebeam and bathymetric LiDAR and the scatter plot of the difference between the two interpolated DSM (c).

Within Table 4.1 the main technical characteristics of the LiDAR HawkEye II sensors are highlighted.

Table 4.1 - Technical features of topographic LiDAR sensor and positioning system.

LiDAR HawkEye II	
Topographic LiDAR Frequency	64,000 Hz
Altitude	From 250 to 500 m
Swath	From 100 to 330 m
Topographic point density	Tipicamente da 1 a 4 punti per m^2
Accuracy of Topographic survey	Horizontal: ± 0,5 m Vertical: ± 0,15 m

With regard to the emerged area to define the accuracy of the data, refer to the Pallotini et al., 2010 published paper. With regard to the performance and accuracy of the submerged LiDAR data we used a singlebeam acquisition (Figure 4.3b) where the comparison was carried out through a traditional assessments accuracy metrics such as the differences (Athearn et al., 2010; Goodman et al., 2008). Figure 4.3a and 4.3d shows, both the spatial resolution of the different measuring points of the seafloor (determined by differences in the acquisition system with singlebeam and bathymetric LiDAR) and the scatter plot of the difference between the two interpolated DSM (Figure 4.3c). The results show a varying constant overestimation of the LiDAR DSM over the singlebeam of about -20 cm that slightly increase offshore above 8 m of depth. The algorithms of the Airborne Hydrography AB (Isaksson, 2009: Schnurr, 2010) used by the Bloom Aereofilms for the final point cloud generation calibrates the data post-processing using a topographic RTK with errors estimated of 50 cm. From literature (Guenther and Thomas, 1984) the specific LiDAR returns from different targets without considering the full waveforms, showing results of beam propagation in water, which expands in a different way after rebound/backscatter. The effective diameter in deep water is half the depth (number of scattering lengths) while in shallow water this causes an overestimation of the bathymetry (Goodman et al., 2008). Bearing in mind the effects of the density number of points available within a single cell (in our case 4x4 m) is it possible to understand how the effect of an overestimation is due to the density of data acquisition. The area ratio and the target cell detection provide, in fact, a value that calculated the accuracy of return. In literature (Guenther et al., 1996), the ratio is 1.78 for 3x3 m, 5x5 m to 0.64, and 0.16 for 10x10 m. This applies only when the result is less than unity. Multiplying the values of literature, the biggest advantage of the actual factor of 1.78 has occurred in the 4x4 m acquisition with a probability of around 0.5 (Guenther et al., 1996).

4.3.2 MIVIS DATA AND VALIDATION MEASUREMENTS

The hyperspectral remote sensing, also known as spectroscopy, is a technology used in the detection and identification of aquatic and terrestrial vegetation, minerals, materials and man-made environments (Alberotanza et al., 1999; Boschetti et al., 2007; Calvo et al., 2003; Giardino et al., 2007; Rainey et al., 2003; Small et al., 2009; van der Wal and Herman, 2007). The high resolution hyperspectral data obtained from the airborne sensors allows to extract information about: chlorophyll and leaf moisture, sediment soil and seabed types, decomposing organic materials, waters and coastal vapour, clouds and many other environmental parameters (Deronde et al., 2006; Ibrahim and Monbaliu 2011).

The MIVIS sensor is an airborne hyperspectral scanner with 102 spectral channels (or bands organized as modular tool, consisting of four spectrometers that simultaneously reproduce the radiation from the Earth in the visible (20 bands between 0.43 and 0.83 µm), near infrared (8 bands between 1.15 and 1.55 µm), middle infrared (64 bands between 2.0 and 2.5 µm) and thermal infrared (10 bands between 8.2 and 12.7 µm).

The acquisition campaign of May 2009 along the coast of Lazio returned with a significant nadir IFOV (Instantaneous Field of View) of 2 mrad, a scanned field of view of 71.059 °, an accuracy of the digitization of 12 bits per pixel and a resolution to soil of 3x3 m (average altitude of 1500 m flight) (Table 4.2).

.

Table 4.2 - Technical features of hyperspectral MIVIS sensor

MIVIS – ***Multispectral Infrared Visible Imaging Spectrometer***

	Wavelenght intervals	Spectral resolution
Spectrometer I	0,4 - 0,8µm	0,2 µm
Spectrometer II	1.2 - 1.5µm	0,5 µm
Spectrometer III	2.0 – 2.5µm	0,09 µm
Spectrometer IV	8.2 – 12.7 µm	3.4-5.4 µm
IFOV	2mrad	
scan/sec	25	
Digital accuracy	12bit x pixel, ±1 bit	

The collection of MIVIS imagery used for the extraction of vegetated dune is made up of 3 images in Band Sequential format (.bsq), georeferenced in UTM 33N WGS-84.

For the extraction of polygons containing areas, the dataset was resampled to 28 bands from 0.43 to 0.83 µm and from 1.15µm to 1.55µm, to consider different degrees of reflectance as a function of the state of stress and penology. The choice of this range is based on the known activities of reflection of the vegetation in the green (0.55 µm) and especially in the NIR between 0.75µm and 0.99µm (Allegrini, 2006).

The MIVIS dataset geometric correction was carried out directly by CGR (General Company of Aerial Acquisition), the company who made the airborne acquisition using techniques based on synthetic GCP points (ISPRA, 2009).

The evaluation of the distribution of brightness and radiance to the atmospheric attenuation measured by the sensor was evaluated taking into account local weather conditions at the time of the survey (ISPRA, 2010b). The error associated with the removal of these effects through the correction process depends on the atmospheric optical path length, the turbidity of the atmosphere and the codes used to remove it considering the conditions of solar illumination, sensor geometry, atmospheric attenuation and irradiance of the sky (Berk et al., 1989; Richter and Schläpfer, 2011).

Available algorithms to minimize variations caused by atmosphere, such as ENVI® FLAASH® module (Fast Line-of-sight Atmospheric Analysis of Spectral Hypercubes, published by Research Systems Inc. 2005), are based on atmospheric and maritime aerosol models as suggested in MODTRAN - moderate resolution atmospheric transmission (Matthew et al., 2000, Kaufman, 1989). The results of the atmospheric corrections return reflectance images with few black-null pixels randomly distributed in the portion of the images with lower values of radiances (sea waters and rivers). The MIVIS signal to noise ratio degrades in the presence of water and a non-differential component for vapour returns reflectance data that seemed source of artifacts (ISPRA, 2012). The results was also compared with a normalization to the irradiance sensor MIVIS for all 92 channels. The effect led to the standardization of reflectance values, especially in water, decreasing the possibility of resolving the individual pixels (Table 4.3).

Table 4.3 - Pearson correlation coefficients for MIVIS radiance/irradiance/reflectance analysis obtained on the image spectral profiles collection before and after the application of the two methodologies.

	At sensor radiance/ irradiance	At sensor radiance/ reflectance
submerged vegetation	0,99	0,85
emerged vegetation	0,99	0,98
submerged sand	0,99	0,96
emerged sand	**0,64**	**0,51**

Based on the analysis and the behaviour of the vegetation both in emerged and submerged area we choose to work directly on the radiance images. The choice is the most comprehensive in terms of the spectral behaviours of targets and gives the possibility to compare products obtained by each MIVIS scene.

Hyperspectral dataset was masked in order to subset the images allowing the reduction of time of processing and giving the possibility of detailed unmixing. MIVIS sensor register 10 thermal bands based on surfaces emissivity and a thermal threshold (17.5 °C) was obtained on spectral profiles cross to the shoreline in order to obtain two complementary masks that separate the onshore from sea. A spectral threshold (1.55 µm) was defined to analyse vegetation presence and variability. Finally a reduction of hyperspectral dataset was enhanced with a spatial reduction obtained with the information extracted by LiDAR that set the 'extent' or the Region of Interests (ROIs).

Measurements were made on several patches of the front shore of the dune belts that are occupied by homogeneous shrubs or herbaceous vegetation, generally greater than 50% of total cover. These areas are well characterized by botanists and ecologists (Pignatti et al., 2009) and a valuable support was obtained by using Trimble Pro-XRS (Trimble Navigation, Inc., Sunnyvale, CA) global positional system (GPS) in random validation test areas, not bigger then 3X3 m. Each area was classified directly with the visual estimation of percentage cover and a quick estimation of the main representatives species (Van der Maarel, 1979). Finally, we classified on the base of the percentage cover and by the type in 'mostly sand-partially vegetated', 'shrub and herbaceous vegetation', 'shrub and trees'. The field observations dataset was validated with land cover and habitat classification available at ISPRA based on ortho-photos (National Acquisition on the 2000 at scale 1:13.000) interpretation, Ground Control Points and other medium-resolution optical imagery (Landsat ETM+) standard classification (Casella et al., 2008; Capogrossi and Augello, 2008).

4.4 METHODS AND METHODOLOGY

The final point cloud of LiDAR was processed to obtain the topographic and bathymetric DSMs on regular grids. According to the points' density, the dimension of the grid cells was set to 2 m for the topographic DSM, and to 4 m for the bathymetric one. The elevation value for each cell was calculated averaging all the points included between the cell's boundary (Innocenti et al., 2011).

4.3.1 ANALYSIS OF LIDAR DATA

The processing of LiDAR data was conducted with the aim of obtaining useful information to the interpretation of the forms and dynamics of coastal areas identified. In this regard, using some basic attributes (elevation, slope, exposure angle, curvature and convexity) the analysis has been applied to different types of processes that have led to the creation of geomorphological parameters. Specifically a procedure was used for the extraction of the foot of the dune and some morphometric parameters from a model of the surface (DSM) developed by LiDAR data. For effective characterization of the coastal dunes, as well as several morphometric parameters that can be obtained with a LiDAR DEM is also necessary to investigate aspects of vegetation, closely linked by feedback mechanisms to the dynamics of aeolian deposits.

4.3.2 SHORELINES EXTRACTION

The shoreline has been identified with the contour lines of 30 cm above sea level. This reference was preferred at 0 m for two main reasons:

- The height of 30 cm is above the majority of maximum tidal levels in the area and thus presumably emerged during both surveys (Tebbens et al. 2002).
- The 30 cm isohypse is extremely more regular than the 0 m ones that tends to be more fragmented. This behavior is probably due both to the surface proprieties of the intertidal zone and to the lesser accuracy of LiDAR around 0 m (Guenther G.C., 2007).

4.3.3 EXTRACTION OF THE FOOT AND THE INNER EDGE OF THE DUNES

The definition of the extent and geometry of the aeolian deposits present within coastal areas were made from the LiDAR DSM by highlighting the position of the foot of the dune (ocean side) and the inner slope. These morphological elements were identified by calculating the slope already used in previous studies for the morphometric analysis of the dunes through the use of LiDAR data (Mitasova et al., 2005) and values of altitude (elevation) (Fig. 4b).

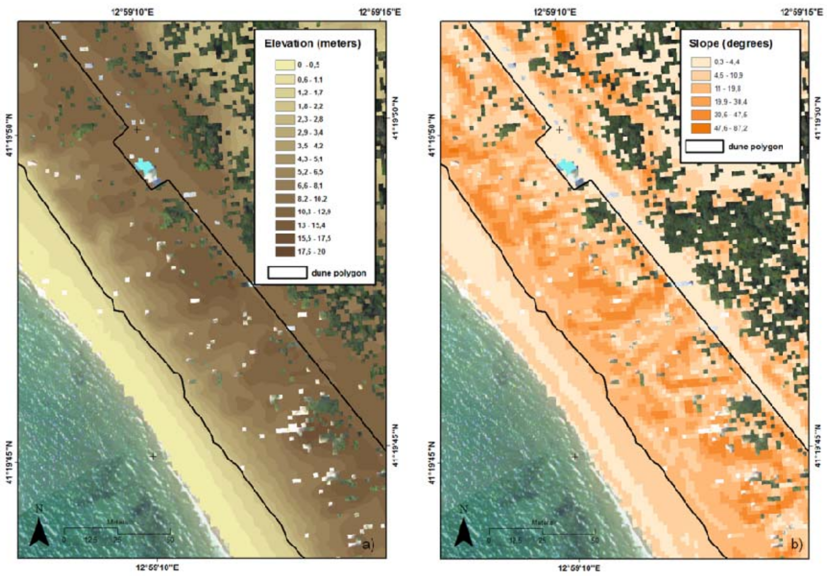

Figure 4.4 - Extraction of the foot and the inner edge of aeolian deposits on the base of elevation a) and b) slope.

The procedure for the extraction of the polygon of the dune was performed through the following steps:

a) Calculation of the slope on the DSM was created using the tool "Surface Analysis / Slope" present in the extension Spatial Analyst in ArcGIS ® 9.3 (Fig. 4.4).

b) Division into classes depending on the values of slope of the topography of the area. Following the steps listed below performed for the definition of classes of values:

I. visualization of isolines calculated from raster "Slope" with 0.5 ° interval.

II. Detection, within only marine side, of the area of thickening of the isolines, indicating a sharp increase in the slope of the land (identified as the transition zone emerged beach-dune). The band in which there was a thickening of the isolines was between the isolines is 4.5 ° and isolines 10 °.

III. Identifying the number of classes appropriate for a range that emphasize the emerged beach-dune transition identified in the previous phase.

c) Subdivision into classes of elevation values as a function of the morphology of the territory. Similar to what was seen for the identification of classes of slope, the definition of classes of values was performed by following the steps listed below:

I. visualization of isolines calculated from DEM with an interval of 0.5 m.

II. Detection, within only marine side, of the area of thickening of the isolines, indicating a significant increase in the slope value (identified as the transition zone emerged beach-dune). The band in which there was a thickening of the isolines was the one between the isolines 2.5 m and the isolines 1.5 m.

III. Identifying the number of classes appropriate for emphasizes emerged beach-dune transition identified in the previous phase.

d) Positioning of the foot of the dune (ocean side) by simultaneous display of orthophotos, elevation values and the values of slope (Display Scale: 1:1500 - 1:1000).

e) Completion of the polygon "Dune" and the definition of its internal limit. To avoid discrepancies where the morphological thresholds value coincides with the inner foot of the dune, it was reconstructed (the scale used to display the position of the limit is 1:3000):

I. where possible by interpreting the morphology of the cord as it appears in the ortho or

II. interpolated using as a support surface, or

III. at the limit of available data, or

IV. Corresponding to different types of man-made elements in the area (for example, limit cultivated fields, roads, buildings, etc...).

f) Validation and correction of the polygon by displaying three-dimensional polygon shape file on the orthophotos. For the 3D visualization software ArcScene was used, which allowed exaggerating the scale of allowances in order to highlight the morphologies observed with respect to sea level. In this case the scale of the vertical exaggeration of the relief is set with a ratio of 1:5.

Associated with the display of orthophotos in ArcScene dimension values were also used to describe the morphology and the identification of different morphological types of discontinuity, by observation of the characteristics of land cover associated with the morphological characteristics (axis of elongation, extension, shape).

4.3.4 MORPHOMETRIC ANALYSIS OF AEOLIAN DEPOSITS

Morphometric analysis of the beach-dune system and its temporal and spatial variation was investigated by using the software Digital Shoreline Analysis System (DSAS) 4.0 (Thieler et al., 2009). DSAS is an extension of ESRI's ArcGIS ® v. 9.x created to calculate the variation of time series of shape files through the generation of linear transects perpendicular to a line of reference (baseline) specially created by the operator. The analysis was used to identify and calculate the amplitude of the emerged beach in relation to dune foot using the LiDAR dataset. DSAS software was used to calculate the amplitude of the emerged beach and Polygon "dune".Morphometric parameters (amplitude of the emerged beach and Polygon "Dune") using the software DSAS 4.0 tool and the procedure described as follow:

a) Creation of the reference line, from which are generated transects (baseline) which is located at the coastal road that runs parallel to the coastline along the crest of the dune.

b) Conversion of the shape file polygon of linear dune in a shape files using the "polygon to line" in ArcGIS ® 9.3;

c) Perform 4.0 with DSAS transects positioned perpendicular to the baseline and with a wheelbase of 250 m. The parameters have been set as shown in Table 4.4;

Tabelle 4.1 - Table 4 -

Table 4.4 - Results of morphometric parameters extraction in nearshore beach dune system

Sector	Dune polygon	Dune amplitude (mean)	Dune elevation (range)	Dune elevation (mean)	Dune slope (range)	Dune slope (mean)	Beach width (range)	Shoreline
A	1 2	35 m	7 m - 12 m	9,5 m	0° - 51,3°	11,75°	12 m - 40 m	In the initial rather is regular. Going SE, pattern is characterized by irregular undulations.
B	3	22 m	7 m - 37 m	8 m	0,1° - 50,7°	14,75°	12 m - 32 m	In the first part of sector is characterized by a trend with the "cusp" that has irregular widths and lengths. Proceeding the shoreline is more regular.
C	4 5	50,3 m	10 m - 16	13 m	0° - 49,5°	13,41°	25 m - 60 m	Is characterized by a trend cuspidate with undulations characterized by irregular widths and lengths.
D	6	92 m	13 m - 27 m	9,9 m	0° - 57,1°	10,23°	15 m - 60 m	Is characterized by a trend cuspidate with undulations characterized by irregular widths and lengths.

Data input foot of the dune

- Shoreline
- Baseline

Main output data transects

- Distance between the baseline and the points of intersection between each transect and shape files

Variables calculated from the data output of the system

- Width beach - dune (distance between the baseline and shoreline)
- Amplitude of Dune (distance between the baseline and the foot of the dune)
- Amplitude of the beach (distance between the shoreline and the foot of the dune

4.3.5 EXTRACTION OF VEGETATED AREAS

The numerical analysis of hyperspectral images quantifies the signal response through products called thematic maps. The thematic map obtained by a classification algorithm, consists of a set of pixels associated to a particular class or category. These classes, such as different response of land use (agricultural areas, forest areas etc) are not recorded directly in the images, but they must be derived indirectly using the evidence contained in the spectral measurements presents the images. The similarity between pixels or groups of pixels is the fundamental concept upon which the majority of classification algorithms allow to divide the image pixels in groups with a certain degree of association. For each dune polygon the Normalized Difference Vegetation Index, that exploits the different response of vegetation cover in the visible spectral bands (red) and near infrared, was then calculated. The NDVI provides a dimensionless numerical value related to the health of plant biomass and photosynthetic processes, theoretically between -1 and +1. The characteristic behaviour of the pigments of the leaves not subjected to stress is in fact to reflect only about 10% of the radiation received in the spectral region of visible light (red), and at the same time reflect over 40% of that received in 'near infrared'.

In this case the evaluation of NDVI was used to get a synoptic view of biomass distribution of vegetation on coastal dunes and to discuss the accuracy of the results. MIVIS spectral wavelength used for NDVI are 12 or 13 for red and 19 or 20 for the infrared (Figure 4.5a).

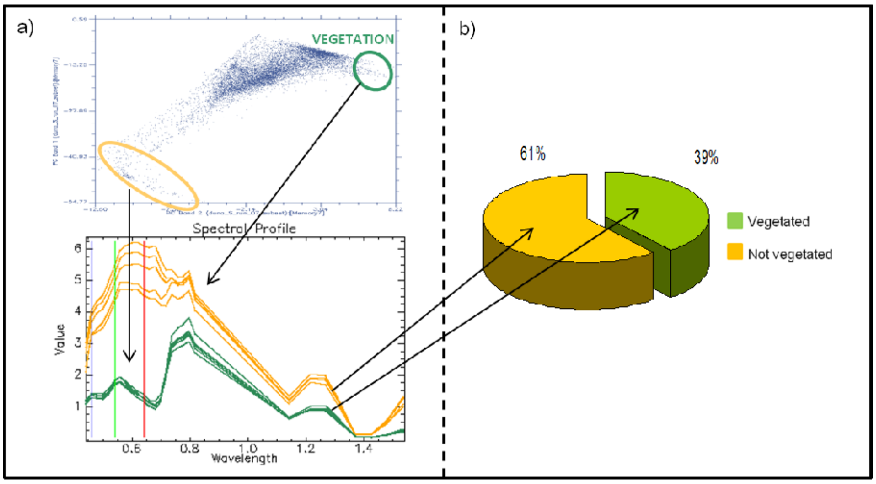

Figure 4.5 - a) Selection of training sets on the PC1vsPC2 scatter plot after the PCA rotation of 28 spectral bands from each MIVIS imagery. b) Example of the application of Supervised (MLLH) classification with selected training sets for vegetation presence/absence analysis.

4.3.6 PRINCIPAL COMPONENT ANALYSIS (PCA)

Among various feature reduction methods, principal component analysis (PCA) is a commonly adopted technique to reduce the dimensionality of remote sensing data. This analysis has advantages over more sophisticated feature reduction techniques: PCA is simple, straightforward, easy to use, and most importantly, has been implemented in almost all available remote sensing image processing and analysis packages (Tsai et al, 2007). In this work we used PCA as the fundamental framework to develop an appropriate feature space extraction helpful to the discrimination of target classes.

The PCA multidimensional space identified for each dune units or polygon on the 28 selected bands, allowed the identification of quotes of the scatter plots on the base of the first two or more dimensions as pure pixels (Boardman and Huntingon, 1997, Kruse et al., 1997). Two, three and four pure pixels were selected for each polygon (Fig. 5b) in order to collect vegetation, sands and eventually atrophic structures (Herold et al., 2004) pure signals (endmember). The spectral profiles that belong to these pixels were identified on the images and the spectra were attributed to the territorial units to which they belong (vegetation, sands and atrophic structures). The remaining pixels, the majority, were then combined in classes or levels according to their similarity with the sample pixels.

4.3.7 PRESENCE/ABSENCE OF VEGETATION

The supervised classification provides training phases of the algorithm chosen to provide examples of spectral behaviour (training set) of classes of interest. Presence and absence of vegetation was associated to pure pixel spectral profiles identified at the apexes of scatterplots. From the reference spectral profiles training areas were defined and used to run the maximum likelihood classification method (MLL - Richards, 1999) that works assigning each pixel to the class for which the conditional probability is greater defined as the probability that selecting a pixel x from the scene, it belongs to a particular class.

The MLL is a hard degree because pixels with radiance values very different from those of the categories initially defined are not included in any class and therefore are not classified. MLL in the classification procedure assumes that the distribution of reflectance values of each class is approximated to a normal distribution of the spectral data in multidimensional space.

The final classification generates two complimentary maps: one for vegetated pixel and the other one for sandy pixels (Figure 4.5b).

4.3.8 LANDFORM VEGETATION COVER STRUCTURE

Once we have extracted the vegetation polygon in the merged area, we choose to detect the potential of the first spectrometer of MIVIS to recognize coastal vegetation structural characteristics by reducing spectral threshold (0.75 µm) and performing again PC analysis on 20 bands In this way the recognition of red-blue wavelength provided a synoptic view of vegetation distribution with a physically based approach (Small, 2004; Small and Lu, 2006). The characterization of beach dunes habitat means that the transitional zones between land and water are detectable by the mixing model. We choose the linear unmixing to recognize the spectral mixing model that can describe the hyperspace of physical response of different vegetated surface. The unmixing linear model allows, in fact, the classification using 3 and 4 endmembers selection showing that mixed reflectance along the shoreline fit with the reality using the Spectral Mixing Analysis (SMA) (Figure 4.6).

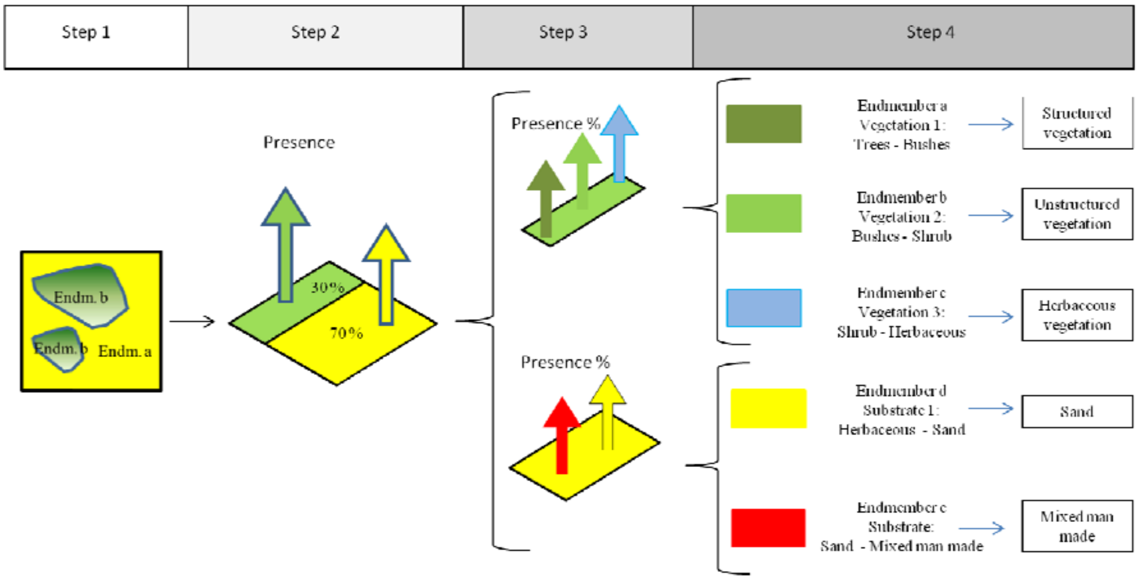

Figure 4.6 - The unmixing model implemented for each pixel of hyperspectral MIVIS imagery. Presence/absence of vegetation is obtained by the MLLH supervised classification, and then after picking up 3 vegetation endmembers and 2 substrates endmember 5 typologies of fraction map are defined.

Spectral Mixture Analysis (SMA) is a methodology for study and interpretation of the image that allows us to model the radiance of each pixel as a linear combination of spectrally pure radiances of targets contained within the pixels themselves (Adams et al. 1993; Boardman, 1989; Small, 2009). The potential of this technique is the ability to solve the information of mixed pixels, i.e. consisting of several reflective elements, based on the physical composition of the surface investigated. This methodology allows then to represent the entire scene as a map of fractions of endmember (pure elements), resolved with extreme accuracy, the spatial variation of different components (Adams et al. 1993; Boardman, 1989, Gillespie et al., 1990, Sabol et al., 1992, Smith et al., 1990;

Small, 2004; Taramelli and Melelli, 2009). The multidimensional space (mixing space) on which the analysis is finally performed for the selection of pure elements (endmember) is based on the Analysis of Principal Components (Adams et al. 1993; Boardman, 1989). As a final step the linear combination of the pure elements selected, weighted according to the fraction that they occupy within the pixel (Linear Mixture Model), returns a dynamic visualization/classification image in terms of variety and percentage of physical response.

The main steps are;

1) Determine mixing space topology and structure by Principal Component Analysis.
2) Determine dimensionality and linearity and select spectral endmembers:
    - Display scatter plots in 2 and 3 Dimensions on the base of cumulative variance
    - Pick endmembers from each apex of the mixing space by picking the endmember near the apex and saving the profile as an ASCII file. Display spectral profiles for each scatter plot.
    - Select the Substrate from the PC1vsPC2 plot and from the PC1vsPC3 (top view) that shows the 3D (in PC3 dimension) divergence of the mixing space approaching the substrate endmembers. Then at the opposite side of the PC1 and along PC2, vegetation endmembers can be selected on the base of single pixel spectral profiles analysis.
    - It is important to pick Substrate, Vegetation and at least 1 Dark endmembers (water) for each scene. More endmember for Substrate if the topology of the mixing space warrants it. We looked especially for sharp apexes within linear edges.
    - The results are sets of images of orthogonal mixing spaces (PC scatter plots) for each scene and at least 4/3endmember spectra :
        - Substrates, sands and manmade structures
        - Vegetation cover and distribution
        - Dark, shadow and water

for each scene combined on the base of vegetation spectral responses intensity.

3) Analyze misfit between estimated endmember.
4) Invert linear mixture model using the electromagnetic spectra, subsetting areas of unmixing in case of high spectral variability.
5) Determine spectrally distinguishable classes and decision boundaries.
6) Calculates the Root Mean Square error (The evaluation of 'RMS error indicates the accuracy of the mathematical results obtained by inversion of the linear model (unmixing) for each pixel for each band (Adams et al., 1993, Roberts et al., 1997, Metternicht and Fermont, 1998, Small, 2004). There is an inverse relationship between the magnitude of the error and the accuracy of the choice of endmember. In general, for values below 0.5 the reliability of the inversion is still accurate, but in general, unless the investigated cases in which the scene does not contain types such as water, soils and vegetation, then spectrally distinguishable, a certain degree error is inevitable).

The method builds and implements a classification system that allowed showing the higher fractions of each vegetation typology we select. Along the steps of the procedure, the endmember selection on the base of the analysis of PCs is based on the experience in vegetation detection. The increasing variance of images due to the extent of dune's ROIs, moving from the north to the south, was modelled by subsetting ecological – spectral units that represent different vegetation patters. At that point step detailed unmixing was used to highlight and select the pure endmembers. Based on the above for all the ROIs the percentage of vegetation cover, sands and anthrophic structures were calculated. Fraction maps were then combined and classified on the base of degrees of presence within each pixel leading to different vegetation patterns classifications. The classification provides 5 biophysical classes that identified no more than 3 ecological sectors of the stretch.

4.5 RESULTS AND DISCUSSION

The Hyper-LiDAR acquisition has generated different parameters to extrapolate high morpho-ecological indicators of the physiographic unit. In order to define the feedback between morphology and ecological parameters we have twisted a specific effort to quantify and map of vegetation fractions pattern in emerged and submerged morphology highlighting the central role of the feedbacks between biological and physical processes that links the sand dune system stabilization to the shallow water seabed morphology (Figure 5.7).

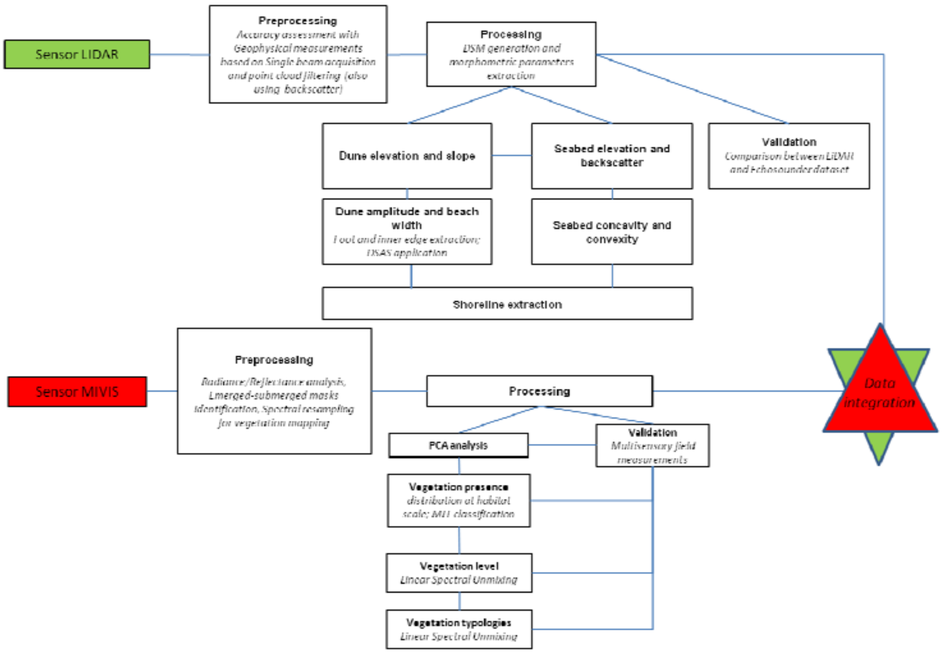

Figure 4.7 - Flow chart of the applied methodology

The below LiDAR parameters (Table 4.5) not only allowed the identification of the position of the foot of the dune, thus allowing their perimeter and the extraction of the area occupied, but also a characterization of detail of the forms (for example, those erosive) and the description of some characteristics of the different sectors, such as the trend of the shoreline. On the contrary the hyper-MIVIS sensor allowed an assessment of the vegetation patterns as an adjunct value to the morphometries at very high resolution (both spectral and spatial).

Table 4.5 - Results of extraction of vegetated and sandy areas of aeolian deposits.

Sector	Dune polygon	dune polygon surface	total vegetation cover (mq)	shape lenght (m/10000)	dune polygon surface/tot	total sands and substrate (mq)	vegetation cover within dune polygon	vegetation cover /total surface	vegetation cover/sector	vegetation cover (vegetation /total) surface %	Vegetation cover level	Vegetation Typologies
A	1	99129,90	28861,29	0,57	8%	70268,61	29%	2%	39%	5%	High level	
	2	70986,03	37257,11	0,31	5%	33728,92	52%	3%			Low level	
B	3	74844,81	19727,54	0,68	6%	55117,27	26%	2%	26%	2%	Presence	
C	4	48221,41	24917,48	0,41	4%	23303,94	52%	2%	32%	10%		Structured vegetation Herbaceous vegetation
	5	354424,64	105566,29	1,37	27%	248858,35	30%	8%				Sand Mixed man made
D	6	644473,80	310167,50	1,51	50%	334306,29	48%	24%	48%	24%		Structured vegetation Unstructured vegetation Mixed man made Sand
STRETCH	tot	1292080,59	526497,21		100%	765583,38		41%				
step 1						step2					step 3	step 4

Vegetation patterns can be considered as part of beach and dune building processes because of the interaction with sand abrasion, salt spray, erosion (loss of sand) and accretion (build-up of sand), wind blasting, dehydration and wave attack that generate different degree of plant structures and typologies. This process is known as succession and is reflected in the formation of distinct "zones" that run parallel to the shore. Coastal vegetation is itself dynamic. Earlier, simpler plant communities pave the way for a series of future, more complex communities that can be recognized as different level of structure, composition and cover.

The results of morphological and vegetation characterization will be exposed proceeding from NW to SE.

From the topo-bathymetric map of the area it is possible to assess the general trend of the surface area investigated. Moving from N to S, relative to the emerged part of the territory, we observe that the structure of aeolian deposits in the tract near Capo Portiere, has size less than 100 m with an average of shares that are below the 5 m. Going down to S, to the mouth of the Rio Martino, the system is larger, exceeding 100 m wide with dimensions that can reach 7 to 8 m. In the stretch of beach in front of the Lake of Monaci is instead the dismantling of aeolian deposits that make the evolution. The trend shows a topographic isolines: the width of the strip of territory occupied by the aeolian deposits rarely exceeds 30 m in width and the odds are found in most cases within 5 m. Moving towards the promontory of Circeo, the aeolian deposits are increasingly structured in particular the stretch of coastline between Lake Caprolace and Sabaudia, where the amplitude of the coastal strip occupied by dunes over 150 meters increase with dimensions approaching 20 m. In the stretch in front of the Lake

Sabaudia, it is highlighted the loss of information due to anthropization and dense vegetation that covers the aeolian deposits of this stretch of coastline.

With regard to the types of seafloor the areas of mobile and mixed seabed derived from the LiDAR survey and the information obtained by the index of concavity-convexity shows a remarkable uniformity of shape and nature of the substrate. The submerged beach is characterized, between Capo Portiere and the mouth of Rio Martino, by forms of interest develop between 100 m and 200 m from the shoreline, beyond that distance, the bottom tends to regularly sloping towards greater depths. From observation of the whole entire area is clearly distinguishable a system of sandy main bar which extends almost parallel to the coastline and which, proceeding from N to S, tends to drift towards greater depths, reaching and exceeding close the mouth of the Rio Martino 200 m from the shoreline. Looking more in detail the forms found on this stretch of coast, it is evident that near the mouth of the Rio Martino, for about 1 km, sandy bar system splits, with the main form tends to develop at a greater distance from the shore and a smaller extension bar that develops between 40 m and 60 m from the shoreline. In particular it should be reported as the external side of the bar of the present large gradients, between 4% and 6%, reaching in some places the 8-9% and marking the move to areas with greater depths. Additional training similar to sand bar is also present at the northern end, about 0.8 km starting from Capo Portiere and in the central section with a length of about 1.4 km. These two forms seem to be the remnant of a second sand bar system that, probably, in other periods of the seasonal cycle is developed throughout the entire coastal stretch. The morphology is typical of the natural barrier that favours the wave breaking of the waves and the defence behind the beach, with the inner side (facing the ground) and the slope steeper outer slopes gently down to greater depths.

Moving towards the south coast the bed forms morphology is characterized by two rows of sand bars that develop almost parallel to the coastline. The system of bar sandy inner splits into two components distinguishable from the central area of the coast, for about 2 km to the southern boundary, while the bar of the second order develops oriented nearly parallel to the coast. The inner bar is developed within the first 100 m from the shoreline and is dimensionally less extensive than the outer bar. With regard to the bar of the second order, proceeding from N to S, we observe that the tendency to drift towards greater depths, in the stretch near the mouth of Rio Martino both forms of the fund will grow within 200 m from the shoreline, while all 'southern end of the field extends well beyond 300 m from the shoreline to about 400 m. The bar sandy, in correspondence with the Idrovora Lavorazione (Figure 4.8), appears structurally reduced for a distance of about 200 m. From a detailed analysis of the bed forms it is shown how the external side of the bar of the first order is the sandy stretch of seabed with higher slopes ranging between 3.5% and 4%, reaching and sometimes exceeding values of 5%.

Beyond the shoreline after Foce Caterattino (Figure 4.8) the stretch is again characterized by two orders of sandy bar with different morphological characteristics. The inner bar develops within 100-120 m from the shoreline and typically has a scalloped pattern. In some parts of the coast area of this form does not appear clearly distinguishable, being juxtaposed to the bottom of lesser depth and forming with it a continuous morphology. In other sections, on the contrary, it is clearly detectable in the form of bar. The sand bar has a clear outer scalloped morphology develops between 180 m and 280 m around the shoreline. This form has an inner side (facing the ground) especially steeper, with slopes ranging between 5% and 6%, and that can reach 9%. On the external side of the bar are visible areas with accumulations of sediment alternated with a similar detachment; it is essentially the areas where the sediment flows offshore under the effect of rip currents to reach areas of accumulation. Other forms related to sediment flows are visible on the external side of the first order sand bar and their characteristics and behaviour are still under investigation. Taking into account the different profiles extracted from the LiDAR bathymetry and the singlebeam DSM (Figure 4.8) to determine the slope of submerged beach it can be notice that above 8 m of depth the difference between the two dataset increases. Such number is close to the closure depth, determined with Hallermaier's (1981) equation.

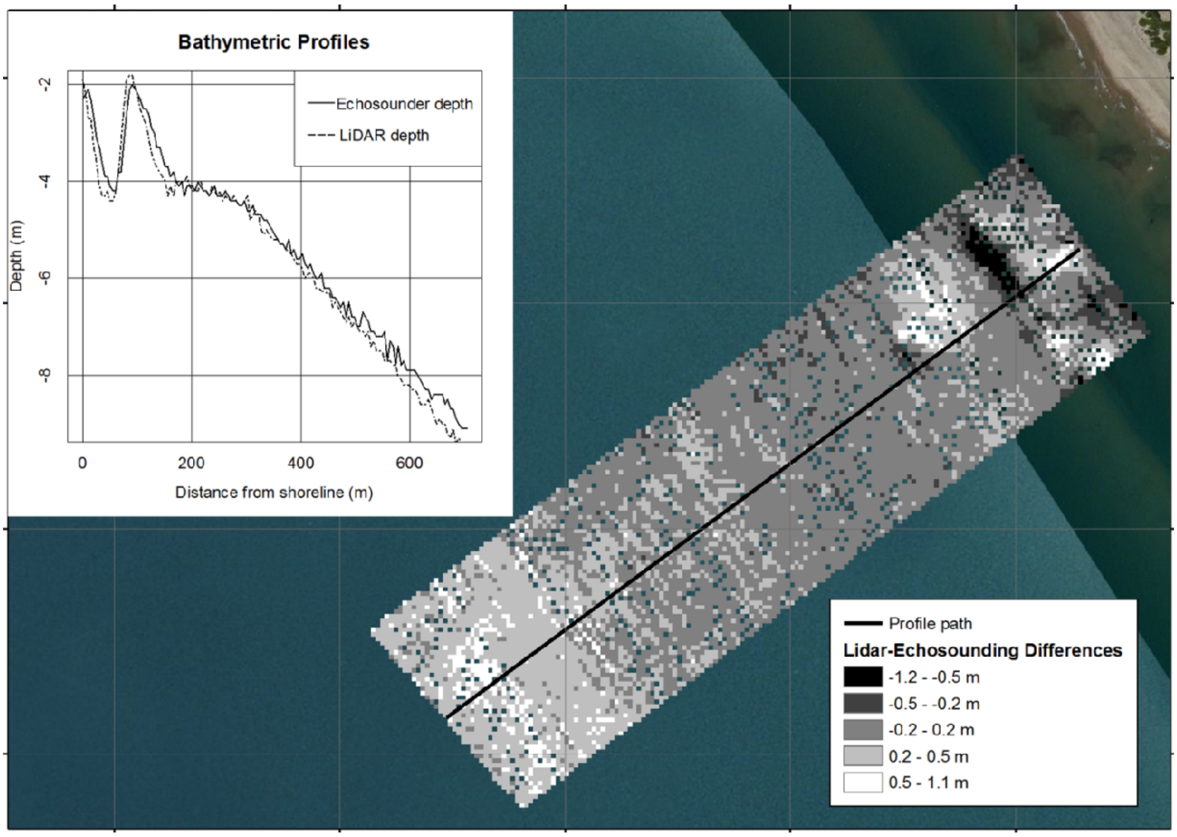

Figure 4.8 – Bathymetric LiDAR DSM and bathymetric echosounding DSM differences

The Authors are now investigating how changes in grain size distribution of the sea floor may influence different tools and procedure for data processing as the closure depth represent the boundary of the sediment dynamic and the sand-sharing within the physiographic unit (Dean and Darlimple, 1991).

Beyond the shoreline Foce Caterattino (Figure 4.9) is again characterized by two orders of sandy bar with different morphological characteristics. The inner bar develops within 100-120 m from the shoreline and typically has a scalloped pattern. In some parts of the coast area of this form does not appear clearly distinguishable, being juxtaposed to the bottom of lesser depth and forming with it a continuous morphology. In other sections, on the contrary, it is clearly detectable in the form of bar. The sand bar has a clear outer scalloped morphology develops between 180 m and 280 m around the shoreline. This form has an inner side (facing the ground) especially steeper, with slopes ranging between 5% and 6%, and that can reach 9%.

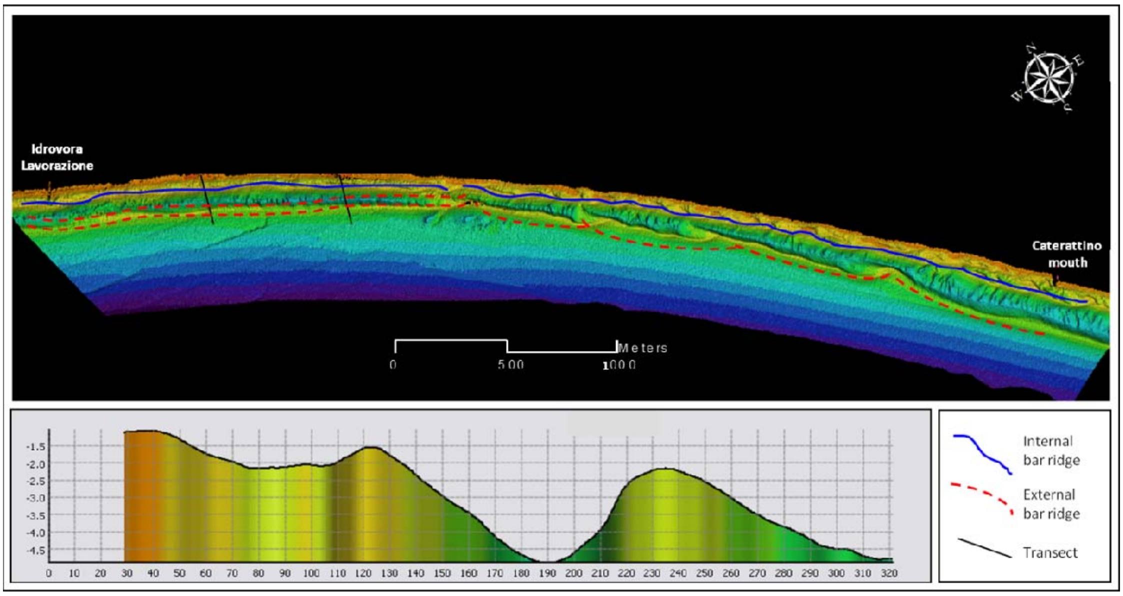

Figure 4.9 - Seabed morphology between Idrovora della Lavorazione and Caterattino mouth

With regard to the nature of the substrate the entire South Area is characterized by the presence of sand, in particular it must be said that, as reported by La Monica and Raffi (1996), the sediment is highly homogeneous to speak of fine sand for the entire coastal area in question, except for the range of the stretch at the shoreline of Lake Sabaudia where there is sand of average grain size. In particular, further confirming the homogeneity of the substrate the same authors speak for the stretch of beach in front of the Lake of Sabaudia pure sand up to 50m deep. The analysis of hyperspectral images MIVIS available to the area did not reveal the presence of vegetated areas except for the section between Torre Astura and Capo Portiere, more precisely in the area surrounding the pier of the Central Tower of Foce Verde was identified as an area characterized by the presence of submerged vegetation, well delimited from the coastline and interspersed with a wide channel mostly sandy. In this case, a selection of the submerged part of the image was carried out a qualitative assessment of the spectral variability, through emphasizing techniques that have shown a certain degree of homogeneity. Subsequently, a PCA on the entire selected stroke, some disturbing elements, i.e. boats, docks and flooded the area closest to the coast where there are sandy bars and submerged structures / emerging sub, were masked.

The dunes system in the sandy stretch of coastline from Capo Portiere and Torre Paola move in parallel to the coastline, and develop for about 25 km. The amplitudes, the elevation and the vegetation structure and continuity of the dune belt system increase

toward south where the vegetation patterns at Torre Paola become lush and stronger separating the beach from four coastal lakes. Basically the dunes in the southernmost part of this coastal arch, the most developed in terms of width and heights differ from the more northern belt for the presence of man-made areas and buildings affecting nearly all of their surface extension and vegetation presence.
Below is reported a detailed description of these aeolian deposits in the area going from N to S with a morphometric characteristics and the vegetation patterns description within the habitat topography on the dune marine apparatus. The area that extends from Capo Portiere to the mouth of Rio Martino develops in the direction NW-SE for a total of 6.5 km. It is characterized by the presence of a sandy beach bordered by a continuous dune belt that separates the beach emerged from behind coastal Lake Fogliano, where it interrupts the New Mouth of Fogliano.

This section presents the beach with an average width of 20 m, varying from a minimum of 12/14 m up to 40 m. The minimum values are found near the New mouth of Fogliano. The shoreline, in the initial rather regular, going SE shows a scalloped pattern characterized by irregular undulations of amplitude and length. The coastal dune has an area of 17.01 hectares, average width of 35-38 m, heights ranging from 7 m to 12 m with an average height of 9.5 m. It extends along the entire sector and has an axis of elongation parallel to the shoreline, at which there is the coastal road. The morphological discontinuities found in this section are both anthropogenic and natural. In the first case it is primarily the coastal road, which also triggers instability phenomena, runoff and blow out (Figure 4.10).

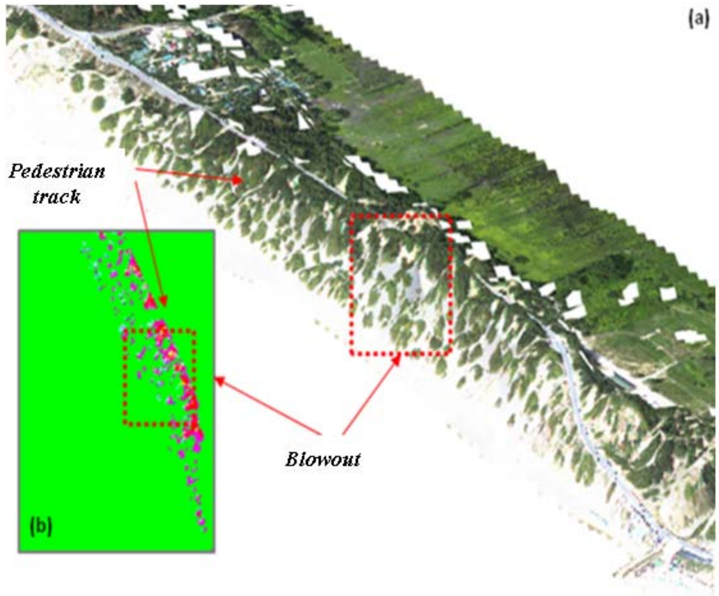

Figure 4.10 - a) 3D visualization of beach dune system topographic LiDAR (Sector 2); b) detail of MIVIS spectral unmixing analysis for blowout identification.

They sailed the ocean side of the dune cordon interrupting the continuity of vegetation cover. Lanes of natural origin are found in ever more frequently moving towards the mouth of the Rio Martino. These are mainly blowout and areas of overwash, in correspondence of which the foot of the dune is more backward and difficult to detect. In these cases vegetation is strictly reduced to grasses and bushes (even if considering the spring season of the airborne acquisition). Endmember fraction maps suggest the presence of vegetation compositions which include few arboreal formations with low density and coverage. The cord appears homogeneously vegetated on the dune slope facing the lake in the back while it shows a more discontinuous vegetation cover in the marine environment, which is proceeding gradually decreasing towards the mouth of Rio Martino where dunes are home to several species of small plants, like shrubs and bushes. On the basis of MIVIS data processing the vegetated surface of this field is equal to 6.61 hectares and represents 39% of the total area. The PCA analysis on hyperspectral image highlighted within the first three dimension (99,97% of total variance) the possibility of picking up two endmembers in view of the low variance associated with the substrates. The two pure endmebers represent an homogeneity of sandy patches that overlap the vegetation endmebers signature. In TABLE 5 the total surface of both dune’s ROIs in sector A (6.61 hectares) are unmixed for 'High vegetation cover' and 'Vegetation partial coverage'. In Figure 11a) examples of graphic representation are showed in accordance with the percentage abundances within each pixel. According to the results, vegetation on the two dunes in front of the Lake of Fogliano appears less variable in terms of structural complexity compared to the areas further south.

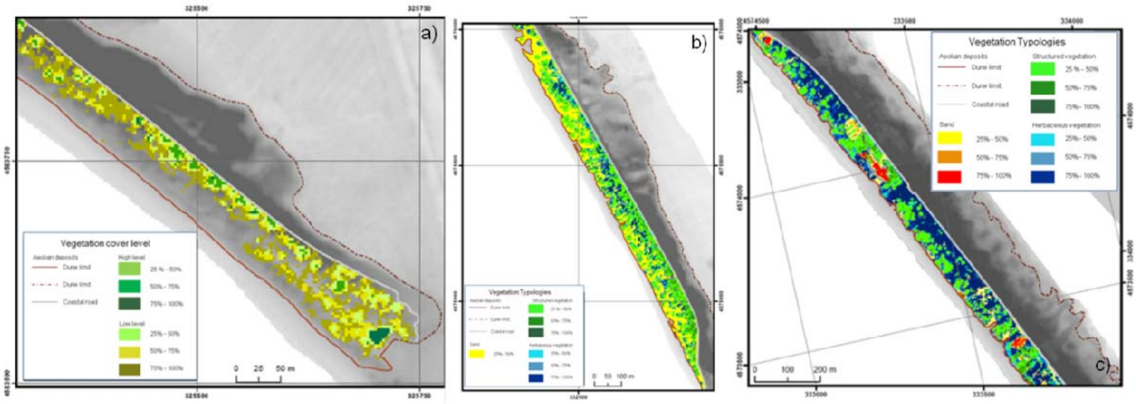

Figure 4.11 - Results of unmixing results proposed visualization for a) Sector A) Sector B and c) Sector C.

High vegetation cover is detectable close to the coastal road, but generally units of 3m x 3m (pixel) didn’t have more than 75% fractions of vegetation. Throughout the study area the plant populations become denser and structured proceeding inland. In particular, in the area of front and unconsolidated dunes, sporadic herbaceous populations *(l’Agropyretum mediterraneum)* suggest pioneer stages of colonization of the primary dunes. In areas with strong erosion features or where fragmented and altered vegetation composition is present with low cover, internal discontinuities showed by low values of ‘Vegetation partial coverage’ suggested replacement with secondary dunes vegetation (*Ammophiletum arundinaceae).*

In agreement with these results, the northern section of the study area dunes, lower in elevation, host plant populations mostly grassy and bushy characterized by a density which increases coverage by the end of front dunes moving towards the coast road (Figure 4.10). In the more stable and internal portion there are individuals of juniper mixed with pioneer communities. The thinning of vegetation, proceeding from the ridge to the foot and the uppermost portion of the beach, can be explained both by the presence, in the range of transition between the beach and dune deposits, of unconsolidated pioneer vegetation, and for the presence of critical issues related to erosion and mechanical cleaning actions that go beyond the beach showed up at the foot of the dune, preventing or hindering the possible formation of new embryo dunes.

The coastline stretching from the mouth of Rio Martino toward the Idrovora Lavorazione develops in the direction NW-SE for a total of 3.5 km. It is characterized by the presence of a sandy beach bordered by a continuous dune belt that separates the beach emerged from the lake behind the Lake of Monaci. In this section there are armed foci that interrupt the continuity of the coast and the coastal road, which runs along the axis of elongation of the dune belt, was closed to traffic in the eighties after a particularly intense storm event. This is the area which presents the minimum amplitudes of the whole stride and which has suffered as a result more prominently the effect of the sea storms that have hit on the coast in the last decades. The beach has emerged an average width of about 20 m, varying from a minimum of 12 m and a maximum of 32 m. The minimum values are found in north-central portion of the field, just to the SW of the mouth of the Rio Martino. The shoreline is characterized by a trend in the first part of that spire, proceeding towards the dewatering processing, is becoming less clear. As in the previous case, here too the "cusp" has irregular widths and lengths. The slope has values ranging from 0° to 5°. Behind the dune, always parallel to the shoreline and consists of a single bead, has an area of 7.48 hectares, average width of 22 m, heights from 37 m 7 but with an average height of 8 m. Except for the first leg, in which the inner slope of the dune is quite large and uniformly vegetated, the dune belt has small amplitude and low vegetation cover. At several points there are clear morphological discontinuities and gaps due to different processes, including leaching and collapse phenomena along the ocean side of the road base, which are the most obvious forms of erosion. There are also traces of trenches and marine erosion at the foot of the dune. Following the removal of the asphalt in the stretch of coastal road closed to traffic during the nineties, there has been a progressive "colonization" of plant communities typical of the dune that partially re-established continuity between the ocean and the side slope internal cord. On the basis of data processing MIVIS the vegetated surface of this field is equal to 1.97 hectares and represents only the 26% of the total area (Table 4.5, sector B). The PCA analysis highlighted within the first dimension (99,95% of total variance) the total amount of polygon spectral variance. Mixing space in this case resulted so aggregated that the possibility of picking up endmembers was reduced, and linear spectral unmixing RMSerror was too high (>0.5). Very low variance was associated both with the mostly sanded/high reflective beach and vegetation homogeneity in species and composition principally generated by sporadic herbaceous populations *(Agropyretum mediterraneum).*

The coastline, which stretches to the mouth of Idrovora della Lavorazione to the Caterattino, develops in the direction of NNW-SSE for a total of about 8 km. Like the previous areas, is characterized by the presence of a sandy beach bordered by a continuous dune belt that separates the beach emerged from the lake Caprolace behind. The beach has more extensive than the previous field, has an average width of about 40 m, varying from a minimum of 25 m and a maximum of 60 m. The minimum values are found in the northern portion of the field, near Idrovora della Lavorazione. As in the section previously discussed, the shoreline is characterized by a trend cuspidate with undulations characterized by irregular widths and lengths. The dune behind it, this stretch more massive, has an area of 40.26 hectares and heights from 16 m 10 but with an average altitude of 13 m. The greater width of the beachfront is reflected in the presence of small avandune incipient in some parts of sector, a result of a favorable condition for the transport and deposition of sand by the wind. Similarly to what was observed previously, also in this section morphological discontinuities are visible due to both natural and anthropogenic causes. Among the latest addition to the coastal road, to walkways and paths, we find evidence of runoff, wind erosion and seawater (overwash). From the point of view of the vegetation cover, the slope dune interior is almost completely vegetated as well as the marine environment, characterized by a vegetation predominantly shrub. On the basis of data processing MIVIS the vegetated surface of this field is equal to 13.05 hectares and represents 32% of the total area. The large amount of information contained in PC1 associated with the spectral variance sand / vegetation suggested the possibility of picking up more than two endmembers in view of the variance associated with the substrates within each of the two spectral apexes in the scatterplot. Substrates, in this case were divided into sand and the contribution of other sources of variance due to the presence of man-made structures. In Table 4.5, the total surface of both dune units in sector C (13.1 hectares) are spectrally unmixed for 'Structured vegetation' representative of trees and shrub, where present, considering that trees are scattered within the two dune units and not comparable with coastal pine woods; 'Herbaceous vegetation' that shows lower values of % cover and lower intensities in the spectral profile; 'Sand' and 'Atrophic substrate'. This last, was introduced, after the reiteration of unmixing to lower RMSerror values that at the beginning of the analysis showed sand fraction maps. Roof, pools, asphalts are considered as a unique source of variance. In Figure 4.11b) examples of graphic representation are showed in accordance with the percentage abundances within each pixel.

Observing processing results, structured vegetation runs at the ridge of sand dunes adjacent to the coastal road. Moving closer to the beach an increase in predominantly sandy areas interspersed with other plant communities that appear less structured and with low % cover. More internally, in contact with the secondary dunes vegetation (*Ammophiletum arundinaceae)*, there are also community typical of the consolidated dune not yet structured as the hemicrypto-chamaephitic vegetation, forming a discontinuous layer of elevation of few decimeters. These formations characterized by the presence of pioneer juniper, which represents the transition between herbaceous phytocoenoses and those of the Mediterranean coastal forestry of consolidated dunes.

In this strip closest to the sea, in the sections most degraded or subject to erosion, the presence of the community appears discontinuous due both to the openings of natural blowout, furrows of erosion, runoff, and man-made walkways and paths, which are reflected in the hyperspectral images that showed very high percentage of sand presence.

The beach in front of the Lake Sabaudia, which extends from the mouth of Caterattino to Torre Paola runs for a total of 7 km NNW-SSE direction. It is characterized by the presence of a sandy beach bordered by a continuous dune belt that separates the beach emerged from the lake behind, Lake Sabaudia. The beach has emerged an average width of about 40 m, varying from a minimum of 15 m and a maximum of 60 m. As in the section previously discussed, the shoreline is characterized by a trend cuspidate with undulations characterized by irregular widths and lengths. In this area behind the dune presents greater morphological complexity as well as the larger dimensions, both as regards the shares obtained (from 13 to 27 m) that with regard to the area (64.47 ha). However, this is the sector most affected by the impact anthropogenic, both directly and indirectly. The coastal dunes in fact, although higher and more developed, are completely rigid buildings, or fences of the gardens of private houses, which often coincide with the foot of the dune itself or even go in the first band of the back beach. On the basis of data processing MIVIS the vegetated surface of this field is equal to 31.02 hectares and represents 48% of the total area. The PCA analysis on hyperspectral image highlighted a spatial aggregation of pixels consisting of many small scattered islands, which in part belong from the same spectral behaviour within groups of vegetation, and in part that belong from the heterogeneity of non-vegetated areas. The processed dune polygon was very large and contains high spectral variability that is not easily to relate to two major sand and vegetation information. The analysis of the components in fact, proceeded by the collection of a greater number of endmembers to be included in the system of linear equations. The spectral variance was very high due to the presence of mixed vegetation, more or less structured and completely sandy areas adjacent to highly reflective manmade buildings, including small paved areas, roofs and swimming pools.

To be able to associate a detailed characterization of the vegetation, an analysis was made within different vegetated areas. The presence of grassland vegetation and unstructured (*Ammophiletum arundinaceae)*, has emerged with lower spectral intensity if compared with the pervious image, therefore we decided to enter one endmember that took into account this information. The endmebers was extracted manually by profiling the image and not through the PCA. Within the PCA, five components were selected in order to consider a cumulative variance of 99,97% and the possibility of picking up at least four spectral endmembers. In Table 4.5, the total surface the dune unit in sector D (64,4 hectares) is unmixed in ‘Structured vegetation’, considering the extensive presence of Junipers and Pines and ‘Unstructured vegetation’, considering the top of the dune, where vegetation is constrained to small islands and corridor strictly interconnected with morphological complexity as well as the larger dimension of the surface (50% of total analyzed dune surface). For the substrates were selected 'Mixed substrates' and ‘Sand and herbaceous’ in view of the presence of completely rigid

buildings, gardens, fences, private houses, pools, which often coincide with the foot of the dune itself or even go in front zone of the back beach.
In Figure 4.11c) examples of graphic representation are showed in accordance with the percentage abundances within each pixel of vegetation structure and san cover.
This unit is undoubtedly the most affected by the anthropogenic impact, both direct and indirect.
Structured vegetation band is in the inner, adjacent to the coastal road, which runs at the ridge of sand dunes proximal to the central area that showed medium vegetation cover and large clearings that contain more than 75% sand. The stretch, walking from the north has more grassland or shrubby areas and larger amounts of sand, indicating lower density of coverage over the entire area. Moving toward the end, almost all of the area closest to the beach, an increase in sandy areas interspersed with less structured plant communities was observed.

The application of lidar in this morpho-ecological study is an area of great potential that is just beginning to be realized based on the results of this data processing. Airborne lidar is primarily used for obtaining elevation data for large areas, but its potential for aiding ecological studies and restoration projects extends well beyond simple ground elevation measurements. In fact, the results of the application and implementation of hyperpsectral Spectral Mixing Analysis (SMA) for the part of emerged vegetation (vegetation on the dune belt) suggest a high-resolution capability of the spectral composition of the vegetated areas. In particular, in addition to the definition of the percentage coverage of each type was possible to distinguish some additional sources of variability that may be present in the investigated areas. The result of the analysis of spectral mixture present in each pixel was strongly influenced by the degree of variance associated with the different areas of study selected, a factor that suggests the possibility of increasing the degree of spectral resolution information, through the selection of areas small, both in terms of surface extension in terms of spectral composition (heterogeneity).
In this paper, based entirely on the direct study of MIVIS hyperspectral images (image-based) without the use of spectroradiometers data validation on the ground, it was decided to differentiate the optical signal of vegetated surfaces in terms of degree of

structure or in some cases, the degree of coverage. Thus emerged a zonation of vegetation representing the main types present on the dunes investigated (meadow, shrub and tree), consistent with what is measurable through the available literature.

With the same conceptual model used for the study of the vegetation of the band emerged, were evaluated for their ability to extract spectral information on the environment of submerged area. The physically based classification has provided the basis of analysis of the different spectral types associated to the bottom and allowed the recognition of the shape and the upper and lateral areas of submerged vegetation and bottom cover up to 6 m depth and a bottom definition of sandy sediments.

4.6 CONCLUSIONS

The Sabaudia coastal area is an highly valued environment where different habitats are linked by complex interactions that determine a state of dynamic equilibrium. It is also the key component of the coastal settlements characterized by different relevant economic and commercial activities. The correct characterization of such complex environmental areas of strategic importance for a proper and integrated management requires tools to analyze the individual components. The scientific research improvements in this study of coastal environments is very promising as it is based on the fact that requiring equipment and applications that provide products and processed with high quality standards in order to represent the territory in a realistic and accurate order. This improves knowledge and management that are in a fast development.

In this context, within this research, which deals with the study of the coastal morphology and ecology through innovative techniques implemented remotely, present a new methodology for acquisition and processing of environmental data through the use of airborne systems. The new systematic approach through new methodologies such as the combined analysis of remotely sensed data (hyperspectral and LiDAR) for the quantitative estimation of different morphometric index is useful for geomorpho-ecological analysis. The new approach shows the impressive results of physical characterization and environmental impact of coastal ecosystems based on integrated use of remote sensing data type LiDAR and hyperspectral MIVIS. The synergy between the two sensors has allowed on one hand to evaluate the morphological characteristics of the surface and on the other hand to investigate the physical nature of the targets, in order to correlate the performance and the morphotypes of the territory with the presence and distribution of some ecological matrices. For example, the integrated use of two datasets, the LiDAR (morphological and quantitative) and the MIVIS (environmental), offered the chance to explore the vast territory from areas, emerged and submerged, by providing high quality information related forms (morphotypes) and the development of the territory but also the distribution and characteristics (structural and physico-ecological) of the region.

The products obtained gives information on morphological and biological parameters allowing the possibility of a first attempt of identifies feedback between habitats and morphodynamics. In particular the use of the MIVIS data, provided information on the physical nature of landforms. The integration of information derived from LiDAR data and the data MIVIS has enabled us to carry out inspections and quantitative characterization of the coastal ecosystem of environmental matrices such as sediment and vegetation cover, large scale bed forms (both above and below msl) allowing for the first time ever to recognize complex conceptual models of land form evolutionary processes which are far beyond the purpose of the present work and still under investigation by the Authors. The results obtained have enabled us to produce cartographic thematic summaries that describe the feedback between habitats and morphodynamics even at the scale of retail.

The results evidenced most from this stage of work is that the integrated LiDAR data with hyperspectral MIVIS data has resulted in better delineation of the system emerged-submerged present in the study area and a better characterization of the morphological and environmental discontinuities. The combined analysis of 2 dataset showed that in almost all cases the dune area of shallow water can be divided into different portions according to the degree of correspondence between the data collected. The coastal marine environment is optically and biologically complex, and many efforts have yet to be made to understand the behavior of radiation in its interactions with different targets.

The hyperspectral remote sensors, such as MIVIS are better suited to describe the spectral variability of these environments, thanks to identify potential small spectral differences between targets that can be found optically similar, but still can not be ignored by a combined use with optical data to the ground if you want to achieve a degree of discrimination between the target that is satisfactory. Following an approach only image-based the work is in fact able to achieve a distinction of the main spectral features that characterize the region of emerged shoreline, the dune belt and the coastal seabed. The combined use of active sensors such as LiDAR, topographic and bathymetric information has provided details, which are the indispensable basis for the interpretation of the variation of radiance less obvious.

Spectral Mixing Analysis has demonstrated a technique with great potential for the study of coastal marine areas. In fact, in addition to having provided a good differentiation of the vegetation on the coastal areas has allowed a significant speculation emerged in the coastal seabed in the absence of a sculpting of the attenuation of the spectral characteristics of the seabed. In particular, SMA allows an interpretation of the marine coastal areas in terms of fractions of spectrally pure endmember and therefore allows decomposing a heterogeneous environment, both spectrally fundamental elements that make up the total response in each pixel.

Acknowledgements

This research is funded by the Lazio Region within the CAMP Project. A special thank is addressed to Eng. Paolo Lupino for his interest through it all.

Thanks for the contribution to the achievement of this work goes to Raffaele Proietti.

4.7 REFERENCES

1 Adam S, De Backer A, De Wever A, Sabbe K, Tooman E A, Vinex M and Monbaliu J. 2011. Bio-physical characterization of sediment stability in mudflat using remote sensing: A laboratory experiment. Continental Shelf Research. 31 (10 supplement): S26-S35 ..

2 Adam S, Vitse I, Johannsen C, Monbaliu J. 2006. Sediment type unsupervised classification of the Molenplaat, Westerschelde estuary, the Netherlands. EARSeL eProceedings **5**: 146-160.

3 Adams JB, Smith MO, Gillespie AR. 1993. Imaging spectroscopy: Interpretation based on spectral mixture analysis. Remote Geochemical Analysis Elemental and Mineralogical Composition **7** : 145–166.

4 Alberotanza L, Brando V, Ravagnan G, Zandonella A. 1999. Hyperspectral aerial images. A valuable tool for submerged vegetation recognition in the Orbetello Lagoons, Italy. International journal of remote sensing **20** : 523–533.

5 Allegrini A, Anselmi S, Cavalli RM, Ambientali LA., IIA-CNR TVR., Manes F, Pignatti S, others. 2006. Multiscale integration of satellite, airborne and field data for Mediterranean vegetation studies in the natural area of the Castelporziano Estate (Rome). Annals Of Geophysics **49**

6 Andrews BD, Gares PA, Colby JD. 2002. Techniques for GIS modeling of coastal dunes. Geomorphology **48** : 289–308.

7 Artigas F, Yang J. 2005. Hyperspectral remote sensing of marsh species and plant vigour gradient in the New Jersey Meadowlands. International Journal of Remote Sensing **26** : 5209–5220.

8 Athearn ND, Takekawa JY, Jaffe B, Hattenbach BJ, Foxgrover AC. 2010. Mapping elevations of tidal wetland restoration sites in San Francisco Bay: comparing accuracy of aerial lidar with a singlebeam echosounder. Journal of Coastal Research : 312–319.

9 Barducci A, Guzzi D, Marcoionni P, Pippi I. 2009. Aerospace wetland monitoring by hyperspectral imaging sensors: A case study in the coastal zone of San Rossore Natural Park. Journal of environmental management **90** : 2278–2286.

10 Bauer BO, Davidson-Arnott RGD. 2003. A general framework for modeling sediment supply to coastal dunes including wind angle, beach geometry, and fetch effects. Geomorphology **49**: 89–108.

11 BEACHMED-e. [Online] Available from: http://www.beachmed.it (accessed on February 2012).

12 Belluco E, M. Camuffo S, Ferrari L, Modenese S, Silvestri A, Marani M, Marani. 2006. Mapping salt-marsh vegetation by multispectral and hyperspectral remote sensing. Remote Sensing of Environment **105**: 54–67, doi:10.1016/j.rse.2006.06.006.

13 Berk A, Anderson G, Bernstein L, Acharya P, Dothe H, Matthew M. 1999. MODTRAN4 radiative transfer modeling for atmospheric correction. presented at the SPIE – The International Society for Optical Engineering. 348–353 pp.

14 Blanc AC, Segre A. 1953. Le quaternaire du Monte Circeo. Livret guide. presented at the IV Congrès INQUA. Rome. 23–108 pp.

15 Boardman J, Huntington J. 1997. Mineralogic and geochemical mapping at Virginia City, Nevada using 1995 AVIRIS data. presented at the Applied Geologic Remote Sensing-International Conference-

16 Boardman JW. 1989. Inversion of imaging spectrometry data using singular value decomposition. presented at the 12th Canadian Symposium on Remote Sensing Geoscience. 2069–2072 pp.

17 Boschetti M, Boschetti L, Oliveri S, Casati L, Canova I. 2007. Tree species mapping with Airborne hyper-spectral MIVIS data: the Ticino Park study case. International Journal of Remote Sensing **28** : 1251–1261.

18 Brock JC, Wright CW, Sallenger AH, Krabill WB, Swift RN. 2002. Basis and methods of NASA airborne topographic mapper lidar surveys for coastal studies. Journal of Coastal Research : 1–13.

19 Brock JC, Purkis MJ. 2009. The Emerging Role of Lidar Remote Sensing in Coastal Research and Resource Management. Journal of Coastal Research**53**: 1-5, DOI: 10.2112/SI53-001.1

20 Calkoen CJ, Hesselmans GHFM, Wensink GJ, Vogelzang J. 2001. The Bathymetry Assessment System: efficient depth mapping in shallow seas using radar images. International Journal of Remote Sensing **22** : 2973–2998. DOI: 10.1080/01431160010031306 [online] Available from: http://www.catchword.com/cgi-bin/cgi?body=linker&ini=xref&reqdoi=10.1080/01431160010031306 (Accessed 24 April 2012)

21 Calvo S, Ciraolo G, La Loggia G. 2003. Monitoring Posidonia oceanica meadows in a Mediterranean coastal lagoon (Stagnone, Italy) by means of neural network and

ISODATA classification methods. International Journal of Remote Sensing **24** : 2703–2716.
22 Campo V, La Monica GB. 2006. Le dune costiere oloceniche prossimali lungo il litorale del Lazio. Studi Costieri **11** : 31–42.
23 Casella L, Agrillo E, Bianco PM, Cardillo A, Laureti L, Lugari A, Spada F. 2008. Carta degli habitat della Regione Lazio per il sistema informativo di Carta della Natura alla scala 1:50.000
24 Cappucci S, Amos CL, Hosoe T, Umgiesser G. 2004. SLIM: a numerical model to evaluate the factors controlling the evolution of intertidal mudflats in Venice Lagoon, Italy, Journal of Marine System, **51/4**: 257-280.
25 Cappucci S, Scarcella D, Rossi L, Taramelli A. 2011. Integrated Coastal Zone Management at Marina di Carrara Harbor: sediment management and policy making. Journal of Ocean and Coastal Management, **54**: 277-289
26 Casella L, Agrillo E, Bianco PM, Cardillo A, Laureti L, Lugari A, Spada F. 2008. Carta degli habitat della Regione Lazio per il sistema informativo di Carta della Natura alla scala 1:50.000
27 Capogrossi R, Augello R. 2008. Applicazione delle procedure informatiche per la Valutazione del Valore Ecologico, Sensibilità Ecologica, Pressione Antropica, Fragilità Ambientale:
28 Cracknell A. 1999. Remote sensing techniques in estuaries and coastal zones an update. International Journal of Remote Sensing **20**: 485–496.
29 Davidson-Arnott RGD. 2005. Conceptual model of the effects of sea level rise on sandy coasts. Journal of Coastal Research: 1166–1172.
30 Davidson-Arnott RGD, MacQuarrie K, Aagaard T. 2005. The effect of wind gusts, moisture content and fetch length on sand transport on a beach. *Geomorphology* **68** : 115–129.
31 Dean RG, Darlimple RA. 1991. Water wave mechanics for engineers and scientists. *World Scientific Press*, Singapore, 353 pp.
32 Deronde B, Houthuys R, Debruyn W, Fransaer D, Lancker VV, Henriet J-P. 2006. Use of Airborne Hyperspectral Data and Laserscan Data to Study Beach Morphodynamics along the Belgian Coast. Journal of Coastal Research **225**: 1108–1117. DOI: 10.2112/04-0264.1 [online] Available from: http://www.bioone.org/doi/abs/10.2112/04-0264.1
33 Giardino C, Brando VE, Dekker AG, Strömbeck N, & Candiani G. 2007. Assessment of water quality in Lake Garda (Italy) using Hyperion. Remote Sensing of Environment, **109**: 183−195.
34 Giovagnotti C, Rondelli F, Pascoletti FT. 1980. Caratteristiche geomorfologiche e sedimentologiche delle formazioni quaternarie del litorale laziale tra T.re Astura e il M. Circeo. Estratto degli Annuali della Facoltà di Agraria dell'Università di Perugia : 173–235.
35 Goetz A. 1992. Principles of narrow band spectrometry in the visible and IR: instruments and data analysis. In Imaging spectroscopy: fundamentals and prospective applications ,. Springer; 21–32.
36 Goodman JA, Lee ZP, Ustin SL. 2008. Influence of atmospheric and sea-surface corrections on retrieval of bottom depth and reflectance using a semi-analytical model: a case study in Kaneohe Bay, Hawaii. Applied optics **47** : F1–F11.
37 Guenther GC. 1986. Wind and nadir angle effects on airborne lidar water'surface' returns. presented at the Ocean optics VIII. Orlando, FL. 277–286 pp.
38 Guenther GC. 2007. Airborne lidar bathymetry. In Digital elevation model technologies and applications: the DEM user's manual ,. American Society of Photogrammetry and Remote Sensing Bethesda, Maryland; 253–320.
39 Guenther GC, Eisler TJ, Riley JL, Perez SW. 1996. Obstruction detection and data decimation for airborne laser hydrography. DTIC Document [online] Available from: http://www.dtic.mil/cgi-bin/GetTRDoc?Location=U2&doc=GetTRDoc.pdf&AD=ADA487820 (Accessed 16 May 2012)
40 Guenther GC, LaRocque PE, Lillycrop WJ. 1994. Multiple surface channels in Scanning Hydrographic Operational Airborne Lidar Survey (SHOALS) airborne lidar. presented at the Ocean Optics XII. 422 pp.
41 Guenther GC, Thomas RWL. 1984. Prediction and Correction of Propagation-induced Depth Measurement Biases Plus Signal Attenuation and Beam Spreading for Airborne Laser Hydrography. NOAA Technical Report NOS. NOAA: Rockville, Md. [online] Available from: http://www.ngs.noaa.gov/PUBS_LIB/PredictionAndCorrectionOfPropagationInducedDepthMeasurementBiasesForAirborneLaserHydrography_TR_NOS106_CGS2.pdf (Accessed 14 May 2012)
42 Hallermeier RJ, 1981. A profile zonation for seasonal sand beaches from wave climate. Coastal Engineering 4, 253-277.

43 Herold M., Roberts D.A., Gardner M.E., Dennison P.E. (2004) - Spectrometry for urban area remote sensing - Development and analysis of a spectral library from 350 to 2400 nm. Remote Sensing of Environment, 91: 304-319.

44 Ibrahim E, Monbaliu J. 2011. Suitability of spaceborne multispectral data for inter-tidal sediment characterization: A case study. Estuarine, Coastal and Shelf Science **92** : 437–445.

45 Innocenti C, Taramelli A, Valentini E, Cappucci S. 2011. Use of airborne LiDAR and hyperspectral data to study the sandy beach morphology along the Lazio region coast (Italy), Geophysical Research Abstracts **13**: EGU2011-8725, 2011 EGU General Assembly 2011

46 Irish JL, White TE. 1998. Coastal engineering applications of high-resolution lidar bathymetry. Coastal Engineering **35** : 47–71.

47 Isaksson A. 2009. Coastal Survey Studio Mark II – Version 2.x – Manual . Airborne Hydrography AB

48 ISPRA. 2009. Rilievo di dettaglio della batimetria costiera laziale con tecnologie LiDAR e valutazione delle caratteristiche fisiche e biologiche in aree marine della costa laziale di specifico interesse ambientale. Fase 1A – Ricerca bibliografica di settore e implementazione della metodologia. ISPRA: 38 pp. (available at http://www.cmgizc.info)

49 ISPRA. 2009b. Rilievo di dettaglio della batimetria costiera laziale con tecnologie LiDAR e valutazione delle caratteristiche fisiche e biologiche in aree marine della costa laziale di specifico interesse ambientale. Fase 1B – Acquisizione e groundthruting. ISPRA: 34 pp. (available at http://www.cmgizc.info)

50 ISPRA. 2010. Rilievo di dettaglio della batimetria costiera laziale con tecnologie LiDAR e valutazione delle caratteristiche fisiche e biologiche in aree marine della costa laziale di specifico interesse ambientale. Fase 2 – Caratterizzazione morfologica. ISPRA: 119 pp. (available at http://www.cmgizc.info)

51 ISPRA (2010b) – Rilievo di dettaglio della batimetria costiera laziale con tecnologie LiDAR e valutazione delle caratteristiche fisiche e biologiche in aree marine della costa laziale di specifico interesse ambientale. Fase 3 – Caratterizzazione ambientale. ISPRA: 153 pp. (available at http://www.cmgizc.info)

52 Kaufman YJ. 1989. The atmospheric effect on remote sensing and its correction. Theory and applications of optical remote sensing : 336–428.

53 Koppari K, Karlsson U, Steinvall O. 1994. Airborne laser depth sounding in Sweden. International hydrographic review. Monaco **71** : 69–90.

54 Kruse FA, Richardson LL, Ambrosia VG. 1997. Techniques developed for geologic analysis of hyperspectral data applied to nearshore hyperspectral ocean data. presented at the Fourth International Conference on Remote Sensing for Marine and Coastal Environments. Orlando, Florida. 19 pp. [online] Available from: http://hgimaging.com/PDF/Kruse_erim97_marine.pdf (Accessed 16 May 2012)

55 Lawrence RL, Wood SD, Sheley RL. 2006. Mapping invasive plants using hyperspectral imagery and Breiman Cutler classifications (RandomForest). Remote Sensing of Environment **100** : 356–362.

56 Van der Maarel E. 1979. Multivariate methods in phytosociology, with reference to the Netherlands. The study of vegetation **161** : 225.

57 Malthus TJ, Mumby PJ. 2003. Remote sensing of the coastal zone: an overview and priorities for future research. International Journal of Remote Sensing **24**

58 Matthew MW et al. 2000. Status of atmospheric correction using a MODTRAN4-based algorithm. presented at the SPIE. 199–207 pp. [online] Available from: ftp://popo.jpl.nasa.gov/pub/docs/workshops/00_docs/matthew_web.pdf (Accessed 16 May 2012).

59 Marani M, Belluco E, Ferrari S, Silvestri S, D'Alpaos A, Lanzoni S, Feola A, Rinaldo A. 2006. Analysis, synthesis and modelling of high-resolution observations of salt-marsh ecogeomorphological patterns in the Venice lagoon. Estuarine, Coastal and Shelf Science **69**: 414-426, doi:10.1016/j.ecss.2006.05.021.

60 Marani M, Silvestri S, Belluco E, Ursino N, Comerlati A, Tosatto O, Putti M. 2006. Spatial organization and ecohydrological interactions in oxygen-limited vegetation ecosystems. Water Resources Research **42**: W06D06, doi:10.1029/2005WR00458.

61 Mason DC, Scott TR, Dance SL., 2010. Remote sensing of intertidal morphological change in Morecambe Bay, U.K., between 1991 and 2007. Estuarine, Coastal and Shelf Science **87**: 487–496

62 Metternicht G, Fermont A. 1998. Estimating erosion surface features by linear mixture modeling. Remote Sensing of Environment **64** : 254–265.

63 Milliken RE, Mustard JF, Poulet F, Jouglet D, Bibring JP, Gondet B, Langevin Y. 2007. Hydration state of the Martian surface as

seen by Mars Express OMEGA: 2. H2O content of the surface. J. Geophys. Res **112** DOI: 10.1029/2006JE002853
64 Mitasova H, Mitas L, Harmon RS. 2005. Simultaneous spline approximation and topographic analysis for lidar elevation data in open-source GIS. Geoscience and Remote Sensing Letters, IEEE **2** : 375–379.
65 La Monica GB, Raffi R. 1996. Morfologia e sedimentologia della spiaggia e della piattaforma continentale interna. Il Mare del Lazio. Universita degli Studi di Roma "'La Sapienza'", Regione Lazio Assessorato Opere e Reti di Servizi e Mobilita : 62–105.
66 Morton RA, Leach MP, Paine JG, Cardoza MA. 1993. Monitoring beach changes using GPS surveying techniques. Journal of Coastal Research **9** : 702–720.
67 Mumby PJ, Edwards AJ. 2002. Mapping marine environments with IKONOS imagery- Enhanced spatial resolution can deliver greater thematic accuracy. Remote Sensing of Environment **82** : 248–257.
68 Pallottini E, Cappucci S. 2009. Beach - dune system interaction and evolution. Rendiconti Online Società Geologica Italiana **8** : 87–97.
69 Pallottini E, Cappucci S, Taramelli A, Innocenti C, Screpanti A. 2010. Variazioni morfologiche stagionali del sistema spiaggia-duna del Parco Nazionale del Circeo. Studi Costieri **17** : 105–124.
70 Pignatti S, Cavalli RM, Cuomo V, Fusilli L, Pascucci S, Poscolieri M, Santini F. 2009. Evaluating Hyperion capability for land cover mapping in a fragmented ecosystem: Pollino National Park, Italy. Remote Sensing of Environment **113** : 622–634.
71 Psuty NP. 1988. Sediment budget and dune/beach interaction. Journal of Coastal Research **3** : 1–4.
72 Quadros ND, Collier PA, Fraser CS. 2008. Integration of bathymetric and topographic lidar: a preliminary investigation. The International Archives of the Photogrammetry Remote Sensing and Spatial Information Sciences **37** : 1299–1304.
73 Rainey MP, Tyler AN, Gilvear DJ, Bryant RG, McDonald P. 2003. Mapping intertidal estuarine sediment grain size distributions through airborne remote sensing. Remote sensing of Environment **86** : 480–490.
74 Research Systems I. 2005. ENVI user's guide . Research Systems
75 Revell DL, Komar PD, Sallenger Jr AH. 2002. An application of LIDAR to analyses of El Niño erosion in the Netarts Littoral Cell, Oregon. Journal of Coastal Research **18** : 792–801.
76 Richter R, Schläpfer D. 2011. Atmospheric/Topographic Correction for Satellite Imagery [online] Available from: http://atcor.com/pdf/atcor3_manual.pdf (Accessed 15 May 2012)
77 Roberts D, Green R, Adams J. 1997. Temporal and spatial patterns in vegetation and atmospheric properties from AVIRIS. Remote Sensing of Environment **62** : 223–240.
78 Roberts D, Green R, Adams J. 1997. Temporal and spatial patterns in vegetation and atmospheric properties from AVIRIS. Remote Sensing of Environment **62** : 223–240.
79 Rodríguez I, Montoya I, Sánchez MJ, Carre\ no F. 2009. Geographic Information Systems applied to Integrated Coastal Zone Management. Geomorphology **107** : 100–105.
80 Sallenger Jr A et al. 2003. Evaluation of airborne topographic lidar for quantifying beach changes. Journal of Coastal Research **19** : 125–133.
81 Saye SE, Van Der Wal D, Pye K, Blott SJ. 2005. Beach–dune morphological relationships and erosion/accretion: an investigation at five sites in England and Wales using LIDAR data. Geomorphology **72** : 128–155.
82 Schnurr D. 2009. High speed Hawk Eye delivers new efficiencies in coastal zone mapping. Port Engineering Management **27**
83 Schnurr D. 2010. How low can you go? Maximum depth achieved with Hawk Eye II during project in 2009. presented at the International LiDAR mapping forum. Denver, Colorado. March
84 Simeoni U, Fontolan G, Tessari U, Corbau C. 2007. Domains of spit evolution in the Goro area, Po Delta, Italy, Geomorphology **86**: 332-348.
85 Silvestri S, Marani M, Marani A. 2003. Hyperspectral remote sensing of salt marsh vegetation, morphology and soil topography. Physics and Chemistry of the Earth **28**: 15–25
86 Small C. 2004. The Landsat ETM+ spectral mixing space. Remote Sensing of Environment **93** : 1–17.
87 Small C. 2009. 4 The Color of Cities. In Global mapping of human settlement: experiences, datasets, and prospects ,. CRC Press; 59–106.
88 Small C, Lu JWT. 2006. Estimation and vicarious validation of urban vegetation abundance by spectral mixture analysis. Remote sensing of environment **100** : 441–456.
89 Small C, Steckler M, Seeber L, Akhter SH, Goodbred Jr S, Mia B, Imam B. 2009.

Spectroscopy of sediments in the Ganges-Brahmaputra delta: Spectral effects of moisture, grain size and lithology. Remote Sensing of Environment **113** : 342–361.
90 Steinvall OK, Koppari KR, Karlsson UCM. 1994. Airborne laser depth sounding: system aspects and performance. presented at the Ocean optics XII. 392 pp.
91 Stockdon H, Holman R, Sallenger A. 2002. Parameterization of incident and infragravity swash variance. presented at the AGU Fall Meeting Abstracts.
92 Taramelli A., Giardino C., Valentini E., Bresciani M., Gasperini L., Zucca F. 2012. Coastal landscape: linking morphology to ecosystem structure using air-borne sensors for monitoring the Earth System, In review JOURNAL OF APPLIED EARTH OBSERVATION AND GEOINFORMATION
93 Taramelli A, Valentini E, Dejana M Zucca F, Mandrone S. 2011. Modelling coastal processes by means of innovative integration of remote sensing time series analysis, 978-1-4577-1005-6/11/ ©2011 IEEE
94 Taramelli A, Giardino C, Valentini E, Bresciani M, Gasperini L. 2010. Linking morphology to ecosystem structure using air-borne sensors for monitoring the Earth System, AGU Fall Meeting, 13-17 December 2010, San Francisco, California, abstract n. 960716
95 Taramelli A., Giardino C., Gasperini L., del Bianco F., Bresciani M., Valentini E., Pizzimenti L., Zucca F., Disperati L. 2010. Biophysical and morphological study of coastal habitats from imaging spectrometry, lidar and in situ data acquisition, Extended abstract, The hyperspectral workshop 2010, ESRIN 17-19 Marzo 2010 Frascati.
96 Tebbens SF, Burroughs SM, Nelson EE. 2002. Wavelet analysis of shoreline change on the Outer Banks of North Carolina: an example of complexity in the marine sciences. Proceedings of the National Academy of Sciences **99** : 2554.
97 Thieler ER, Himmelstoss EA, Zichichi JL, Ergul A. 2009. The Digital Shoreline Analysis System(DSAS) Version 4. 0- An ArcGIS Extension for Calculating Shoreline Change . U. S. Geological Survey
98 Thomas RWL, Guenther GC. 1990. Water surface detection strategy for an airborne laser bathymeter. presented at the Ocean Optics X. Orlando, FL, USA. 597 pp.
99 Tsai F, Lin EK, Yoshino K. 2007. Spectrally segmented principal component analysis of hyperspectral imagery for mapping invasive plant species. International Journal of Remote Sensing **28** : 1023–1039.
100 Valentini E, Bresciani M, Giardino C, Innocenti C, Taramelli A. 2009. Characterization of submerged macrophytes in a shallow lake using a combined approach of hyperspectral and LiDAR data. Eos Trans. AGU **90**
101 van der Wal D, Herman PMJ. 2007. Regression-based synergy of optical, shortwave infrared and microwave remote sensing for monitoring the grain-size of intertidal sediments. Remote Sensing of Environment **111** : 89–106.
102 Wensink G, Hesselmans G, Calkoen C, Vogelzang J. 1997. The bathymetry assessment system. Elsevier Oceanography Series **62** : 214–223.

5. Habitat mapping with combined field, hyperspectral and LiDAR detection in a shallow muddy lake

Emiliana Valentini[(1)], Andrea Taramelli[(1)], Claudia Giardino[(2)], Mariano Bresciani[(2)]

[(1)] *ISPRA Istituto Superiore Protezione e Ricerca Ambientale, Roma*
[(2] *CNR – IREA Istituto per il Rilevamento Elettromagnetico Ambientale, Milano*

ABSTRACT

Wetlands and transitional habitats between aquatic and terrestrial environments are key elements of freshwaters network and they require specific conservation and management strategies. There is a need for decision users of high resolution biophysical maps that can represent product where habitat distribution is synthetically described and predicting indicators for ecosystem changes in terms of ecological and geomorphologic features can be measured. In order to study and monitoring the quality of waters and the erosion thresholds of coastal soils, updates of these parameters are periodically required. In the present paper we test an integrate analysis of multisource data with biophysical approaches for optical analysis in a shallow freshwater lake where coastal reeds areal distribution and macrophytes assemblage are influenced by water quality, through optical properties. Contemporary MIVIS hyperspectral, bathymetric LiDAR and field spectral data acquired in the spring 2009 were classified according to a parallel supervised and unsupervised classification. Two significant issues were noted in the classification process: a) the Spectral Mixture Analysis (SMA) based on end-member fraction distributions of the hyperspectral bottom revealed a deep dependencies on optical properties of total suspended matters (TSM) so that b) on the base of bathymetric model obtained with LiDAR and by bio optical TSM models field and image data were used to achieve an increased accuracy in mapping environmental matrix. Based on these results, individual vegetation communities are included into habitat classes: reed and macrophytes are crosschecked with the available 2007 and 2005 maps and by field measurements showing accuracy of 87 and 92% respectively. These assessment lead to a fine scale habitat map and allowed to explore the capabilities of airborne hyperspectral remote sensing for aquatic vegetation survey.

5.1 INTRODUCTION

Climate variability, dynamical and surface process such as marine, fluvial and ground water strictly influenced by anthropogenic uses, can generate spatially and temporally highly variable environmental conditions, mostly in wetland areas (Zedler, 1996, 2005). Wetlands are complex and vulnerable ecosystems, characterized by different soil conditions in adjacent uplands, and by vegetation adapted to different wet conditions. Under this variability, the structure and growth of shallow freshwaters fluctuate over time in response to seasonal pattern of water levels. Such transitional zones may be diversity hotspots, because of the edge effect that enhances species richness, ecosystem services provision (Harris, 1988; Costanza et al., 2008) and natural waste because of their natural role in nutrient cycling.

In this context, ecological and physical measures are integrated to establish an updated habitat classification and this would provide a tool to stakeholders to efficiently manage coastal freshwaters.

Aquatic macrophytes, both submerged and coastal reeds have an important influence on freshwaters quality and ecosystem functions because they strictly interact with physical and biological processes (Frodge et al., 1990; Kiraly et al., 1990) so that they have to be periodically inventoried as indicators and managed wisely as limiting factors in lake exploitation.

The 92/43/EC 'Habitat' Directive, represent the realization of a coherent European ecological network of special areas of conservation and habitats of species at risk, and it is strictly interconnected with the protection areas network classified in accordance with 79/409/CE 'Birds' Directive. The indicators proposed in the guidelines for the management of these sites concern complexity and spatial mosaic organization of flora and vegetation structure and they require information geographically digitalized and referenced.

This research focuses on developing and testing a model for mapping macrophytes and reeds abundance, frequency and distribution on the base of airborne hyperspectral imagery, topographic Light Detection and Ranging (LiDAR), photography and field sample collection. In this, remote sensing supported the assessment of water quality parameters, the investigation of freshwaters costal habitats both aquatic and areal, the evaluation of vegetation forms, erosion thresholds and soil moisture optical properties.

This study would contribute to Lake Trasimeno multi-disciplinary studies for refining the water management plan of the lake. Remote sensing can be one of the supporting tools for the assessment of water quality, the investigation of coastal habitats and the land use/cover change analysis.

The hyperspectral remote sensing, also known as spectroscopy, is a technology used in the detection and in the identification of aquatic and terrestrial habitat networks through the classification of vegetation, minerals, materials and man-made environments (Alberotanza et al., 1999; Boschetti et al., 2007; Cavalli 2006;van der Wal and Herman, 2007). The high resolution of hyperspectral data obtained from airborne acquisitions, allows to extract information about chlorophyll, sediment and soil properties, water quality parameters such as Total Suspended Matter, clouds and many other environmental indicators and indexes (Deronde et al., 2006; Ibrahim and Monbaliu, 2011). Retrieval methods may involve classification techniques (Reguzzoni et al., 2003), decision tree classifier (Bresciani et al., 2010) and semi-analytical bio-optical modelling (Giardino et al., 2007), the latter able to simultaneously derive a number of water quality components (e.g., chlorophyll-a, suspended solid concentrations) beside bottom albedo and bottom depth (Brando et al., 2009; Lee et al., 2001).

Multispectral and hyperspectral remote sensing provides data sets allowing, for example, mapping habitat heterogeneity (Artigas and Yang, 2005; Pignatti et al., 2009) study of vegetation cover in wetlands (Barducci et al., 2009), mapping of invasive plants distribution (Lawrence et al., 2006; Tsai et al., 2007), and plant species (Boschetti et al., 2007; Calvo et al., 2003; Giardino et al., 2009; Marani et al., 2006). Hyperspectral remote sensing has been used to make large-scale inventories of macrophytes, seagrasses and corals (Pinnel et al., 2006) because data generally has shown a linear relationship between chlorophyll-a and the difference between the emergent energy in the primarily scattering range (0.700-0.705 µm) and the primarily chlorophyll-a absorption range (0.675-0.680 µm).

A lot of studies has been made in view of quantifying benthic cover and they demonstrate the improvement in detail that field spectral radiometry offer to measures reflectance in simultaneous, narrow, contiguous bands in helping to resolve absorption caused by vegetation pigments (Hochberg et al., 2006; Murphy et al 2005). Many pigments have in vivo absorption features between 0.40µm nm and 0.75µm nm. These parameters are important for identifying feeding areas, for evaluation of erosion/deposition processes function of the system exposure, for advancement/retreat monitoring of the coastline on the properties and for vegetation on both emerged and submerged areas (Valentini et al., 2012; Disperati et al., 2012).

The bathymetric LiDAR system (Irish and Withe, 1998; Guenther et al., 2000) is an airborne laser that detects sea bottom at high vertical accuracy and high horizontal resolutions in shallow coastal waters (<50 m). to provide a more cost-effective alternative to ship-borne echosounders, for mapping and monitoring shallow water coral reef ecosystems (Costa et al., 2009). There is an increasing number of uses of the bathymetric LiDAR in coastal applications, such as mapping the morphology of shallow-water coral reefs (Costa et al., 2009), shoreline detection and delimitation (Boak and Turner, 2005), predicting fish communities with seafloor features (Kuffner et al., 2007), and defining benthic habitat complexity (Wedding et al., 2008).

LIDAR acquisition, including integrated GPS, is the most suitable techniques to measure morphometric status and to establish the baseline reference for accurate future assessment of evolutionary trend in coastal areas. Numerous examples of coastal monitoring studies may be cited, that integrate field data with remote sensing data (Adams et al., 2010; Davidson-Arnott et al. 2005a, b; Goodman et al., 2008;). Besides morphometric analysis, other study approaches based on the use of Geomatics techniques can provide important support for the study of health/vulnerability status of coastal systems.

5.2 CASE STUDY

Lake Trasimeno (Figure 5.1) is the fourth largest lake for extension in Italy (124 km^2). Fluvial in origin and also tectonic, it is located in central Italy and it belongs to the Tevere river basin. From the geological point of view, alluvial and swamp deposits can be distinguished in the lake basin. The catchment area of Lake Trasimeno covers approximately 30,900 hectares and it has not natural emissary (Orsomando et al., 1993; Orsomando et al., 1991). Along its shores, the hygrophilous wood and the extensive reeds barriers, once present, are now quite completely replaced by intensive cultivations and controlled mowing.

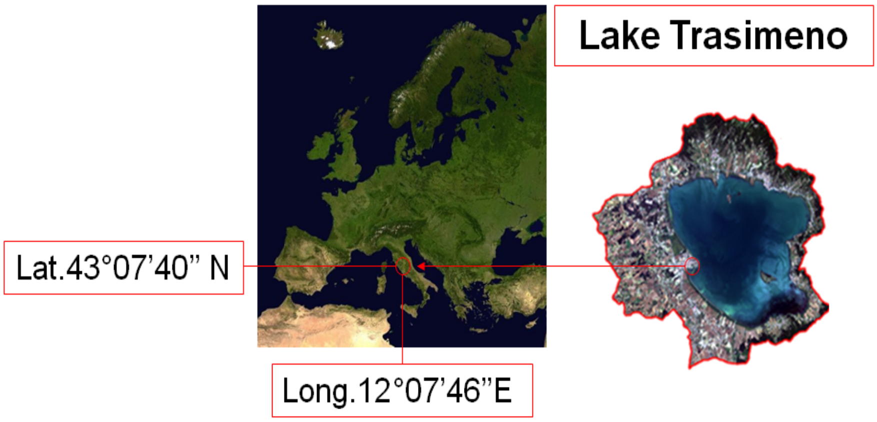

Figure 5.1 - Lake Trasimeno is located in central Italy in a sub-basin of the Tevere river.

The basin has an artificial outlet, excavated in 1898, which threshold overflow is placed at an altitude of 257.33 m a.s.l, this level represents the hydrometric zero (Venanzoni et al., 2006) for water level variation. The lake is roughly circular (Table 5.1), with three small islands: the Maggiore and the Minore are close to the northern shores, while the Polvese lies close to the south-eastern corner where an open bay is colonized by macrophytes. Trasimeno is a close lake, with un-stratified and very shallow waters characterized by an irregular hydrological regime of about 24 years of spare time. The high concentration of phytoplankton and the suspended solids, make lake waters unclear (less than 1 m) threatened by drought and anoxia and the consequent impacts over fish populations and over the stability of the trophic chains. Since 2000, the lacustrine ecosystem is a protected area (Natura 2000 sites) for its exceptional value for flora and fauna richness and species diversity.

Table 5.1 - Lake Trasimeno environmental characteristics

LAKE TOTAL SURFACE	124 KM^2
CENTRE LAKE COORDINATES	43°06'N; 12°07'E
MEAN DIAMETER	CIRCULAR, 11 KM
DEPTH	AVERAGE BOTTOM DEPTH 4.5 M MAXIMUM DEPTH 6 M
PERIOD OF RENEWAL OF WATER	24 YEARS
RATE OF EVAPORATION	(155X106 M3/YEAR)
SECCHI DISC	DEPTH 1 M

The actual annual rainfall recorded at the Monte del Lago station is about 754 mm; with a main maximum in autumn and a secondary in the spring. The average annual temperature is 14° C and the maximum value is recorded in July. Based on the calculation of bioclimatic indexes (Biondi & Baldoni, 1994) the bioclimatic typology moving from the north to the south, is meso - Mediterranean to sub - humid (Venanzoni et al., 2006).

The reeds of Lake Trasimeno, for which in 1988 was estimated an area of 10.48 km^2 (PUT data in Mearelli et al., 1990) and in 2005 just 3.56 km^2, are probably amongst the largest of peninsular Italy and are certainly dominated by *Phragmites australis*. Environmental issues that have historically threatened the lake ecosystem are mainly attributable to the phenomena of eutrophication of anthropogenic origin and at the present are accentuated by highly irregular water regime that, in the absence of tributaries of relief, is subject to the contribution of precipitation and river basin (Mearelli et al., 1990, Viotti et al., 2002).

The helophytic vegetation of the coastal water basin of Lake Trasimeno can be grouped in *Phragmites australis* and association of *Typha angustifolia*, *Scirpus maritimus,* and *Scirpus lacustris*. These species, especially in the southern east coast of the lake border, the line of hydrophytes mostly represented by the hydrophilic and rooting reeds and by submerged hydrophytes in opener waters. Examples are *Carex pseudocyperus, Potamogeton, Najas marina, Ceratophyllum demersum*, *Miriophyllum spicatum* and a variety of *Charophytes*. The macroalgal group of *Charophytesv* is considered a carbonatic bottom indicator because and colonizes carbonatic unconsolidated substrates by building benthic prairies that provide both sediment traps and lakebed habitat stabilization.

The major pressures in Trasimeno catchment are represented by tourism, agriculture and livestock breeding: Cultivated lands cover about 70% of the catchment's area of the lake even if intensive agriculture with irrigation s is present in only 28% of the area (Mearelli et al., 1981). The annual charge of organic carbon (500t), nitrogen (550t) and phosphorus (30t), even if not consistent, negatively affects water quality because of the specific seasonal temperature cycle coupled with irregular lake bed properties (Teatini, 1961; Mearelli et al., 1990, Bresciani et al., 2010).

The presence of boundaries represented by agricultural land use, actually prevents the natural readjustment of vegetation under the changing land-water gradient, and this generate disappearance of wetland in large areas and a reduction of helophytic communities, mainly represented by reeds. Reeds extension in 1994 was reduced by 19.1% compared to 1957. This phenomenon of subtraction of spaces is causing the gradual deterioration of marshes dominated by *Phragmites australis*, deeply fragmented (Venanzoni et al., 2008).

5.3 MATERIALS AND METHDOS

The region of interest of the lake considered in the present study has the extent of the available hyperspectral image and includes the eastern coasts until the Polvese Island.

On 12 May 2009 MIVIS hyperspectral and LiDAR data of eastern part of Lake Trasimeno were collected from an altitude of 2000 m. The Multispectral Infrared and Visible Imaging Spectrometer (MIVIS) is a hyperspectral whiskbroom scanner which consists of 4 spectrometers that simultaneously measure the radiation coming from the earth's surface in the visible, near – medium infrared, and thermal. Radiance values are automatically and simultaneously recorded in 102 bands on different tracks of the mass memory connected to the MIVIS sensor. Hyperspectral image was converted into remote sensing reflectance Rrs using the empirical line method calibrated with synchronous Rrs in situ data.

Bathymetry and reflectivity data were using an Airborne Hydrography (Sweden) LiDAR Hawkeye II, operated by BLOOM-CGR. The Hawkeye II altimeter has the

unique feature of using infrared (1064 nm) and green (532nm) wavelengths to acquire respectively topographic and bathymetric data. This provided a 4 m resolution Digital Surface Models (DSM) on the same Region of Interest. Point cloud filtering has been obtained on the base of hyperspectral contribution.
Synchronously to the airborne overpass limnological parameters such as concentrations of chlorophyll-a (chl-a), suspended particulate matter (SPM), coloured dissolved organic matter and absorption spectra of vegetation species and remote sensing reflectance (Rrs) of waters has been collected. Field data include in situ measurements from extensive field sampling surveys performed during the project. That represents the comprehensive dataset of water quality parameters, apparent and inherent optical properties and a spectral library of aquatic vegetation that can be used for both data quality assessment and products accuracy estimate.
The purposes of the field observations were twofold. First, field observations allowed identification of biophysical habitats and properties associated both to radiometric and limnological features. Secondly, field reconnaissance and laboratory analysis allowed the identification of significant parameters involved in image processing of the water quality and the physical environment. The spectral library of aquatic vegetation coupled with the turbidity measures, gave an overview of spectral features and albedo and enhanced the ability of benthic classification through image processing.

5.3.1 BIO OPTICAL MODELING OF WATERS

The first step of the analysis is based on the parameterisation of a bio-optical model used to assess water quality parameters (Giardino et al., 2012). The total absorption coefficient and the total backscattering coefficient were modelled as functions of concentrations of chl-a, SPM and CDOM. The specific backscattering coefficients were obtained indirectly by knowing Rrs data, the total absorption coefficient and concentrations of chl-a, SPM and CDOM.
In order to invert MIVIS Rrs data a bio-optical model (Lee1998a, b and Albert & Mobley, 2003) the modelled remote sensing reflectance Rrs, was expressed as a function of the subsurface irradiance reflectance coming from optically deep waters. The model was parameterised to run in optically deep waters because water lens above the macrophytes beds was little to generate a signal separable from the bottom (not

shown in this study). Once the model was calibrated it was applied to Rrs values derived from MIVIS data by running an optimization process through the minimization of a function δ which measures the spectral distance between modelled and image derived Rrs values. Starting from initial values of the unknowns (chl-a, SPM and CDOM), the predictor-corrector procedure change these values computing the distance function δ, at each step. The algorithm repeats this process until δ reaches a minimum value corresponding to the δ minimum and optimum (the best) set for the unknown variables (Giardino et al., 2012).

5.3.2 DOUBLE STEP CLASSIFICATION

LiDAR 4x4m DSM was generated on the base of MIVIS hyperspectral grid and stacked on the subset as an adjunct band. By calculating the standard deviation of the LiDAR point cloud on a 4 x 4 m grid, we observed and classified seafloor shapes (slope and aspect) that helps in categorize the seabed in vegetated and unconsolidated. Through the analysis of morphological parameters and by standard deviation classification we calculate the correlation with hyperspectral MIVIS bands in order to define the spatial mask for a reduction of the spectral subset. The contribution of LiDAR reflectance for classification purposes was assessed for those habitats by adding this information to the biological features. Several habitats, occurring below lake surface at the acquisition of the hyperspectral image, were not visible because of sun glint and/or water turbidity. This limitation enabled the assessment of the potential of hyperspectral LiDAR information for habitat discrimination.

Step 1. For these areas we applied a reliable technique in resolving spectral mixture of turbid waters. Spectral Mixture Analysis (SMA) is a methodology whereby an observed radiance is modelled as a linear mixture of spectrally pure endmember radiances. Linear mixture models are based on the observation that, in many situations, radiances reflected from surfaces with different "endmember" reflectance mix linearly in proportion to the area of each endmember within the Instantaneous Field Of View (IFOV) (Singer and McCord, 1979). This observation has made possible the development of a systematic methodology for spectral mixture analysis (Adams et al., 1993; Adams et al., 1986; Gillespie et al., 1990; Sabol et al., 1992) in which surface reflectance variations are described by a set of endmember fraction images representing spatial variations in the areal abundance of each endmember. By determining the mixing space topology generated on the base of Principal Component the dimensionality (Figure 5.2) and linearity of a system can be based on a collection of endmembers:

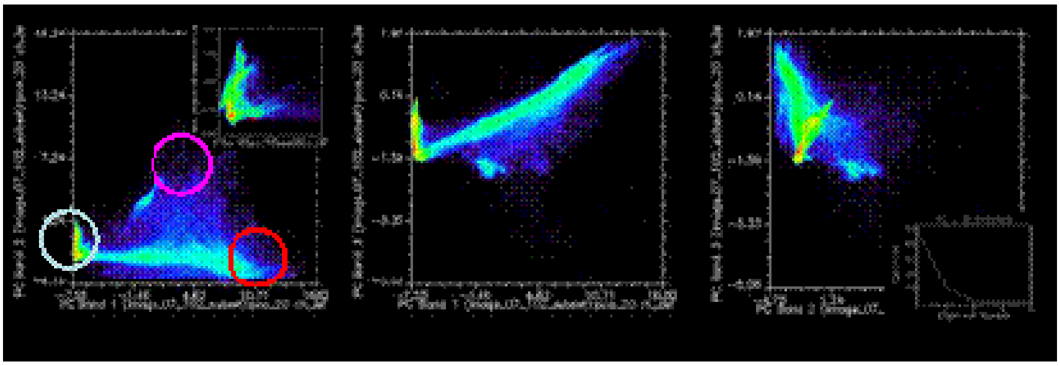

Figure 5.2 - a) 2D scatter plots of the 3 orthogonal views of the first 3 PCs (e.g. 1vs2, 1vs3, 3vs2) as in the Side, Top and End views; Circle identify the apexes were spectral profiles of endmembers are collected; b) examples of spectral collection from the 2d scatter plot.

The broadband multispectral imagery provided by MIVIS was used to classify and map the extent of vegetation presence and to distinguish them from dark and substrates. The estimated endmember fractions were then combined in colour composite maps to provide thresholds for expert decision boundaries.

Step2. The performance of the airborne hyperspectral data coupled with field spectral libraries to enhance the accuracy of habitat mapping was tested using a decision tree classification implemented in ENVI 5.0. This classification extracts a statistical signature for each habitat class based upon the mean and the variance of each spectral dataset, using only the training areas and signatures that represents physical features of bottom. The contribution of hyperspectral and topographic layers in the subsequent spectral unmixing classification was assessed individually and jointly to the visible bands conventionally used for photo-interpretation. A classification was computed firstly by introducing the bands corresponding to reeds and macrophytes and then to TSM. Subsequently, the bathymetry and the standard deviation whilst the classification accuracy when compared with the results of the non-bathymetric maximum likelihood classification.

5.4 RESULTS AND DISCUSSION

5.4.1 WATER QUALITY MAPS

The MIVIS derived images of chl-a, CDOM and SPM concentrations were overlaid to field measurements performed in five stations. For chl-a the agreement was higher (*r*=0.86) than for CDOM (*r*=0.68) but in both cases the MIVIS derived maps slightly underestimated in situ data. For SPM the validation in situ data collected at higher spatial resolution reduced the uncertainties commonly arising when remote sensing data are compared to in situ sampling (e.g., scale mismatching, time delay). Figure 5.3b and c shows the comparison, from north to south, of SPM concentrations derived from MIVIS data and of NTU values (Figure 5.3a) measured in situ with a flow-through system (FATA). In the northern part the match is good while a divergence occur in the lake centre. At the time of image acquisition the agreement was good, confirming the capabilities of MIVIS in describing the spatial variation of water quality in the lake.

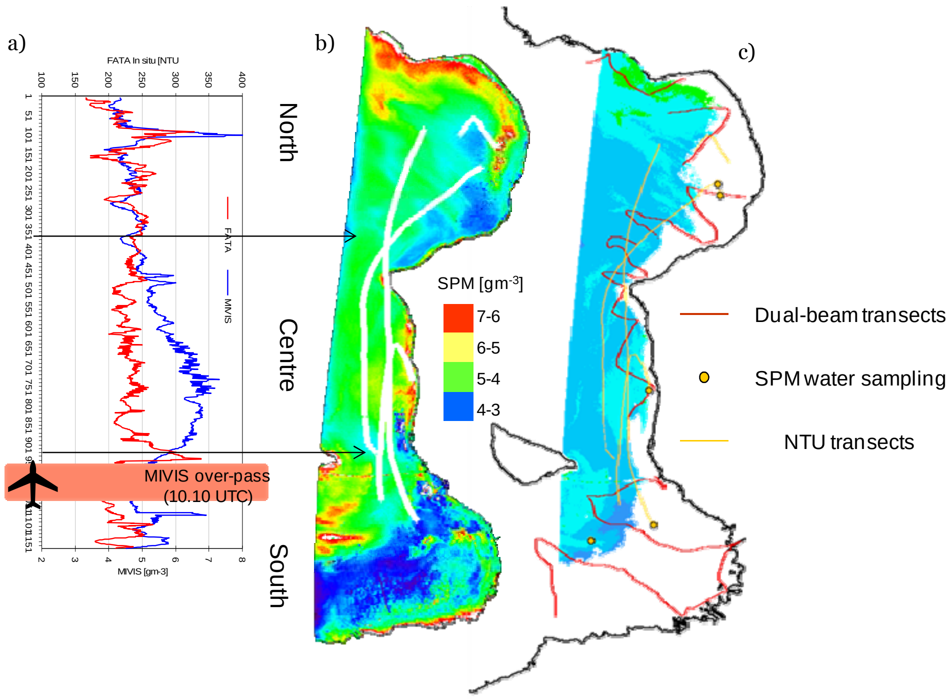

Figure 5.3 - Comparison of in situ measured and MIVIS derived water parameters values. a) Turbidity transect and spectral MIVIS response during the overpass. b) SPM modelled with bio optical parameterization; c) subsection into two subareas: in light blues optically deep waters.

The southern part of the processed image was not accessible with boat because of the presence of surface and submerged macrophytes coupled with the shallower bathymetries. In this area the transparency of waters is considered generally high because of the sediment capping action of macrophytes and the higher oxygen values. In this area residual reeds determine the high heterogeneity of lake bed bathymetries.

5.4.2 STEP 1. LIDAR DSM ANALYSIS

Through the analysis of LiDAR derived products interesting evidence has been observed for vegetated and not vegetated lake bed. The most representative calculated parameter starting to the filtered point cloud has been the standard deviation (Figure 5.4a). By weighing this parameter and the slope, we obtained classes of bottom rugosity that were associated to the main lake bed habitat typologies: surface or submerged macrophytes, sparse and dense reed. We threshold slope values to determine where DSM can represent lake bed habitat properties.

a) b)

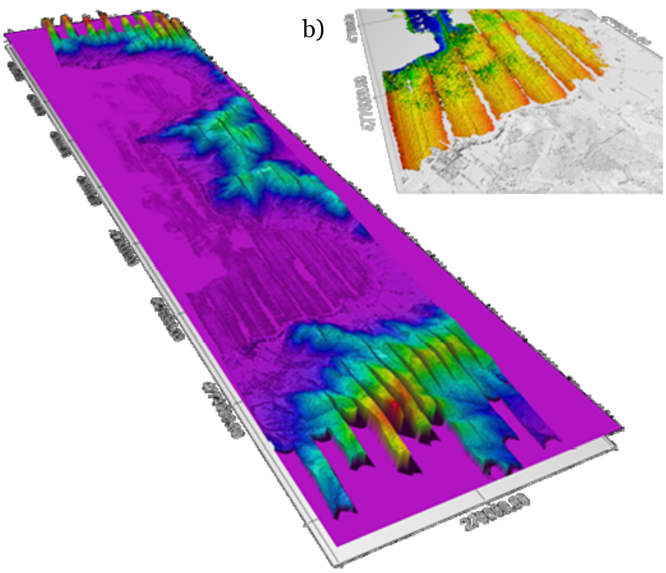

Figure 5.4 - 3d LiDAR DSM visualizations. a) The sum of backscatter expressed from yellow to red color scale; darker areas in the lakebed represent macrophytes and reeds root. b) Lakebed reflectance from LiDAR intensity, after filtering spikes and outliers. The view has been compared with the IGM cartography and improved in altimetry.

The most striking characteristic of LiDAR data is the low power of returns over areas like the ones with submerged macrophytes. Figure 5.5 shows the 3D views obtained with reflectance of the frontal reeds view. The deeper bathymetries stand out by their very low backscatter (Figure 5.5a). From submerged to semi submerged areas, increased heterogeneity of signals can be observed and reeds roof can be detected at both emerged and submerged level (Figure 5.5b).

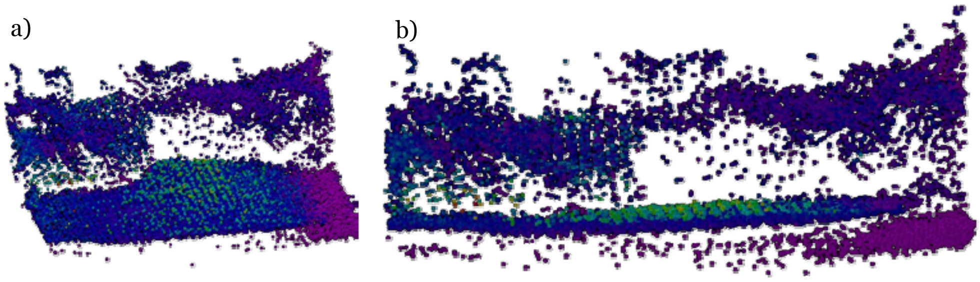

Figure 5.5 – LiDAR 3d reflectance points. In a) standing reeds are present and represent one of the tree color layers. b) Frontal view where the three level of vegetation are evident, Blu green coloured points represent the roof of submerged macrophytes. Purple can be either consolidated sediments or reeds root.

5.4.3 AQUATIC VEGETATION MAPS

The MIVIS image was georeferenced by a third degree polynomial function with ground control points and an interactive enhancement was obtained in the southern part in view of classification. We obtained PCA on the 20 hyperspectral bands between 440 and 750 nm. In this way the recognition of visible wavelength provided a synoptic view both aquatic and areal vegetation distribution. The preliminary habitat characterization has been achieved with the decision tree approach by integrating field observation and spectral libraries to image processing. This empirical approach led to the classification of the 30% of image with surface macrophytes that represent the 4% and 2% of the image covered by common reeds that correspond to about 42 ha (Figure 5.6).

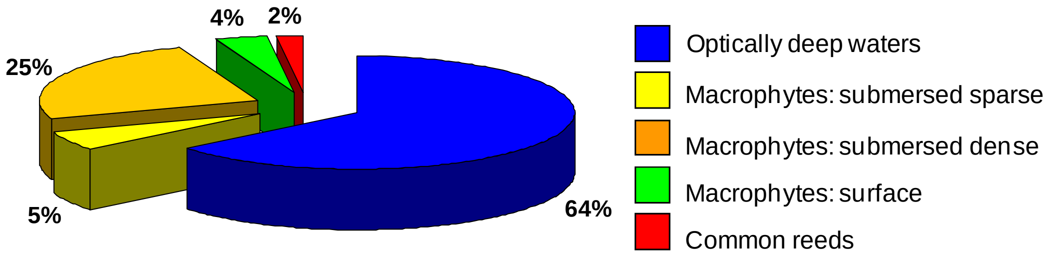

Figure 5.6 - Classification of aquatic vegetation from MIVIS data with field and image based decision tree classifier.

Spectral Mixture Analysis (SMA) classifies individual mixed pixels according to the distribution of spectrally pure endmember fractions and provides a tool for discrimination among different types of reflectance properties in each pixel. So that by selecting tree and four spectral signatures, of turbid water, of substrate and vegetation typologies the spectral mixture model allowed generating a variety of fraction of information for each pixel.

By using the ‘common reeds’ class to create the subset area where reeds are certainly presents, through the application of an image based SMA we analysed both plant composition and distribution (Figure 5.7). The southern area, showed across the original continuous reed the fragmented aquatic edge that represent the retreatment process (Figure 5.7 b). By analysing substrate fraction maps both the terrestrial and the aquatic front of reeds appear as transitional from reed to non-reed marshes with lower level of density. It is evident the dissection in two subareas due to the managed enlargement of a main channel (Figure 5.7 c, d, e) that run across the coastline and enlarge his bed at the connection with the open waters.

In the aquatic front we measured the presence of lower cover of reeds, with values that varies from 30% to 60%.

The distribution of the turbidity fraction map suggested the presence of a heterogeneous lake bed in the aquatic front of reeds and this also coupling with the TSM modelling . Whereas, moving along transect from land to waters, the density of plant increases until 80% - 100% of presence per pixel.

The lake front of this area is totally occupied by sparse reeds and a growing channel network. Reflectance along the analysed subset of the coast quantitatively fit with the NDVI providing accuracy of 92% (Figure 5.7 f). Less has been the overlap between the decision tree (Figure 5.7 g) classification based on field observation and radiometry either if the overall comparison suggest the presence of different spatial patterns.

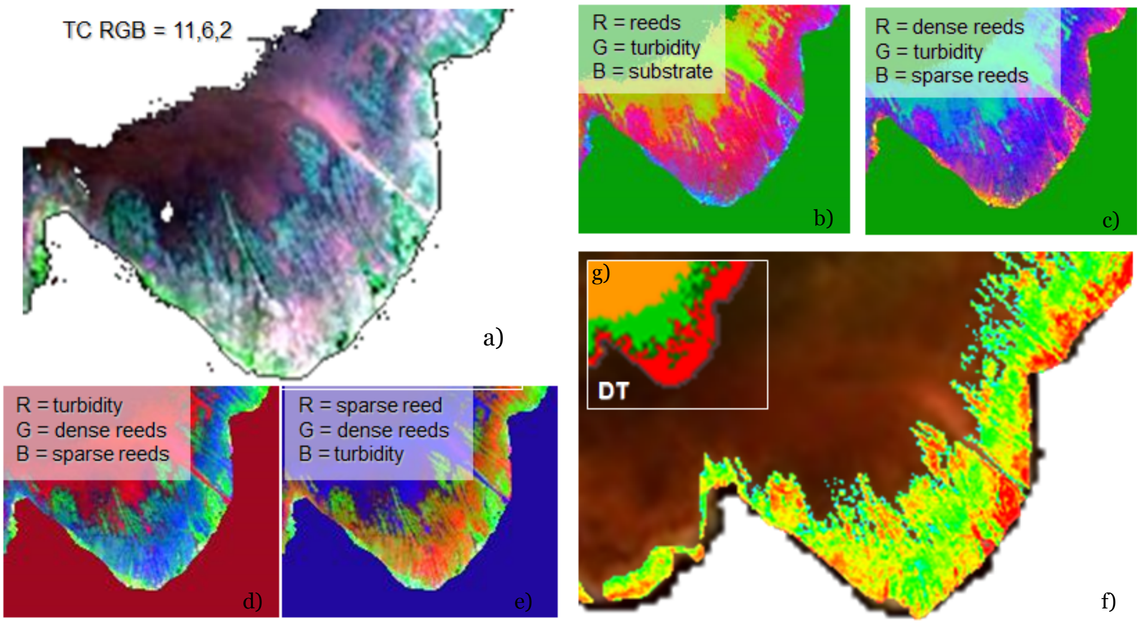

Figure 5.7 - Aquatic and terrestrial side of reeds. a) RGB true colour composite. b) – e) RGB composite of fraction maps: in b) substrate is represented in yellow while reeds are blue and violet - purple; in c) sparse reeds are mixed with turbidity in blue green gradients; in d)-e) enhancement of blue and red respectively indicate sparse reeds in coastal side; f) NDVI; g) Decision Tree.

SMA applied to the reed subset provided the possibility of collecting a couple of spectral profiles associated with dense reed and sparse reeds.

Results of validation are based on the diachronic map of reeds changes from 1954 to 2005 (Filipponi et al., 2010) of the southern part of the lake (Figure 5.8a). This map is based on ortophoto interpretation and is considered a valid reference in terms of accuracy to define growing reed and the past extension of plants.

SMA showed interesting gradients moving from small and circular patches probably residual of the retreatment (Figure 5.8b-c) and densely populated areas (Figure 5.8d). Hyperspectral fraction abundances showed very high capacities in reeds retrieving, both in areal and aquatic areas and gave back details useful to lake bed reconnaissance.

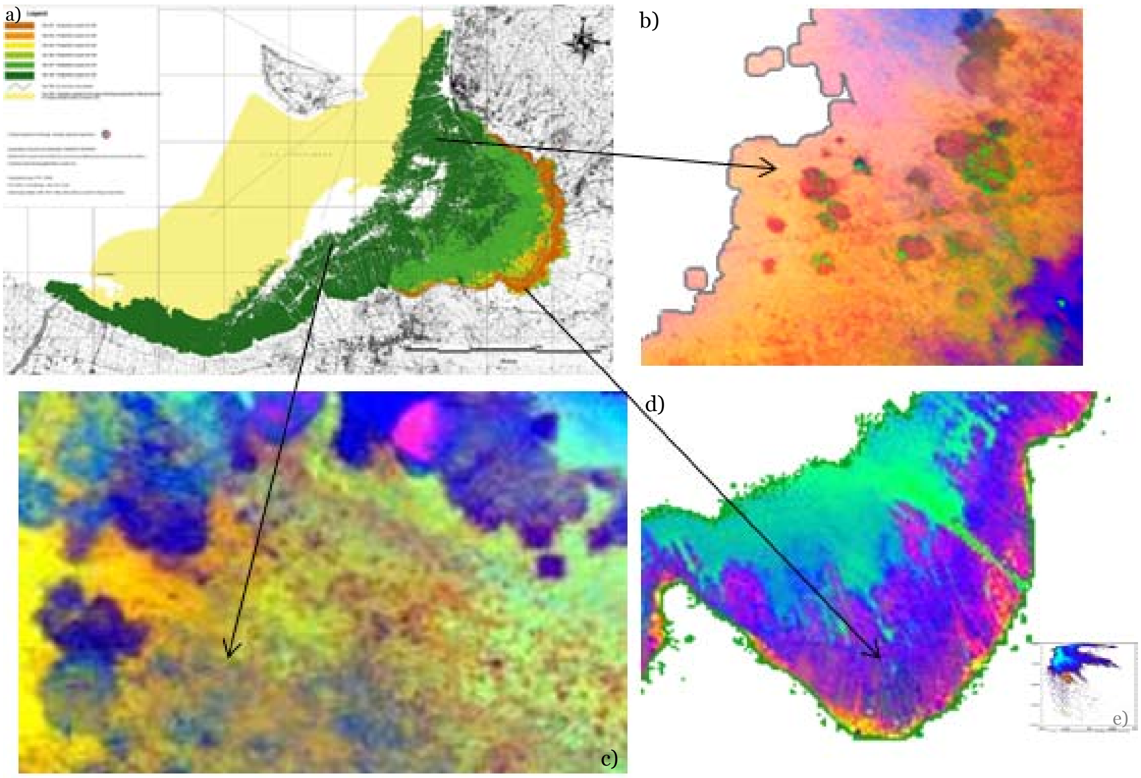

Figure 5.8 - Reeds: a) 2005 map (Filipponi et., al 2006); b) small and circular patches of reeds roots or pioneer patches; c) sparse vegetation signals from the bottom; d) reeds and water turbity obtained to highlight coastal vegetation patterns (violet- blue); e) multidimensional space with orange selection of coastal sediments.

Looking at the standard deviation of lake bed classified from LiDAR and bio optical turbidity maps the lake bed resulted complex in terms of morphologies and spectral properties due to the presence of submerged and surface macrophytes intersected with the residual root network of the past reed.

When SMA was applied to the aquatic areas in view of retrieving macrophytes we observed a mixture of gradients in vegetation signal that mix linearly with the turbidity fraction. This highlighted the possibility of dissecting water from lake bed signal and mapping also dense submerged macrophytes, almost where the level of sediment concentration measured by the turbidity fraction would results lower (Figure 5.9). An important issue arose from the 5 endmember mixture model. The lower values of reflectance fraction of reeds usually correspond to the higher transparency and in general to the presence of macrophytes on the lake bed.

More significant evidences are detectable if LIDAR DSM and standard deviation are associated with the hyperspectral derived fraction maps.

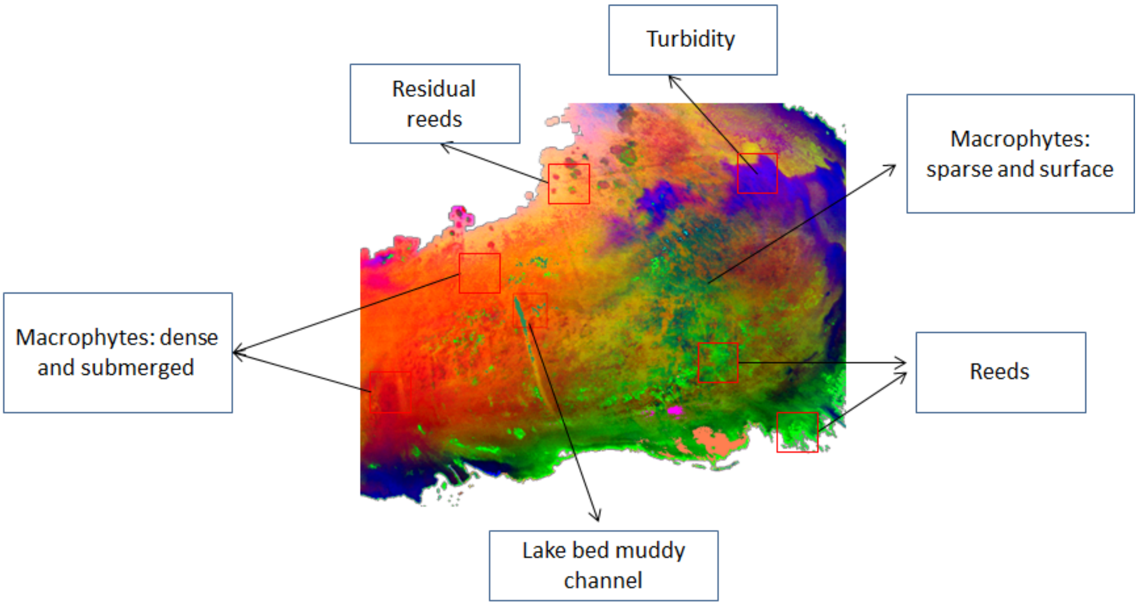

Figure 5.9 – RGB composite of fraction maps on the base of LiDAR and field hyperspectral library analysis. All the validated details are highlighted and gradients of features can be seen through the RGB color composite analysis.

The objectives of the LiDAR-MIVIS analysis combined with field validation were to provide a baseline to lake bed cover discrimination through vegetation mapping and bathymetries retrieving.

By representing a multispectral feature space with the low order PCs the topology as a 2D space was used to retrieve the physical effect due to the morphology (Figure 5.9). The LIDAR bathymetry and the standard deviation values revealed their particular use for augmenting the MIVIS surface classification being added to the multidimensional space. Smoother surfaces showed smaller roughness than rough surfaces such as vegetated areas or muddy bottom. This multisource mixture space provided the possibility of building a final map by overlaying all vegetation classes on the ratios between standard deviation and the total suspended matters.

This opportunity, due to the contemporary acquisition, led to the definition of the presence of macrophytes along the northern east coast of the area.

Moving through areas validated with field spectral radiometer the 75% of randomly selected pixel match the spectral profile identified by the endmember collection. The point with major erroneous mismatching were among macrophytes at depths below the water level minimum variation with a variety of the values of water transparency that at the end, determines the deep influence of TSM in both LiDAR and MIVIS recorded signals.

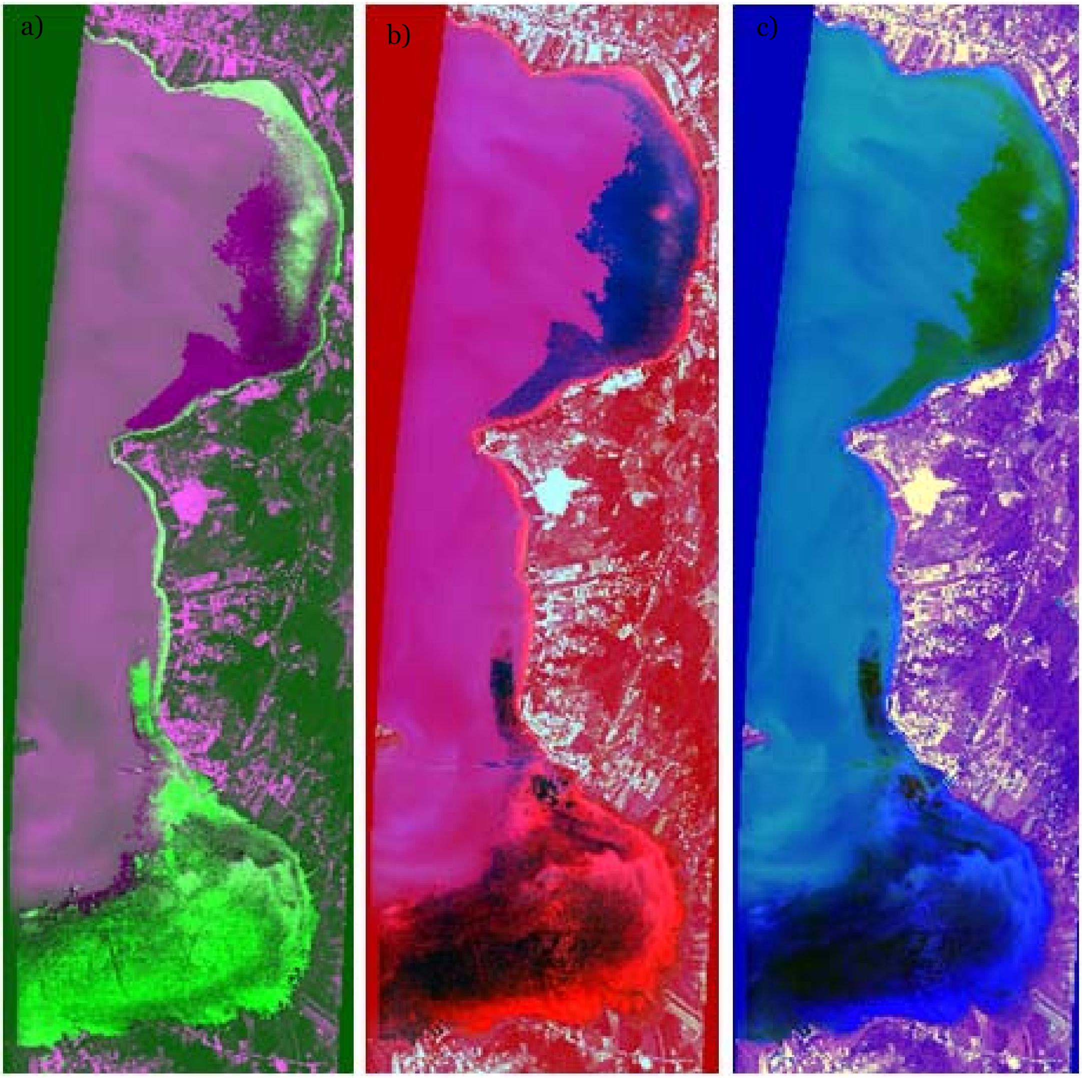

Figure 5.10 - Color composite RGB of vegetation and turbidity fraction maps. In a) reeds and surface vegetation are enhanced with green, and purple is the mostly submerged macrophytes area; in b) and c) mixture of submerged and emerged vegetation are highlighted in the south while the northern basin resulted poor of emerged vegetation. High definition is obtained also for the middle lake coast.

The generation of a final map of the entire region separately analysed gave the finest scale of mapping and a multi-layered dataset for both empirical and modelled parameterization of pattern and process.

The preliminary classification based on the spectral evidence measured with field instrumentation provided a set of masks with specific spectral common properties in that defined different regions of interest. Then, by coupling the powerful analysis of spectral mixture and bio optical models with the physical retrieving of LiDAR altimetry, vegetation has been mapped at the finest scale.

Physical and biological compositions are the primary determinants of the inherent reflectance properties at a landscape scale. In shallow waters environments, optical responses are strictly dependent by the turbidity and by nutrient availability that can drive algal blooms (transparency (cm) = 130-150; Chl-a (µg/l) = 1.5—4.3 during the survey). The effectiveness of classification with hyperspectral data that has undergone SMA showed that the effort in endmember selection in a complex landscape has to be enhanced by the use of field observation. In this way, the decision trees are based both on spectral libraries and image endmember collection. Proxy for mixture interpretation and the results of the present work flow demonstrate that accuracy depend on the endmember collection and that hyperspectral data allow to enlarge the linear mixture model to more than three/four endmember. Resolution of separate classification (Figures 5.11) of each unmixed pixels and LiDAR reflectance/backscatter gives the necessary extent to the habitat analysis providing feedback from both bottom and water physical properties.

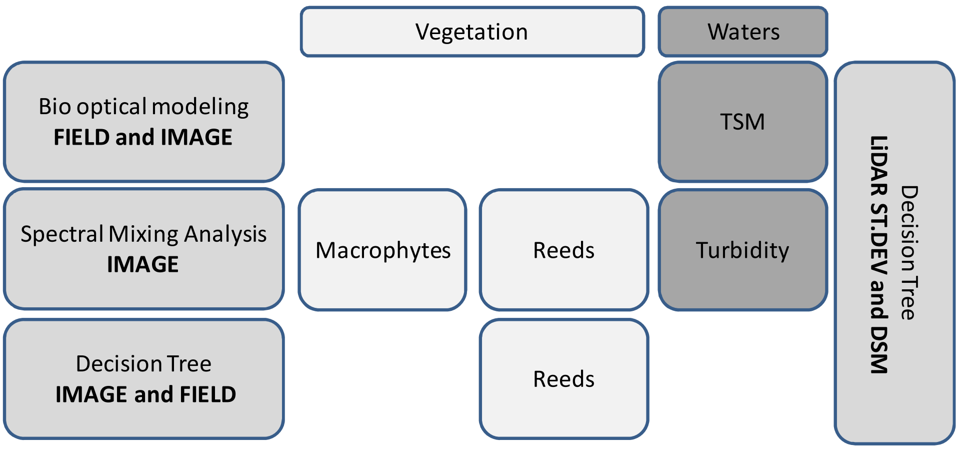

Figure 5.11 – Products and processing blocks

The first evidence of this approach is that remote observation gives a synoptic view of environmental variability and allows a conservative view of that variability. This is the base to predict ecosystem structure and function changes.

5.5 CONCLUSIONS

The decreasing of both biodiversity of the fish fauna and the complexity of aquatic vegetation of Trasimeno Lakeis is causing changes in the distribution and nature of the submerged vegetation. In particular, these changes represent a sign of instability and potential ecological health alert. Among the various hypotheses to attempt at the identification of the causes of such degradation, the water quality, deeply affected by inputs of organic matter and minerals, is probably one of the main driver coupled with the natural filling tendency of the basin.

Our strategy is to model aquatic vegetation from MIVIS hyperspectral imagery by using field observation to verify the accuracy of the model and to use spectral mixture analysis to represent lake bed reflectance as continuum of biophysical properties with LiDAR altimetry.

Among LiDAR metrics (i.e coastal depth and roughness) and the biotic and optical properties from MIVIS (i.e coastal lakebed habitat), the questions that different surfaces, with their shapes and features may influence the reflected signature of physical targets revealed different ways of target mixtures.

The combined analysis of the lake bed revealed some interesting ecological features of Lake Trasimeno and suggests developing the interpretation of numerical results into a systematic ecosystem analysis. This would be possible by using this mapping dataset to models (e.g. hydrology) or to temporal series in order to participate with quantitative answer to conservation and management strategies.

ACKNOWLEDGEMENTS

Thanks to Dr. Luca Gasperini for funding through the agreement "CNR-ISMAR Bologna & Regione Umbria for the paleoclimatic reconstruction of Trasimeno Lake" the LiDAR – MIVIS acquisition.

5.6 REFERENCES

1 Adams et al., 1993; Adams et al., 1986. Gillespie et al., 1990; Sabol et al., 1992

2 Adams, J.B., M.O. Smith, and A.R. Gillespie, 1993. Imaging Spectroscopy: Interpretation based on spectral mixture analysis, in Remote Geochemical Analysis: Elemental and Mineralogical Composition, edited by C.M. Pieters, and P. Englert, pp. 145-166, Cambridge University Press, New York.

3 Adams, J.B., M.O. Smith, and P.E. Johnson, Spectral mixture modeling; A new analysis of rock and soil types at the Viking Lander 1 site, Journal of Geophysical Research, 91, 8098-8122, 1986.

4 Alberotanza L, Brando VE, Ravagnan G, Zandonella A. (1999), "Hyperspectral aerial images. A valuable tool for submerged vegetation recognition in the Orbetello Lagoons, Italy," International Journal Of Remote Sensing, 20: 523-533

5 Albert, A., & Mobley, C.D. (2003). An analytical model for subsurface irradiance and remote sensing reflectance in deep and shallow case-2 waters. *Opt. Exp.,* **11**, 2873-2890.

6 Artigas F, Yang J. 2005. Hyperspectral remote sensing of marsh species and plant vigour gradient in the New Jersey Meadowlands. *International Journal of Remote Sensing* 26 : 5209–5220.

7 Barducci A, Guzzi D, Marcoionni P, Pippi I. 2009. Aerospace wetland monitoring by hyperspectral imaging sensors: A case study in the coastal zone of San Rossore Natural Park. *Journal of environmental managemen*t. 90: 2278–2286.

8 Brando, V.E., Anstee, J.M., Wettle M., Dekker A.G., Phinn S.R., & Roelfsema, C. (2009). A physics based retrieval and quality assessment of bathymetry from suboptimal hyperspectral data, *Rem. Sens. of Environ*., **113**, 775-770.

9 Biondi, E., & Baldoni, M. (1994). Climate and vegetation of the Italian peninsula. *Anais do Instituto Superior de Agronomia*, *44*(1), 75-135.

10 Boak, E. H., & Turner, I. L. (2005). Shoreline definition and detection: a review. *Journal of Coastal Research*, 688-703.

11 Boschetti M, Boschetti L, Oliveri S, Casati L, Canova I. 2007. Tree species mapping with Airborne hyper-spectral MIVIS data: the Ticino Park study case. *International Journal of Remote Sensing* 28: 1251–1261.

12 Brando, V.E., Anstee, J.M., Wettle M., Dekker A.G., Phinn S.R., & Roelfsema, C. (2009). A physics based retrieval and quality assessment of bathymetry from suboptimal hyperspectral data, *Rem. Sens. of Environ*., 113, 775-770.

13 Bresciani, M., Giardino, C., Musanti, M., Martinelli, A., Taramelli, A., & Valentini, E. (2010). *Mappatura delle macrofite del lago Trasimeno tramite tecniche di telerilevamento.* Special Issue Conference SITE, Bolzano 2009 (In press).

14 Calvo S, Ciraolo G, La Loggia G. 2003. Monitoring *Posidonia oceanica* meadows in a Mediterranean coastal lagoon (Stagnone, Italy) by means of neural network and ISODATA

classification methods. *International Journal of Remote Sensing* 24 : 2703–2716.

15 Cingolani L, Marchetti G, Martinelli A, Rapi G, Cantucci A (2005) Misure per il contenimento del carico diffuso nel Piano di Tutela delle acque della Regione Umbria. 2nd Int. Conf. LIFE. Libri ARPA Umbria, Italy.

16 Coppin, P, Jonckheere, I, Nackaerts, K, Muys, B, & Lambin, E. (2004). Digital change detection in ecosystem monitoring. *Int. J. Rem. Sens*., **25**, 1565-1596.

17 Costa, B. M., Battista, T. A., & Pittman, S. J. (2009). Comparative evaluation of airborne LiDAR and ship-based multibeam SoNAR bathymetry and intensity for mapping coral reef ecosystems. *Remote Sensing of Environment*, 113(5), 1082-1100.

18 Costanza, R., & WALLACE, K. (2008). Ecosystem services: Multiple classification systems are needed. Authors' reply. Biological conservation, 141(2), 350-354.Arnot, C., Fisher, P. F., Wadsworth, R., & Wellens, J. (2004). Landscape metrics with ecotones: pattern under uncertainty. *Landscape Ecology*, *19*, 181-195.

19 Davidson-Arnott RGD, MacQuarrie K, Aagaard T. 2005b. The effect of wind gusts, moisture content and fetch length on sand transport on a beach. Geomorphology 68: 115–129.

20 Deronde B, Houthuys R, Debruyn W, Fransaer D, Lancker VV, Henriet J-P. 2006. Use of Airborne Hyperspectral Data and Laserscan Data to Study Beach Morphodynamics along the Belgian Coast. *Journal of Coastal Research* 225 : 1108–1117. DOI: 10.2112/04-0264.1

21 Davidson-Arnott RGD. 2005a. Conceptual model of the effects of sea level rise on sandy coasts. Journal of Coastal Research : 1166–1172.

22 Filipponi F., Gigante D., Venanzoni R, 2010. 46° Conference Socirtà Italiana di Scienze della Vegetazione. Pavia, 17-19/02/2010.

23 Giardino C., Candiani G., Bresciani M., Lee Z., Gagliano S., Pepe M., (2012). BOMBER: a tool for estimating water quality and bottom properties from remote sensing images. *Computers & Geosciences*, doi:10.1016/j.cageo. 2011.11.022.

24 Giardino, C., Bartoli, M., Candiani, G., Bresciani, M., & Pellegrini, L. (2007). Recent changes in macrophyte colonisation patterns: an imaging spectrometry-based evaluation of southern Lake Garda (northern Italy). *J. of App. Rem. Sens*., (SPIE), **1**, 011509.

25 Gillespie, A., M. Smith, J. Adarns, and S. Willis, 1990. Spectral mixture analysis of multispectral thermal infrared images, Proc. 2nd Thermal IR Multispectral Scanner (TIMS) Workshop, JPL Publ. 90-33, pp. 57-74.

26 Goodman JA, Lee ZP, Ustin SL. 2008. Influence of atmospheric and sea-surface corrections on retrieval of bottom depth and reflectance using a semi-analytical model: a case study in Kaneohe Bay, Hawaii. *Applied optics* 47: F1–F11.

27 Guenther GC. 2007. Airborne lidar bathymetry. In Digital elevation model technologies and applications: the DEM user's manual ,. *American Society of Photogrammetry and Remote Sensing* Bethesda, Maryland; 253–320.

28 Hochberg, E. J., & Atkinson, M. J. (2003). Capabilities of remote sensors to classify coral, algae, and sand as pure and mixed spectra. *Remote Sensing of Environment*, 85, 174−189.

29 Ibrahim E, Monbaliu J. 2011. Suitability of spaceborne multispectral data for inter-tidal sediment characterization: A case study. Estuarine, *Coastal and Shelf Science* 92 : 437–445.

30 Irish JL, White TE. 1998. Coastal engineering applications of high-resolution lidar bathymetry. *Coastal Engineering* 35: 47–71.

31 Jeppesen, E., Søndergaard, M., Søndergaard, M., & Christoffersen, K. (Eds.) (1998). *The Structuring Role of Submerged Macrophytes in Lakes*. *Ecological Series* (vol. 131), Springer-Verlag. 58

32 Kuffner IB, Brock JC, Grober-Dunsmore R, Bonito VE, Hickey TD, Wright CW (2007) Relationships between reef fish communities and remotely sensed rugosity measurements in Biscayne National Park, Florida, USA. Environ Biol Fish 78:71-

33 Lawrence RL, Wood SD, Sheley RL. 2006. Mapping invasive plants using hyperspectral imagery and Breiman Cutler classifications (RandomForest). *Remote Sensing of Environment* 100: 356–362.

34 Lee, Z., Carder, K.L., Chen, R.F., & Peacock, T.G. (2001). Properties of the water column and bottom derived from Airborne Visible Infrared Imaging Specrometer (AVIRIS) data. *J. Geophys. Res.*, **106**, 11,639-11,651.

35 Lee, Z., Carder, K.L., Mobley, C.D., Steward R.G., & Patch, J.S. (1998a). Hyperspectral remote sensing for shallow waters: 1. A semi analytical model. *Appl. Opt.*, **37**, 6329-6338.

36 Lee, Z., Carder, K.L., Mobley, C.D., Steward R.G., & Patch, J.S. (1998b). Hyperspectral remote sensing for shallow waters: 2. Deriving bottom depths and water properties by optimization. *Appl. Opt.*, **38**, 3831-3843.

37 Marani M, Belluco E, Ferrari S, Silvestri S, D'Alpaos A, Lanzoni S, Feola A, Rinaldo A. 2006. Analysis, synthesis and modelling of high-resolution observations of salt-marsh ecogeomorphological patterns in the Venice lagoon. *Estuarine, Coastal and Shelf Science* 69: 414-426, doi: 10.1016/j.ecss.2006.05.021.

38 Mearelli M., Lorenzoni M., Mantilacci L., 1990. Il Lago Trasimeno. Riv. Idrobiol., 29 (1): 353-389.

39 Mearelli M., Lorenzoni M., Ruffini F., 1981. Determinazione dello stato trofico del lago Trasimeno attraverso la valutazione indiretta dell'azoto e del fosforo. Riv. Idrobiol., 20, (3): 572-587.

40 Orsomando E., 1993. Carte della vegetazione dei fogli Passignano su Trasimeno e Foligno. Braun-Blanquetia, 10: 3-26, . Camerino.

41 Orsomando E., Catorci A., 1991. Carta della vegetazione del Comprensorio del Trasimeno. Associazione Comuni del Trasimeno, Dip. di Botanica ed Ecologia dell'Università di Camerino, 11-74.

42 Pinnel, N. (2007). A method for mapping submerged macrophytes in lakes using hyperspectral remote sensing. Ph.D. Thesis, Department für Ökologie und Ökosystemmanagement, Fachbereich für Limnologie, Technische Universität München, Germany (2007).

43 Reguzzoni, M., Sansò, F., Venuti, G., & Brivio, P.A. (2003). Bayesian classification by data augmentation. *Int. J. Rem. Sens.* **24**, 3961-3981.

44 Sabol, D.E., J.B. Adams, and M.O. Smith, (1992). Quantitative sub-pixel spectral detection of targets in multispectral images, *Journal of Geophysical Research*, 97, 2659-2672.

45 Singer, R.B., and T.B. McCord, Mars: Large scale mixing of bright and dark surface materials and implications for analysis of spectral reflectance, in 10th Lunar and Planetary Science Conference, pp. 1835-1848, *American Geophysical Union*, 1979.

46 Singer, R.B., Near-infrared spextral reflectance of mineral mixtures: systematic combinations of pyroxenes, olivie and iron oxides, Journal of Geophysical Research, 86, 7967-7982, 1981.

47 Taramelli A., Giardino C., Gasperini L, Del Bianco F., Bresciani M., Valentini E., et al., 2010. Biophysical and morphological study of coastal habitats from imaging spectrometry, lidar and in situ data acquisition, proceedings of 'hyperspectral 2010 workshop', (esa sp-683, may 2010).

48 Teatini D., 1961. Il Trasimeno sulla china della decadenza. Conferenza promossa dal Rotary Club di Perugia.

49 Tsai F, Lin EK, Yoshino K. 2007. Spectrally segmented principal component analysis of hyperspectral imagery for mapping invasive plant species. *International Journal of Remote Sensing,* 28: 1023–1039.

50 van der Wal D, Herman PMJ. 2007. Regression-based synergy of optical, shortwave infrared and microwave remote sensing for monitoring the grain-size of intertidal sediments. *Remote Sensing of Environment* 111: 89–106.

51 Venanzoni R., Gigante D., Montagnoli L., Frattegiani M., (2006). Habitat e Specie della Direttiva 92/43/CEE ed altri aspetti di rilevanza naturalistica al Lago Trasimeno. Perugia. AP&elle s.r.l. 96 pp.

52 Venanzoni R., Gigante D., Pedini A., Ficola M., Reale L., 2008. Intervento di riqualificazione del canneto per la conservazione della biodiversità del Lago Trasimeno. Rapporto conclusivo interno all'Ente. Provincia di Perugia. 77 pp.

53 Viotti P., Galeotti L., Sbaffoni S., Sappa G., Leccese M., Stracqualursi N., 2002. Analisi sperimentale dei flussi di fosforo dai sedimenti di un lago: il caso del Lago Trasimeno (Italia). VI Simpósio Ítalo Brasileiro de Engenharia Sanitária e Ambiental.

54 Wedding, L. M., Friedlander, A. M., McGranaghan, M., Yost, R. S., & Monaco, M. E. (2008). Using bathymetric lidar to define nearshore benthic habitat complexity: Implications for management of reef fish assemblages in Hawaii. *Remote Sensing of Environment*, 112(11), 4159-4165.

55 Zedler, J. B. (2000). Progress in wetland restoration ecology. *Trends in Ecology & Evolution*, 15(10), 402-407.

56 Zedler, J. B., & Kercher, S. (2005). Wetland resources: status, trends, ecosystem services, and restorability. *Annu. Rev. Environ. Resour.*, 30, 39-7.

6. CONCLUSIONS

Ecological and economical goals can be mutually beneficial and according to the objective of delivering the huge amount of information from Earth Observation to the decision process, this research targets natural resources monitoring from the most recent remote sensing technologies through biophysical mapping. A new paradigm arises when biophysical mapping means that biological properties can be integrated with geomorphic features such as topography or roughness into quantitative spatial analysis and models. This would provide new insight in landscape classification because of the possibility of observing both pattern and process through a contemporary detailed and synoptic scale.

The built up methodology is based on the implementation of an innovative approach to use consolidated processing methodologies and knowledge into formal procedures. FHyL represents the main achievement of the present work being a set of modules for repeatable and flexible processing process and being able to delineate the way of data fusion and integration from: field (both radiometry and characterization) and airborne (hyperspectral imagery and LiDAR altimetry) measures, to map complex coastal ecosystem. A multidimensional space based on the Principal Component Analysis of multisource datasets allows the identification of a variety of habitat features as well as the arrangements of landforms that host biological communities. FHyL can be considered a first attempt to analyze feedback from ecology and geomorphology by scaling down ecological observation from landscape level to habitat components through recent remote sensing technologies.

Dealing with aquatic and terrestrial environments and moving from marine coasts to the freshwater wetlands a lot of technical enhancement in data management and analysis grew up during that research. Highlights are in the case of:

- <u>Shallow seabed</u>, where the transparency of waters allowed the development of a physically based approach in spectral mixture analysis. Both field and laboratory measurements revealed unique constrains to simulate benthic seabed properties under coastal waters. The benthic habitat mapping has been achieved with very high accuracy until – 6/ - 8 m of depth and vegetation composition retrieval provided seagrass and seaweeds presence and cover per pixel. The availability of high resolution LiDAR point cloud and derived DSM products represented the innovation of the approach in seabed mapping. Moreover LiDAR bathymetry and standard deviation provides the adjunct band to define limits in optical retrieving of seabed. That information defines boundaries of consolidated and unconsolidated seafloor (standard deviation) and thresholds of optical changes moving along coastal depth.

- Beach dune system, where the combined use of active and passive sensors showed the capability of retrieving vegetation presence and structure. By integrating field measurements and botanical assessment, hyperspectral mixture analysis lead the bases for a new classification system based on spectral libraries implementation and more comprehensive definition of habitat indicators
- Shallow muddy lake bed, where the developed algorithm revealed the possibility of taking into account the turbidity effects more than the bathymetry to normalize vegetation analysis. Coupling consolidated bio optical modeling of water quality parameters with the spectral mixture analysis provided the possibility of identifying benthic and surface macrophytes. Moreover a focus on riparian reeds showed the ability of recognizing intra-specific differences between patches of reeds. Reed distribution in the lake varies from sparse to dense and interesting features has been detected adding the 3D visualization from LiDAR reflectance.

Remote sensing data and services they provide and the information they store in, delivered the ability to foster the creation of environmental analysis and resources management.

In example, the detailed resolution obtained for the spatial distribution of seaweeds, not only indicates a quantitative presence of seaweeds in this area, but also suggests, if combined with the cover % map of *P. oceanica*, to speculate the spread of seaweeds near defense coastal structures.

This analysis defines a methodological process of spatial and spectral scaling down and scaling up on the base of emerged and submerged vegetation typologies and landforms. Biophysical indicators are obtained by relating physical maps into habitat hyper layers of measures able to describe landscape from the tridimensional canopy of lake reeds to

the presence of specific beach dune plant association on the base of their physical structures.
In the last decade, ecologists have focused on estimating the economic value of some ecosystem services and on the evaluation of gains and losses with respect to changes in current levels. Primary production, for example, plays a key role in the functional processes of ecosystems; affecting the circulation and the presence of species, water quality and substrate stability, especially in transitional and shallow waters.
So that biophysical maps are now largely used as decision support and thematic layers in coastal modeling could be in a near future used as input in natural capital estimation as well as in vulnerability and exposure analysis.
Within a context of Ecology and biological resources management, airborne and field techniques has revealed interesting options in monitoring coastal nearshore zones. Airborne multisensory acquisition has been an important cost of this research (~1600€/km^2) mostly because of the mobilization and demobilization of sensors and airplanes. Field data collection, laboratory analysis, logistics and surveys were about 2/3 more per kilometer. In this monitoring test, the first in Italy in its own characteristics, the highest effort has been certainly processing and post processing effort because of the unavailability of already implemented procedures for coastal integrated analysis and because of the groundtruth effort required with new remote sensing technologies implementation. With this work and the overall results of these research standards for data and processing tools have been developed hoping this will determines also a reduction of processing and post processing effort.

7. KEY DISSEMINATION ACTIVITIES

2012-2013

Submitted paper

Emiliana Valentini, Andrea Taramelli, Carlo Innocenti, 2013. FHyL: Field spectral libraries, airborne Hyperspectral images and LiDAR altimetry for complex coastal seabed mapping. *Remote Sensing of Environment.*

Andrea Taramelli, **Emiliana Valentini**, Carlo Innocenti, Sergio Cappucci, Matteo Conti, Elena Pallottini, Use of Airborne Lidar and Hyperspectral data to study the sandy beach morphology along the Lazio region coast (Italy), 2013. *Earth Surface Processes and Landforms.*

Submitted extended abstractt

Andrea Taramelli, **Emiliana Valentini**, Carlo Innocenti, Sergio Cappucci, 2013. FHyL: Field Spectral Libraries, Airborne Hyperspectral Images And Topographic And Bathymetric LiDAR Data For Complex Coastal Mapping. *IEEE International Geoscience and Remote Sensing Symposium.*

Carlo Innocenti, Federico Filipponi, **Emiliana Valentini**, Andrea Taramelli, 2013. A. multisensory data fusion method for the estimation of beach sediment features: mineralogical, grain size and moisture. *IEEE International Geoscience and Remote Sensing Symposium.*

2009 - 2012

Emiliana Valentini, Andrea Taramelli, Mariano Bresciani, Claudia Giardino, Federico Filipponi, Monica Targusi, Ciro Manzo, Leonardo Disperati. Spectral Libraries for emerged and submerged sandy beach using hyperspectral data. *ESA, Ecological Society of America* - 97th Annual Meeting. Portland (OR USA) 03-10/08/2012.

Loreta Cornacchia, Andrea Taramelli, **Emiliana Valentini**, Jaak A Monbaliu, Koen Sabbe. 2012. Magnitudes and spatial and temporal patterns of self-organized processes between geomorphology and biota that drive salt marsh evolution. *AGU Fall Meeting*. San Francisco 2-8/12/2012. CONTROL ID: 1482183.

Andrea Taramelli**, Emiliana Valentini**, Carlo Innocenti, Federico Filipponi, Raffaele Proietti, Luisa Nicoletti, Massimo Gabellini. 2012. Linking morphology to ecosystem structure using air-borne lidar and Hyperspectral sensors for monitoring the Coastal Landscape. *AGU Fall Meeting.* San Francisco 2-8/12/2012. Ecogeomorphology: EP31B- 0810.

Emiliana Valentini. II best project at the 'Licinio Ferretti' with the proposal "Coregistrazione e fusione di dati geospaziali multi sorgente e multitemporali". Parma, *ASITA Conference*, 15-18/11/2011. Reggia di Colorno, Parma. http://www.asita.it/cms/index.php?option=com_content&task=view&id=122&Itemid=95.

Carlo Innocenti, Andrea Taramelli, **Emiliana Valentini**, and Sergio Cappucci. Poster: Use of airborne LiDAR and hyperspectral data to study the sandy beach morphology along the Lazio region coast (Italy). EGU General Assembly 2011, Vienna, Austria. *Geophysical Research Abstracts*, 03-08/04/2011, Vol. 13, EGU2011-8725.

Andrea Taramelli, **Emiliana Valentini,** Mariangela Dejana, Francesco Zucca & Stefania Mandrone, 2011. Modeling coastal processes by means of innovative integration of remote sensing time series analysis. In Geoscience and Remote Sensing Symposium (IGARSS). *IEEE International*, 1547-1550.

Emiliana Valentini, Monica Targusi, Elena Pallottini, AnnaRita Fornari, Mariano Bresciani, Claudia Giardino, Luisa Nicoletti & Andrea Taramelli. 2010. Coastal landscape: Hyperspectral measurements of emerged and marine submerged vegetation. *Site – Società Italiana di Ecologia*. Rome, 09/2010.

Emiliana Valentini, Matteo Conti, Giancarlo Bovina, Massimo Gabellini, 2010. Articolo: Integrating ecological and hydrological features to assess coastal wetland restoration. In Bottarin R., Schirpke U., Tappeiner U. (eds) 2010, EURAC book - Analisi spazio-temporali: dinamiche e processi a confronto, *Proceedings of XIX SItE Conference*, VOL. II, 15-18/09/2009, Bolzano, 57: 113 - 122.

Luisa Nicoletti, **Emiliana Valentini**, Monica Targusi, Paola LaValle, AnnaRita Fornari, Andrea Taramelli. 2010. Characterization of *Posidonia oceanica* meadows using both hyperspectral and lidar data: a new approach, 46° Società Italiana di Biologia Marina *(SIBM) Conference*. Rapallo (GE), 19/06/2010.

Nicoletta Gazzea, Andrea Taramelli, **Emiliana Valentini**, Maria Elena Piccione, 2009. Articolo: Integrating fuzzy logic and GIS analysis to assess sediment characterization within a confined harbour. *Lecture Notes in Computer Science*, Part I, 5592: 33–49.